HEAT PIPE TECHNOLOGY

FOR

ADVANCED ROCKET THRUST CHAMBERS

Interim Report on Contract NAS 7-697

Report 697-I

24 July 1970

AEROJET LIQUID ROCKET COMPANY
A DIVISION OF AEROJET-GENERAL
SACRAMENTO, CALIFORNIA

HEAT PIPE TECHNOLOGY

FOR

ADVANCED ROCKET THRUST CHAMBERS

Interim Report on Contract NAS 7-697

by

D. C. Rousar

Report 697-I

24 July 1970

Prepared for

NATIONAL AERONAUTICS AND SPACE ADMINISTRATION
4800 Oak Grove Drive
Pasadena, California 91103

A E R O J E T L I Q U I D R O C K E T C O M P A N Y

FOREWORD

This is an interim report for Contract NAS 7-697, Heat Pipe Technology for Advanced Rocket Thrust Chambers; the work reported was performed during the period 3 January 1969 to 2 May 1970. The program is being conducted for NASA/JPL by the Engine Components Department of Aerojet Liquid Rocket Company, Sacramento, California. Heat pipe design, fabrication, and testing work was done on a subcontract by the Electronics Components Department, RCA Corporation, Lancaster, Pennsylvania. The JPL technical manager was R. W. Riebling and the NASA project manager was F. E. Compitello. At Aerojet, the project manager was R. J. La Botz and the project engineer was D. C. Rousar. The TCA subcontract management consisted of G. Y. Eastman, program manager, and R. W. Longsderff, project engineer. Significant contributions to this program were also made by P. A. Van and E. H. Green at Aerojet; and by R. A. Freggens and W. E. Harbaugh at RCA.

TABLE OF CONTENTS

LIST OF TABLES

LIST OF FIGURES

LIST OF FIGURES (cont.)

LIST OF FIGURES (cont.)

NOMENCLATURE

A	=	heat transfer area
A_F	=	fluid flow area
A/A_t	=	local area ratio of thrust chamber
a	=	acceleration
b	=	dimensionless constant characterizing a capillary structure, 10-20 for realistic geometries
C_g	=	correlation coefficient
C_p	=	specific heat of liquid
C'_p	=	specific heat of the vapor
D_c	=	local thrust chamber diameter
D	=	diameter
F	=	thrust, lb_f
F_B	=	black body shape factor from the thrust chamber interior to space. (An average value of 0.285 was used).
F'	=	barrier cooling fracture
g_c	=	gravitational constant
H	=	transport property correction factor
ΔH	=	represents one of several small axial elements
h_g	=	gas-side heat transfer coefficient
i	=	represents one of several small axial elements
K	=	permeability
k	=	thermal conductivity
L	=	heat pipe length
L'	=	flow length between evaporator midpoint and condenser midpoint
L^*	=	volume upstream of nozzle throat/throat area
N_2	=	liquid figure of merit
Nu	=	Nusselt number
P	=	pressure
Pr	=	Prandtl number = $\mu C_p/k$
P_c	=	Chamber pressure, psia
ΔP_{cap}	=	net pressure difference across liquid meniscus in evaporator and condenser wicks

NOMENCLATURE (cont.)

ΔP_{liq}	=	pressure loss in liquid flow
ΔP_{vap}	=	pressure loss in vapor flow
ΔP_{acc}	=	acceleration pressure head
Q	=	total heat transfer rate
Q_c	=	convective-heat transfer rate
Q_E	=	$F\varepsilon\sigma A\ T_{HP}^4$ = radiant heat transfer through the nozzle exit
q/A	=	heat flux
R	=	meniscus radius of curvature
Re	=	axial flow Reynolds number = $\rho\ V\ D_c/\mu$
Rr	=	radial flow Reynolds number (defined in Section II,B)
r	=	equivalent pore radius
r_b	=	bubble radius
St	=	Stanton number = $h_g/\rho\ V\ C_p$
T	=	temperature
T_F	=	film coolant temperature
T_{aw}	=	adiabatic wall temperature
T_{cr}	=	critical temperature = 522°R for B_2H_6 and 387°R for OF_2
T_{Fo}	=	inlet film coolant temperature (assumed equal to T_{sat})
T_{HP}	=	heat pipe temperature
T_{sat}	=	saturation temperature
t	=	thickness
ΔT_{SH}	=	wall superheat or excess temperature over the local boiling point
ΔT_{sub}	=	subcooling
V	=	velocity
w	=	mass flow rate
X	=	distance along thrust chamber wall downstream of the liquid film cooled length
Z	=	heat pipe length

NOMENCLATURE (cont.)

GREEK LETTERS

ε	=	emissivity, assumed to be 0.8
σ	=	surface tension or Stephan-Boltzmann constant
ϕ	=	angle of heat pipe axis with direction of gravity
ρ	=	density
θ	=	wetting angle
μ	=	viscosity
χ	=	quality

SUBSCRIPTS

b	=	bulk temperature
c	=	condenser
e	=	evaporator
FC	=	film coolant
fs	=	free stream
L	=	liquid film cooled region
ℓ	=	liquid
NB	=	normal boiling point
s.p.	=	single phase
v	=	vapor
w	=	wall condition
1	=	inside
2	=	outside

I. INTRODUCTION

Very high thermal conductance, heat flux averaging, and a heat flux transformer capability are unique properties which make adaptation of the heat pipe principle attractive for the cooling of rocket thrust chambers. A pressure fed rocket engine with a thrust chamber cooled by the heat pipe principle is currently being considered for unmanned space missions (1). The desired operating conditions are: 100 psig chamber pressure, 1000 lb_f thrust, and 1000 sec duration with OF_2 and B_2H_6 propellants.

A heat pipe consists of three basic elements: a container, a wick, and a working fluid. The container is closed and evacuated, and its walls are lined with a capillary structure, the wick, which is saturated with liquid working fluid. Operation of a heat pipe, shown in Figure 1 for a cylindrical configuration, is initiated by inputting heat to the evaporator region. This causes the working fluid to vaporize, flow to the condenser region (where external cooling is applied), and condense. Capillary action returns the working fluid to the evaporator. Heat-pipe-cooled rocket thrust chambers are not necessarily cylindrical in shape.

This report summarizes the initial design study of heat-pipe-cooled thrust chambers performed under Contract NAS 7-697. The program is being conducted by the Aerojet Liquid Rocket Company for the Jet Propulsion Laboratory, with RCA Corporation contributing as a heat pipe subcontractor. The program objective is to apply heat pipe technology to the cooling of high energy space storable propellants and a specific program goal is the design and fabrication of a working model OF_2/B_2H_6 thrust chamber which is cooled by the heat pipe principle.

The work on this program consisted of three tasks: Task I - Heat Pipe Technology Review, Task II - Analysis and Experimentation, and Task III - Working Model Design.

I, Introduction (cont.)

During Task I the existing heat pipe technology was reviewed and evaluated in view of the liquid rocket thrust chamber requirements. A summary of this technology review was prepared and is contained in Section II of this report. Design considerations relevant to heat-pipe-cooled thrust chambers are discussed in Section III. A heat pipe bibliography was also prepared and is given as Appendix A.

Task II comprised the bulk of the program. The three major efforts of this task were: concept selection, the fabrication experiment, and cylindrical heat pipe testing. Three possible design concepts were established and the feasibility of each for near term application with OF_2/B_2H_6 was evaluated analytically. The analysis results and descriptions of each concept are given in Section IV. A regeneratively cooled condenser concept and a sodium/nickel heat pipe system were chosen for the working model design.

The objective of the fabrication experiment was to evaluate the fabrication problems peculiar to a heat pipe constructed in the shape of a thrust chamber. An unoptimized design was fabricated and was operated successfully as a heat pipe. It is anticipated that the general configuration of the working model OF_2/B_2H_6 design will be similar to this fabrication experiment thrust chamber. The fabrication experiment is discussed in Section V.

The primary objective of the cylindrical heat pipe testing was to evaluate the evaporator heat flux capabilities of sodium/nickel heat pipes. This testing program is described in Section VI. Seven different evaporator wick configurations were tested and the maximum heat flux achieved was 5 Btu/in.^{2} sec. This is more than twice the maximum heat flux previously reported for sodium heat pipes.

I, Introduction (cont.)

The original objective of Task III was to establish a detailed design of a working model thrust chamber which incorporated the design concepts chosen and tested during Task II. However, despite the significant advances made during the Task II work, it was felt at the end of Task II that additional cylindrical heat pipe tests were needed to further evaluate the heat flux capabilities of sodium/nickel heat pipes and to solve certain problems exposed by the first year's effort. Consequently, Task III was modified to consist of preliminary design analyses so that a portion of the Task III funding can be combined with forthcoming funds for follow-on work. The preliminary design analysis work conducted during Task III is described in Section VII.

II. HEAT PIPE TECHNOLOGY REVIEW

Although the heat pipe is a relatively new device, it is the subject of a considerable amount of literature. At the start of this program, the majority of the literature was reviewed with regard to the rocket thrust chamber cooling problem. This literature work and pertinent discussions with heat pipe personnel at RCA Corporation and at the Los Alamos Scientific Laboratory (LASL) comprised the heat pipe technology review which is summarized in the following paragraphs. In addition, a heat pipe bibliography was prepared and is presented as Appendix A of this report. A complete review of the heat pipe field is not intended and technology areas applicable to the thrust chamber cooling problem have been emphasized. A comprehensive review of the heat pipe field is given in Reference 2 and basic introductory articles are given in References 3 and 4.

A. HISTORICAL

The heat pipe was invented by G. M. Grover at LASL in 1963 and most of the fundamental heat pipe work was subsequently done at LASL. The first heat pipe article was written by Grover and co-workers and described the operation of a sodium heat pipe and a water heat pipe (5). A similar device was proposed by Gaugler in 1942 but the principle involved was not effectively utilized until it was independently conceived by Grover. Although several individuals and organizations have contributed to the technology of heat pipes, the work at LASL is considered the most significant, especially the theoretical work of Cotter (6,7) and the experiments reported by Kemme (8,9,10). Previous publications concerning rocket engine applications are listed as References 11 and 12.

B. BASIC THEORY

The three essential elements of a heat pipe are: a working fluid, a wick, and a container. The principle of operation is demonstrated in

II, B, Basic Theory (cont.)

Figure 1 which is taken from Reference 4. Input heat evaporates the working fluid at what is referred to as the evaporator region of the heat pipe. The vapor pressure of the evaporated working fluid causes vapor flow to the condenser region where heat is removed and the fluid returns to the liquid state. Capillary action within the wick returns the liquid to the evaporator.

The basic theory describing steady state heat pipe operation has been discussed by Cotter (6), Cheung (2), Cosgrove (13), Haskin (14), Schlapback (15) and Feldman (16). It consists essentially of a pressure balance in which the pressure losses due to friction and acceleration effects are compared to the maximum capillary pressure difference which can be supported by the wick. Laminar liquid and vapor flow is generally assumed; however, turbulent vapor flow is also possible and has been considered.

A pressure balance for a heat pipe is written as Equation 1. This relationship must exist for successful operation.

$$\Delta P_{cap} \geq \Delta P_{liq} + \Delta P_{vap} + \Delta P_{acc} \qquad \text{Eq. 1}$$

$$\Delta P_{cap} = 2\,\sigma \left(\frac{1}{R_e} - \frac{1}{R_c} \right)$$

For a cylindrical heat pipe oriented with respect to the local acceleration as shown in Figure 1, the following expression applies

$$\Delta P_{acc} = \frac{\rho \ell}{g_c} \, La \cos \phi$$

In calculating the capillary pressure difference, ΔP_{cap}, the meniscus radius of curvature in the condenser is often assumed to be quite large since the working fluid tends to "puddle" in the condenser, so ΔP_{cap} can

II, B, Basic Theory (cont.)

be approximated with the following equations (note in Figure 1 that cos θ = r_e/R_e).

$$\Delta P_{cap} \simeq \frac{2\sigma}{R_e} = \frac{2\sigma}{r_e} \cos \theta_e$$

$$(\Delta P_{cap})_{max\ possible} = \frac{2\sigma}{r_e} \qquad \text{Eq. 2}$$

The liquid pressure, drop, ΔP_{liq}, can be calculated from Darcy's Law, Equation 3, provided some experimental data for permeability exist for the particular wick of interest (16).

$$\Delta P_{liq} = \frac{L'}{Kg_c} \left(\frac{\mu_\ell}{\rho_\ell}\right) \left(\frac{w}{A_F}\right) \qquad \text{Eq. 3}$$

Alternate expressions for ΔP_{liq} obtained through modification of Poiseuilles equation for capillary tube pressure drop are presented in Reference 17 for arterial, groove, screen, concentric annulus, and crescent annulus type wicks.

The vapor pressure drop, ΔP_{vap}, can often be neglected since it is usually small. Cotter (6) gives the expressions listed as Equations 4 and 5 for laminar vapor flow in a cylindrical heat pipe with the evaporator and condenser located on the cylindrical surface and zero adiabatic length.

$$\Delta P_{vap} = \frac{4\ \mu_v L\ Q}{\pi \rho_v\ r_v^4\ \Delta H} \quad R_r << 1 \qquad \text{Eq. 4}$$

$$\Delta P_{vap} = \frac{(1-4/\pi^2)\ Q^2}{8\ \rho_v\ r_v^4\ \Delta H^2} \quad R_r >> 1 \qquad \text{Eq. 5}$$

II, B, Basic Theory (cont.)

where: R_r = Radial flow Reynolds Number = $\frac{\rho_v V_r r_v}{\mu_v}$

An analysis which includes non-zero adiabatic length is presented by Haskin (14). For cylindrical heat pipe geometry tested on this program (heating on one of the circular end surfaces - see Section VII), the vapor pressure drop can be estimated from the laminar flow equation listed as Equation 6 (18).

$$\Delta P_{vap} = \frac{32 \mu_v L_v V_{ave}}{g_c D^2} \qquad \text{Eq. 6}$$

Equations more appropriate for turbulent flow are discussed by Cheung (2). Vapor compressibility effects are usually small except at low operating pressures and very large total heat transfer rates. This case has been investigated by Levy (19) and Kemme (10).

For a heat pipe with negligible vapor pressure drop, Equations 1, 2 and 3 can be combined and solved for the maximum heat transfer rate (note that $Q = w \Delta H$). The resulting expression is shown as Equation 7.

$$Q_{max} = \left(\frac{\rho_\ell \sigma \Delta H}{\mu_\ell} \right) \left(\frac{K A_F g_c}{L'} \right) \left(\frac{2}{r_e} - \frac{\rho_\ell aL}{\sigma} \cos \phi \right) \qquad \text{Eq. 7}$$

C. HEAT PIPE DESIGN CONSIDERATIONS

1. Wicks

The wick is certainly the most important component of a heat pipe since it controls to a large extent the heat flux, total thermal load, and startup characteristics of a given heat pipe. The primary wick function

II, C, Heat Pipe Design Considerations (cont.)

is to produce sufficiently high capillary pumping forces and sufficiently low liquid pressure losses so that the desired quantity of working fluid can be circulated. These two requirements tend to be conflicting since small pore sizes are required for high capillary pressure differences and large pores are desired for low flow resistance. This situation leads to an optimum pore size for maximum thermal load in cylindrical heat pipes with uniform porosity wicks and with no auxiliary liquid return passages.

Other wick requirements arise depending on the application and the working fluid. For example, a relatively thin wick is needed for high heat flux operation to reduce the wick temperature drop and avoid boiling within the wick (generally regarded as detrimental). An additional consideration for cylindrical heat pipes is that high vapor velocities can produce entrainment of the liquid by the vapor unless the wick pore size is sufficiently small.

An evolution of wick designs for cylindrical heat pipes is apparent in the LASL literature as thermal load levels were increased and a summary of the LASL wick configurations is given in Reference 17. Initially, screen mesh wicks were utilized, then grooved channels with and without screen coverings, and most recently an annular liquid flow passage formed by a very fine porosity tube. This latter configuration provides the attractive combination of very high capillary forces and very low flow resistance.

2. Working Fluids

A wide variety of working fluids and operating temperatures have been employed in heat pipes ranging from nitrogen at -250°F (14) to silver at 3630°F (20). A partial tabulation of reported heat pipe work is given as Table 1.

II, C, Heat Pipe Design Considerations (cont.)

The working fluid is often chosen for its heat transport capability and vapor pressure at the particular operating temperature of interest. The heat transport capability is in part described by the liquid transport factor, N_L, which is defined in Equation 8.

$$N_L = \frac{\rho_\ell \sigma \Delta H}{\mu_\ell} \qquad \text{Eq. 8}$$

By inspection of Equation 7, it can be seen that this factor is indicative of the thermal load a fluid can transport for a given wick geometry and orientation assuming the heat pipe is liquid flow limited. The liquid transport factor values given for 8 fluids in Reference 21 are shown as Figure 2. A high liquid thermal conductivity is also desirable for high heat flux operation since heat transfer through the wick is essentially a conduction process.

Vapor properties can also be important and a vapor transport factor, N_v, analogous to N_L, has been defined (22). The ultimate limit of heat transport at a given temperature occurs when sonic velocity is achieved in the vapor and therefore the vapor density is an important property to consider.

The liquid metals are the fluids of interest for thrust chamber applications because of their good heat transport characteristics and high operating temperatures. In addition they have the high values of liquid thermal conductivity which are necessary to operate at high heat fluxes with a reasonable value of non-boiling superheat.

The operating temperature range of a working fluid depends on the particular heat load requirements and geometrical restraints; however, an operating temperature near the normal boiling point is generally chosen because

II, C, Heat Pipe Design Considerations (cont.)

high vapor velocities occur at lower temperatures and excessive vapor pressures develop at higher temperatures. The normal boiling points of several liquid metals are listed below. Melting point values are also given. The melting point becomes important in evaluating startup with a frozen working fluid.

Metal	Cs	K	Na	Li	Ag
Melting Point, °F	83.5	146	208	356	1762
Normal Boiling Point, °F	1242	1402	1622	2430	3542

3. Materials

The container material must be chemically compatible with the working fluid and must be wet by it. Chemical reactions can produce noncondensible gases which block off heat transfer at the condenser. Poor wetting also leads to low heat transport rates. In addition, solubility in the working fluid must be low. Any solids which dissolve in the working fluid will be deposited in the evaporator and curtail the operating life of the heat pipe.

4. Startup

Some difficulties have been experienced in starting heat pipes and this is a potential problem area for heat-pipe-cooled thrust chambers. The work in this area is not extensive, but the essentials of the problem have been defined by Cotter (7). Problems associated with melting the working fluid and operating limits due to sonic vapor flow, liquid entrainment, and evaporation kinetics can be encountered.

II, C, Heat Pipe Design Considerations (cont.)

5. Shapes

Most of the heat pipe work has been done with the cylindrical shape. In more complex geometries, difficulties are sometimes experienced in maintaining a continuous wick structure which remains in close contact with the wall. Cleanliness and the prevention of leaks are also more difficult with complex shapes. RCA has done most of the significant work on unconventional shaped heat pipes including right angle, flexible, and star geometries.

D. HEAT PIPE OPERATING LIMITS

Four heat pipe operating limits have been defined, they are: (1) wicking limit (dryout), (2) sonic flow limit, (3) entrainment limit, and (4) boiling limit. These limits are discussed throughout the literature and a good summary is given in Reference 17. This summary provides the basis for the following discussions.

1. Wicking Limit (Dryout)

An anlytical statement of the wicking limit is given as Equation 1. The wicking limit, also termed dryout, is reached when the sum of the system pressure losses equal the pressure difference capability of the evaporator meniscus. Wicking pressure losses therefore limit the total heat transfer rate since flow rate and consequently the total rate of heat transfer are proportional to them. Drying and overheating of the evaporator wick occurs if this limit is exceeded.

Wicking limits seem to be most restrictive for simple cylindrical heat pipes with mesh type wicks as they have inherently high liquid flow resistance. It appears that the problem can be alleviated by providing

II, C, Heat Pipe Design Considerations (cont.)

large liquid flow areas and relatively short liquid flow lengths. The annular geometry of a heat pipe thrust chamber is particularly attractive from this standpoint because radially oriented liquid return paths can be situated between the condenser and evaporator at whatever location is desired.

2. Sonic Flow Limit

Sonic flow of the vapor can occur at low operating temperatures (low pressures) where the vapor densities are also low. This can be seen in Equation 9 which relates the input heat flux and evaporative mass flux for a flat plate heat pipe (heat flow and vapor flow normal to the evaporator wick).

$$\frac{Q}{A} = \rho_v V_v \Delta H \qquad \text{Eq. 9}$$

For a given heat flux, the vapor velocity depends on the vapor density and latent heat. The velocity cannot exceed sonic and therefore a heat flux limit exists which is dependent on operating temperature. Heat pipes operating at the sonic flow condition have been experimentally investigated by Kemme (10).

Values of sonic limit heat fluxes from Reference 17 are given in the following table for four liquid metals. Assuming an upper limit heat flux of about 1 to 2 Kw/cm^2 (6.1 to 12.2 $Btu/in.^2$ sec), it is seen that the sonic heat flux limit becomes significant for cesium and potassium at temperatures below 500°C (930°F), for sodium below 600°C (1112°F) and for lithium below 900°C (1652°F).

II, D, Heat Pipe Operating Limits (cont.)

Temperature, (°C) °F		Sonic Heat Flux Limit, (Kw/cm^2) $Btu/in.^2$ sec							
		Cs		K		Na		Li	
(400)	752	(1.0)	6.1	(0.5)	3	-		-	
(500)	932	(4.6)	28	(2.9)	18	(0.6)	3.7	-	
(600)	1112	(14.9)	91	(12.1)	74	(3.5)	21	-	
(700)	1292	(37.3)	228	(36.6)	220	(13.2)	81	-	
(800)	1472					(38.9)	240	(1.0)	6.1
(900)	1652					(94.2)	576	(3.9)	24
(1000)	1832							(12.0)	73.5
(1100)	2012							(31.1)	191
(1200)	2192							(71.1)	435

3. Entrainment Limit

Some liquid from the return wick may be entrained by the vapor if the liquid return passage is not impervious and if the vapor velocities are sufficiently high. This limit is generally encountered at temperatures higher than where the sonic condition is limiting. Kemme has measured entrainment limits in screen covered channel wicks (9) and found that the entrainment limit could be predicted reasonably well assuming a critical Weber number of 1 where the Weber number is based on screen wire diameter, d. With this criterion, the entrainment limit expressed as an axial heat flux (based on vapor flow area) is given by Equation 10.

$$\left(\frac{Q}{A}\right)_{axial} = \left[\frac{2\pi \rho_v \sigma \Delta H^2}{d}\right]^{1/2} \qquad \text{Eq. 10}$$

It is apparent from Equation 10 that entrainment can be inhibited by covering the flow channels with fine screens and this is corroborated by Kemme's data.

II, D, Heat Pipe Operating Limits (cont.)

4. Boiling Limit

The boiling limit is one of the more critical technology areas for application of the heat pipe principle to the cooling of thrust chambers because not much is known about the boiling limit in general. The data available for liquid metals are meager but the indications are that relatively large heat fluxes can be accommodated before boiling phenomena produce evaporator hot spots.

General agreement does not appear to have been reached regarding the extent, if any, to which boiling can occur in a heat pipe wick. A simplified, and possibly conservative, phenomenological model of the boiling limit for liquid metals is obtained by assuming that the boiling limit is reached when the conditions are such that a nucleated bubble can grow. This occurs when the excess pressure within a bubble becomes large enough to overcome surface tension forces. A force balance on a bubble, Equation 11, then defines the limiting condition.

$$P_1 - P_2 = \frac{2\sigma}{r_b} \qquad \text{Eq. 11}$$

The interior and exterior pressures P_1 and P_2 in Equation 11 correspond to temperatures in accordance with the vapor pressure curve for a particular working fluid. Since P_2 corresponds to the local boiling point, Equation 11, in effect, defines the allowable superheat in a system with nucleation sites of radius r. At this point it is assumed that the fluid motion within the wick is slow and the heat transfer mechanism is essentially conduction. The heat flux is then given by the relation shown as Equation 12 (radial conduction effects are neglected since they will be small on heat pipe cooled thrust chambers).

II, D, Heat Pipe Operating Limits (cont.)

$$\left(\frac{Q}{A}\right)_{\text{boiling limit}} = \frac{\Delta T_{SH}}{(t/k)_{wick}} \qquad \text{Eq. 12}$$

Equation 12 shows that high boiling limit heat flux values can be achieved if relatively thin, high conductivity wick structures are employed and if the allowable superheats are high. The data in References 23 and 25 show that incipient boiling superheats are higher on smooth, clean surfaces and that the superheat increases with decreasing system pressure. These data trends are explained by examination of Equation 11. It is apparent from this equation that high superheats are obtained if the nucleation site radius, r, is small and small r values would be expected for smooth, clean surfaces. Equation 11 predicts higher superheats at low pressures for two reasons: (1) lower pressure corresponds to lower boiling point and the surface tension of liquids characteristically increases with decreasing temperature; (2) a given excess pressure is equivalent to a greater temperature difference at lower pressure due to the exponential shape of vapor pressure curves.

The allowable superheat is not well defined but values in the 100°F to 400°F have been measured for sodium and potassium and a few very high values (950°F for sodium, 500°F for potassium) have been reported (24). Analysis of the cylindrical heat pipe data obtained on this program has indicated that a maximum superheat of 500°F was achieved with sodium during testing on Heat Pipe No. 7 (see Section VII).

Analytical models for the prediction of incipient boiling superheat have recently been published by Holtz (25) and by Chen (26). The Holtz model is particularly interesting because it predicts a pressure-temperature history effect which is verified reasonably well by potassium and sodium data. Pressure provides the major effect and increased values of superheat are indicated for higher previous system pressures. Predictions for

II, D, Heat Pipe Operating Limits (cont.)

sodium from the Holtz model are shown in Figure 3. The indicated pressure effect suggests a preconditioning of heat pipes by pressurization before actual operation to increase the boiling limit. The effect may also be dependent on the original surface condition, of course, and little improvement may be found for surfaces which are initially very smooth and clean.

III. THRUST CHAMBER DESIGN CONSIDERATIONS

The major design considerations for heat-pipe-cooled thrust chambers are: (a) choice of working fluid and appropriate container material, (b) method of condenser cooling, (c) allowable evaporator heat flux levels, (d) fabrication capabilities, (e) size and total heat transfer rate, (f) the startup procedure, and (g) acceleration and vibration levels. These areas are discussed in the following paragraphs.

A. WORKING FLUID

Three combinations of working fluid and container materials are considered potentially suitable for thrust chamber applications: sodium and nidkel, lithium and molybdenum, silver and TZM. These working fluids provide a wide range of operating temperatures, about 1000°F to 3600°F. They rate high from the standpoint of total heat transfer capability (see for example the figure of merit for sodium in Figure 2) and they are potentially applicable at conditions of high local heat flux due to their high thermal conductivity. The candidate container materials were chosen on the basis of successful previous experience at RCA and at the Los Alamos Scientific Laboratory.

The sodium/nickel heat pipe system was chosen for the OF_2/B_2H_6 thrust chamber application because of the good compatibility of nickel and the combustion products at the wall temperature levels necessary for sodium heat pipes (1400 to 1800°F). Higher local heat flux and total heat transfer rate values may be possible with lithium and silver heat pipes but the container materials for these working fluids have not been shown to be compatible with OF_2/B_2H_6 combustion gases at the required operating temperatures (about 2500°F for lithium and 3500°F for silver). Graphite lined heat pipe thrust chambers may provide a solution to this problem for other propellant combinations.

III, Thrust Chamber Design Considerations (cont.)

B. CONDENSER COOLING

Heat pipe cooling of thrust chambers is feasible only if a suitable means of cooling the heat pipe condenser is available. Condenser cooling can be accomplished by one of three existing thrust chamber cooling techniques which characterize the three concepts evaluated in Section IV: regenerative cooling, radiation cooling, and internal regenerative cooling.

In the regenerative cooled system, heat is transmitted through the heat pipe to one or both of the propellants at a heat flux level substantially lower than exists at the thrust chamber wall. This heat flux reduction is also conducive to the utilization of the relatively low heat fluxes obtainable with thermal radiation for condenser cooling. Heat pipes provide the ultimate in wall thermal conductance and could replace the heavier high thermal conductivity metal walls (copper, beryllium) currently being used in internal regenerative cooled systems. These concepts are illustrated in Figure 4 and discussed in detail in Section V.

C. EVAPORATOR HEAT FLUX

The evaporator wick heat flux limit is one of the more crucial aspects of heat pipe thrust chamber design and is highly dependent on the evaporator wick. Maximum heat fluxes in the range of 4 to 6 Btu/in.^{2} sec are anticipated during steady state operation of the heat-pipe-cooled OF_2/B_2H_6 space engine. An evaporator heat flux capability in the range of 6 to 8 Btu/in.^{2} sec is therefore desirable to provide an adequate safety margin.

Evaporator heat flux limits had not been explored extensively prior to this program. The heat fluxes which had been achieved by LASL and RCA were 1.34 Btu/in.^{2} sec for a sodium heat pipe and 2.75 Btu/in.^{2} sec for a

III, C, Evaporator Heat Flux (cont.)

lithium heat pipe. These are low heat flux levels by thrust chamber standards but it is emphasized that these are achievement levels and not necessarily limits. Reiss and Schretzmann report a boiling limit heat flux of 12.2 Btu/in.^{2} sec in a sodium heat pipe; however, their data are difficult to interpret because of two-dimensional conduction effects. It is believed that their input heat flux of 1.8 Btu/in.^{2} sec is a more appropriate value for comparison to other systems (27).

The desired evaporator heat flux range has been approached during recent testing on sodium heat pipes. A heat flux of 5 Btu/in.^{2} sec was achieved with a cylindrical-shaped device on this program (see Section VII) and a peak heat flux of 5.6 Btu/in.^{2} sec was reached with an annular configuration on an Aerojet IR&D test program.

D. FABRICATION

The feasibility of fabricating heat-pipe-cooled thrust chambers was demonstrated on this program by the fabrication of a non-optimized design. Construction of this thrust chamber comprised the fabrication experiment which is described in Section VI. The completed thrust chamber was heated at a low heat flux and was found to function as a heat pipe.

E. PHYSICAL SIZE AND TOTAL HEAT TRANSFER RATE

Technology level limits with regard to total heat transfer capability and physical size are encountered when applying the heat pipe principle to thrust chamber cooling. A maximum total thermal load of 17 Btu/sec has been transported via a heat pipe and this capability must be increased by more than an order of magnitude for relatively small rocket engine applications. Physical size is not a particular problem for the application currently being

III, E, Physical Size and Total Heat Transfer Rate (cont.)

considered but may become troublesome in the future. These technology limits can be significantly extended through experience since they are essentially a matter of scale and technique in heat pipe fabrication and processing.

F. STARTUP

There are two major aspects of the startup problem: (1) the heat pipe must be "thawed" before the evaporator working fluid is depleted, and (2) the maximum heat transport rate is limited at low heat pipe temperatures. The scope of the present contract did not allow for rigorous investigation of startup procedures; however, sufficient experimental and analytical work was conducted to indicate that startup is not an insurmountable problem. One of the RCA cylindrical test devices was tested with step input heat flux and it was found that relatively high heat fluxes could be accommodated when the sodium was initially a low temperature liquid (see Section VII). It is believed that the problems associated with the rapid startup of rocket engines can be avoided through design. A heat pipe design for rapid, high heat flux starts with solid sodium was conceived and is discussed in Section VII. If necessary, a programmed startup rate can be utilized to alleviate the problems of startup.

G. ACCELERATION AND VIBRATION

Heat pipe performance can be significantly degraded by acceleration forces since the pumping capability of a capillary wick is somewhat limited. Much of the existing heat pipe data has been obtained working against a 1g gravitational field. The acceleration effects are definitely size sensitive (longer pipes give greater hydrostatic effects) and are readily treated analytically. A 1g acceleration level is not severe for a liquid metal system and this is the maximum acceleration currently assumed.

III, G, Acceleration and Vibration (cont.)

It is believed that higher accelerations can be accommodated by proper design. Operation at quite high accelerations may be possible by locating the condenser forward of the evaporator so that acceleration effects aid in the return of liquid working fluid to the evaporator and only the relatively low density vapor flows in the direction of the acceleration.

The influence of thrust chamber vibrations on heat pipe performance is an area of uncertainty. However, a study reported for a water heat pipe (Ref. 26) indicates that vibration is beneficial to heat pipe performance. This unit was not tested near its maximum power level but it appears possible that vibration may enhance the heat flux capabilities of heat pipes by inhibiting bubble formation in the evaporator wick.

IV. CONCEPT EVALUATION

Analytical studies were conducted to evaluate design concepts for heat-pipe-cooled OF_2/B_2H_6 thrust chambers which incorporate regenerative, radiation, and internal regenerative cooled condensers. These three concepts are illustrated in Figure 4. Methods of analysis and the results obtained are given in the following sections and the range of operating conditions considered are shown below.

Thrust	100 to 100,000 lb
Chamber Pressure	10 to 500 psia
Propellants	OF_2/B_2H_6
Mixture Ratio	3.0
Contraction Ratio	1.56

Sodium/nickel heat pipes and the 1000 lbf thrust, 100 psia chamber pressure operating condition were emphasized in the analyses because this heat pipe system and operating condition are planned for the working model design which will be designed and fabricated during the next year.

A conical thrust chamber geometry with 7.5 in. L*, 15° divergence angle, and variable exit area ratio were assumed in the internal-regenerative and radiation cooled calculations. A 12 in. L* geometry with cylindrical combustion chamber and 5/1 exit area ratio was used in the regenerative cooled analysis. Both thrust chamber configurations are shown in Figure 5. In both cases, combustion chamber L* was assumed constant for all thrusts and chamber pressures. The 12 L* configuration has been designated by JPL as the thrust chamber geometry for the working model design. The 7.5 in. L* geometry was utilized on a previous OF_2/B_2H_6 program (27) and in the fabrication experiment on this program.

As a result of these concept evaluation studies, the regenerative cooled condenser concept was chosen for the working model design. This design is discussed further in Section VIII.

IV, Concept Evaluation (cont.)

A. REGENERATIVE COOLED CONDENSER CONCEPT

1. Concept Description

In a regenerative cooled system the entire thrust chamber wall functions as a heat pipe evaporator. The wall consists of a structural layer of nickel backed by an evaporator wick which contains working fluid in the liquid state. Heat from the combustion gases vaporizes the working fluid and the vapors flow in a radial direction to the condenser which surrounds the evaporator. During the condensation process, heat is transferred to the cooling jacket through an appropriate condenser wall thermal resistance. The return of liquid working fluid to the evaporator is facilitated by radially oriented flow passages which connect the condenser and evaporator wicks.

The heat flux transmitted to the cooling jacket is substantially lower than at the thrust chamber wall because of the larger surface area (heat flux transformer characteristic). In addition, sufficient longitudinal and circumferential vapor flow occurs to equalize the vapor pressure at the condenser surface and thereby produce a relatively uniform cooling jacket heat flux (heat flux averaging characteristic).

Consequently, the coolant passage design for a regenerative cooled heat pipe thrust chamber is less complex than in a conventional regenerative system and the limits due to critical heat flux, pressure drop, or total heat capacity are eliminated or significantly extended. In addition, the heat pipe tends to act as a "heat distributor" as the local regions which tend to operate at higher temperatures will receive less heat. This mechanism will prevent the occurrence of local coolant passage burnout. Two-phase flow and a complete change of phase (liquid to gas) within the coolant passages appear feasible.

IV, A, Regenerative Cooled Condenser Concept (cont.)

The design approach for a regeneratively cooled condenser will be to achieve a sufficiently low condenser heat flux so that the required condenser thermal resistance is much larger than the thermal resistance in the coolant boundary layer. The excess thermal resistance will be built into the condenser wall so that large variations in coolant heat transfer coefficient (nucleate boiling to film boiling for example) will yield relatively small variations in overall heat transfer rate.

2. Analysis

The feasibility of regenerative cooling the condenser of a sodium heat pipe (1500°F temperature) with B_2H_6, OF_2, or both propellants was evaluated on an energy balance basis by comparing the total convective heat transfer rate to the heat required to: (1) increase the coolant temperature to the saturation temperature, (2) vaporize the coolant, and (3) increase the vapor temperature to 1500°F. This type of analysis yields an initial evaluation of regenerative cooling. Other factors, such as pressure drop and coolant passage geometry, startup phenomena, and shutdown phenomena must ultimately be considered in designing a regeneratively cooled system. It was assumed that adequate cooling passages can be designed to accommodate the appropriate rate of heat transfer and no pressure drop, startup, or shutdown analyses were performed. The criterion for feasibility used was that the coolant supplied to the injector must be either all gas or all liquid so that two-phase flow in the injector is avoided.

Figure 6 shows how the regenerative cooling feasibility was evaluated. The (1) lines represent the heat Q_1 required to raise the coolant (OF_2, B_2H_6, or OF_2 and B_2H_6) from the inlet temperature (-240°F) to the boiling point at 100 psia pressure. The Q_1 values increase with thrust due to the increase in flow rates.

IV, A, Regenerative Cooled Condenser Concept (cont.)

$$Q_1 = \dot{w}_c C_p (T_{sat} + 240) \qquad \text{Eq. 13}$$

Flow rates were calculated using 100 psia chamber pressure and 1000 lb thrust condition as a reference case.

$\underline{B_2H_6}$: $\dot{w}_c = 0.65\ (F/1000)$, lb/sec

$\underline{OF_2}$: $\dot{w}_c = 1.95\ (F/1000)$, lb/sec

The (2) lines in Figure 6 give the total heat Q_2 required to completely vaporize the coolants, starting from subcooled liquid at -240°F.

$$Q_2 = \dot{w}_c [C_p (T_{sat} + 240) + \Delta H] , \qquad \text{Eq. 14}$$

The (3) lines in Figure 6 show the maximum possible heat transfer rate which the coolant can absorb, termed Q_3, which is the heat necessary to bring the vaporized coolants to 1500°F (the assumed heat pipe temperature), starting with subcooled liquid at -240°F.

$$Q_3 = \dot{w}_c [C_p (T_{sat} + 240) + \Delta H + C_p' (1500 - T_{sat})] \qquad \text{Eq. 15}$$

In the foregoing calculations, it was also assumed that the pressure drop in the coolant passages and across the injector was 20% of the coolant pressure. Liquid specific heats were taken from Reference 28 and ideal gas specific heats (Ref. 29) were assumed for the OF_2 and B_2H_6 vapors. The variation of latent heat with pressure was estimated using the Watson method (Ref. 30) given as Equation 16.

$$\Delta H = \Delta H_{NB} \left[\frac{1 - (T/T_{cr})}{1 - (T_{NB}/T_{cr})} \right]^{0.38} \qquad \text{Eq. 16}$$

IV, A, Regenerative Cooled Condenser Concept (cont.)

The dashed line in Figure 6 is the total convective heat transfer rate which the coolants are required to absorb from the combustion gases. Intersection of the dashed line with the others determined the values of thrust and chamber pressure for which the coolant is heated to its boiling point, completely vaporized, and heated in the gaseous state to 1500°F. The total convective heat transfer rate was calculated through use of an average heat transfer coefficient, $\bar{h}_g$, as shown in Equation 17.

$$\Sigma Q = \bar{h}_g (T_r - T_{HP}) A \qquad \text{Eq. 17}$$

The relationships used to evaluate $\bar{h}_g$ are given in Appendix B. It was assumed that the thrust chamber operates without film or barrier cooling. This assumption tends to yield total heat loads that are conservative.

3. Discussion of Results

A series of plots similar to Figure 6 yielded the final results shown in Figure 7 which is a feasibility chart for regenerative cooling a 1500°F heat pipe thrust chamber with OF_2, B_2H_6, or both OF_2 and B_2H_6. An explanation of this chart is given in the following paragraphs.

The three curves labeled (1) in the upper right hand corner of Figure 7 represent the combinations of thrust (F) and chamber pressure (P_c) which yield saturated liquid at the outlet of the coolant passages. Thrust-P_c combinations to the right of these curves (higher F, higher P_c) yield subcooled liquid, and two-phase flow is encountered to the left (lower F, lower P_c). The (1) curves therefore define one boundary of the two phase flow region.

Saturated vapor curves are labeled as the (2) curves in Figure 7. They lie at a slight angle to the horizontal and further define the

IV, A, Regenerative Cooled Condenser Concept (cont.)

two phase region: F-P_c combinations above the curves yield two phase flow at the coolant outlet while superheated vapor is obtained for the F-P_c values below them.

A maximum possible heat transfer rate condition is defined by the curves labeled (3) which lie near the bottom of Figure 7. Thrust-P_c values above the curves yield superheated vapor at the injector at a temperature between T_{sat} and 1500°F. Operation at F-P_c combinations below the (3) curves is not possible at the assumed conditions since this would require outlet temperatures greater than the heat pipe temperature.

In summary of Figure 7, it is clear that the F-P_c combination of a completely regeneratively cooled system must lie either to the right of the (1) curves (subcooled liquid at the injector) or between the (2) and (3) curves (superheated vapor) if two-phase flow at the injector is to be avoided. Operation with subcooled liquid at the injector is possible only at high values of thrust; for example, about one million lb thrust is indicated for 100 psia chamber pressure. Operation with superheated vapor at the outlet is indicated for moderate thrust levels (about 500 to 10,000 lb thrust) for the chamber pressure range evaluated.

The 100 psia/1000 lbf operating point is indicated as a feasible condition for a regeneratively cooled condenser with superheated-vapor at the outlet. Feasibility is indicated for all three coolant combinations: OF_2 only, B_2H_6 only, and both OF_2 and B_2H_6. The highest vapor temperature is indicated for OF_2 cooling and the lowest vapor temperature is indicated for both OF_2 and B_2H_6 cooling. Other factors such as system design ramifications, chemical reaction phenomena, startup characteristics, and coolant passage design must be considered before choosing among these three possible regenerative cooling techniques. The indicated feasibility for a 50 psia chamber

IV, A, Regenerative Cooled Condenser Concept (cont.)

pressure, 1000 lbf thrust chamber is much the same as the 100 psia/1000 lbf case. Boundary cooling tends to decrease the total heat transfer rate and consequently if Figure 7 were drawn for a boundary cooled thrust chamber the (1) curves would shift to the left and the (2) and (3) curves would shift downward.

B. RADIATION COOLED CONDENSER CONCEPT

1. Concept Description

A radiation cooled condenser is attractive because of its inherent simplicity; however, relatively high exterior temperatures are required and heat transfer to adjacent spacecraft components can be appreciable. The design is virtually the same as described for the regenerative cooled case except that the outer surface of the condenser is a radiator instead of a cooling jacket.

2. Analysis

An analysis to evaluate the feasibility of the radiation cooled concept was conducted by performing an energy balance in which radiation heat transfer to space from a cylindrical condenser surface and from the divergent nozzle surface was equated to the convective heat transfer from the combustion gases to the thrust chamber wall. Design parameters considered were condenser diameter, exit area ratio, and heat pipe temperature.

The assumed geometry was such that the diameter of the cylindrical condenser ranged from one to two times the nozzle exit diameter. This is believed to represent the range of practical condenser surface areas. Large extended radiator surfaces would be difficult to contain in a compact launch

IV, B, Radiation Cooled Condenser Concept (cont.)

package and would also complicate the heat pipe design. Irregular or star shaped condenser surfaces may also be utilized; however, the increased area of these configurations (over a smooth cylinder and for the same diameter restraints) was small enough to be neglected in this feasibility analysis. The condenser length was assumed equal to the thrust chamber length.

The total convective heat transfer rate into the thrust chamber wall was calculated from Equation 18.

$$Q_c = \sum_i h_{g_i} A_i (T_r - T_{HP}) \qquad \text{Eq. 18}$$

It is assumed that the thrust chamber operated without boundary cooling and the temperature drop through the heat pipe was neglected. Gas-side heat transfer coefficients were calculated as a function of thrust, chamber pressure, and exit area ratio as described in Appendix B.

The feasibility criterion used was simply whether or not the thrust chamber heat could be radiated to space from a condenser of a size within the assumed geometrical constraints. An analysis considering boundary cooling would indicate smaller condenser area requirements than those obtained.

Required condenser areas were calculated from Equation 19.

$$A = \frac{Q_c - Q_E}{\varepsilon \sigma T_{HP}^4} \qquad \text{Eq. 19}$$

The surface area ratios R_1 and R_2, defined by Equations 20 and 21, were used to evaluate the feasibility of a radiation cooled system. Feasibility was indicated if the R value was less than or equal to 1.0.

IV, B, Radiation Cooled Condenser Concept (cont.)

$$R_1 = \frac{\text{Required Condenser Area (A)}}{\text{Area of Cylinder with Diameter = Exit Diameter}} \qquad \text{Eq. 20}$$

$$R_2 = \frac{\text{Required Condenser Area (A)}}{\text{Area of Cylinder with Diameter = 2 (Exit Diameter)}} \qquad \text{Eq. 21}$$

3. Discussion of Results

Some typical results for a 1500°F heat pipe thrust chamber with 50/1 nozzle exit area ratio are shown in Figure 8. The ratio R_1 is shown as a function of chamber pressure and thrust. (The R_2 ratio behaves in a similar manner). The R_1 values increase with chamber pressure (fixed thrust) because higher convective heat transfer rates and smaller condenser areas are obtained as the chamber pressure is increased. Increased thrust yields decreased R_1 values because the heat transfer coefficients decrease and the condenser area increases more than the convective heat transfer rate.

Plots similar to Figure 8 were used to generate the radiation cooling feasibility charts shown in Figures 9, 10, and 11. The values of thrust and chamber pressure at which R_1 and R_2 equal 1.0 are shown for heat pipe temperatures of 1500°F (sodium working fluid), 2500°F (lithium), and 3500°F (silver). The R_2 configuration is always feasible at higher chamber pressures than the R_1 configuration because of the higher available surface area. The feasible chamber pressure increases with exit area ratio because higher area ratios yield larger condenser surface areas and lower average evaporator heat fluxes.

For the 100 psia chamber pressure, 1000 lb_f thrust operating condition, radiation cooling is not feasible with a sodium heat pipe chamber because excessively large condenser areas are required. However, the concept is feasible for higher temperature working fluids. Feasibility is indicated

IV, B, Radiation Cooled Condenser Concept (cont.)

for area ratios greater than about 25/1 for lithium heat pipe thrust chambers and for area ratios greater than about 5/1 for heat pipe chambers utilizing silver as the working fluid. Lithium and silver were not chosen as working fluids for the OF_2/B_2H_6 thrust chamber because the required container materials (TZM, Ta-Sw) have not been shown to be compatible with these propellants and their combustion products at the required operating temperatures.

The condenser area requirement for a sodium working fluid thrust chamber is reduced at lower chamber pressures because of the lower heat load. At the 50 psia chamber pressure and 1000 lb_f operating condition, a nozzle exit area ratio of about 100 is required.

C. INTERNAL REGENERATIVE COOLED CONDENSER CONCEPT

1. Concept Description

The internal regenerative system differs from the regenerative and radiation cooled system in that both the evaporator and condenser are located on the thrust chamber wall. In the condenser region, located near the injector, heat is transferred into fuel film coolant which is injected along the wall. The evaporator region is located downstream where sufficient mixing of the film coolant and core gas streams has occurred to produce heat flow into the wall. Vapor flows axially forward to the condenser and the condensed liquid flows axially towards the nozzle exit plane through axial flow passages or arteries and within the condenser and evaporator wicks.

Practical design considerations detract from the internal regenerative concept because of the complex thrust chamber wall design which is required. In the condenser region, a low heat flux out of the wall is desired for a relatively large temperature drop (about equal to $T_{Hp}-T_{sat}$) and therefore a high wall thermal resistance is required. The opposite condition

IV, C, Internal Regenerative Cooled Condenser Concept (cont.)

exists in the evaporator region where a low wall thermal resistance is needed so that a relatively high heat flux may flow into the wall without producing excessive wall temperatures. Therefore, a variable thermal resistance wall is indicated. The design and ultimate operating temperature of such a wall are highly dependent on the gas side boundary conditions and these are difficult to accurately predict in an internal regenerative system. In addition, it has very recently been reported (1) that only relatively small liquid film lengths can be maintained with liquid B_2H_6 due to its thermophysical properties and therefore internal regenerative cooling does not appear attractive for this propellant. However, the internal regenerative concept presents a less severe startup problem than the regenerative concept and appears advantageous in this respect. For this reason the concept was retained for the purpose of this analysis.

2. Analysis

A simplified analysis of a sodium heat pipe thrust chamber with an internal regenerative cooled condenser was conducted which provides an evaluation of the relative effects of thrust and chamber pressure on the feasibility of this concept. The more refined analytical models available (Ref. 31 for example) were not utilized because they are difficult to apply in a study which considers such a large range of operating conditions. The analysis consisted of two parts: the liquid film cooled region (heat transfer out of the wall) and the gas film cooled region located downstream of the liquid film cooled region (mostly heat transfer into the wall). A film coolant flow rate equal to 40% of the total fuel flow rate was assumed.

Liquid film cooled lengths were estimated by performing an energy balance on the liquid film. The energy balance used, written as Equation 22, tends to yield optimistic values of liquid length because entrainment of the liquid by combustion gases was neglected. However, the procedure

IV, C, Internal Regenerative Cooled Condenser Concept (cont.)

used to estimate heat transfer downstream of the liquid length is conservative and this tends to compensate for the lack of entrainment considerations.

Heat Required to Vaporize Liquid Film Coolant	=	Heat Transfer Directly from Combustion Gases	+	Heat Transfer from the Heat Pipe Condenser

$$w_{Fc} (C_p \Delta T_{sub} + \Delta H) = h_g A_L (T_r - T_{sat}) + \Sigma_i h_{g_i} A_i (T_{F_i} - T_w) \quad \text{Eq. 22}$$

Film coolant temperatures in the gas film cooled region were estimated from a simplified version of one of Aerojet's gaseous film cooling models. The manner in which this was done is described in Appendix B.

The criterion for feasibility used was that the heat flux from the condenser to the liquid fuel film coolant could be no greater than 1.0 Btu/in.^{2} sec. This heat flux is defined by Equation 23.

$$\phi = \frac{\Sigma_i h_{g_i} A_i (T_{F_i} - T_w)}{A_L} \quad \text{Eq. 23}$$

This maximum heat flux criterion is indicated by the B_2H_6 film cooling test results obtained on Contract NAS 7-659 which show that a nucleate-boiling-like heat transfer mechanism can be maintained in a B_2H_6 liquid film at heat fluxes below 1.0 Btu/in.^{2} sec (Ref. 31). This nucleate-boiling-like mechanism is desirable for maintaining high liquid-film-to-wall heat transfer coefficients and relatively low wall temperatures. High wall temperatures (1000°F or more) and undesirable B_2H_6 decomposition are likely to occur at higher heat fluxes. The Contract NAS 7-659 data were obtained at -110°F inlet temperature and the maximum heat flux may be higher for the lower inlet temperatures (about -240°F) anticipated in an actual space mission. Additional testing is needed to investigate this possibility.

IV, C, Internal Regenerative Cooled Condenser Concept (cont.)

3. Discussion of Results

Some typical heat flux results obtained for an evaporator wall temperature of 1500°F (representative of a sodium heat pipe) are shown as a function of thrust and chamber pressure in Figure 12. The heat flux increases with chamber pressure (for a given thrust) due to the increased heat transfer rates. The effect of chamber pressure is more pronounced for small area ratios. This is because the h_g and T_f values both change with chamber pressure in the chamber-throat-low area ratio region whereas T_f approaches a constant at the larger area ratios and only h_g varies appreciably with pressure. Increased thrust at fixed chamber pressure yields a reduced heat flux due to the corresponding increase in film coolant flow rate.

A cross plot of results such as those in Figure 12 yielded the feasibility chart for internal regenerative cooling, Figure 13. Combinations of thrust and chamber pressure which yield a 1.0 Btu/in.^{2} sec heat flux are indicated by a family of curves with exit area ratio as a parameter. Thrust-chamber pressure combinations to the right of these curves are not feasible because the heat flux is excessive. Similarly F-P_c values to the left of the curves yield an allowable heat flux and are therefore considered feasible. In general, the most favorable conditions exist at low chamber pressure and high thrust.

For the 100 psia chamber pressure and 1000 lb_f thrust operating condition, feasible operation is indicated for a 1.0 exit area ratio but not for exit area ratios greater than 1.0. This does not provide for an acceptable thrust chamber configuration and therefore the concept does not appear applicable to the OF_2/B_2H_6 thrust chamber.

Limited feasibility is indicated for operation at 50 psia chamber pressure and 1000 lb_f thrust, as exit area ratios up to about 2 appear

IV, C, Internal Regenerative Cooled Condenser Concept (cont.)

allowable. This indication, obtained on the basis of energy balance considerations, must be evaluated in light of the liquid length results recently reported in Reference 1.

V. FABRICATION EXPERIMENT

A. PURPOSE

The fabrication experiment consisted of the design, fabrication, and processing of a heat pipe thrust chamber to specifications within the present heat pipe technology. The objective of this work was to evaluate the problems and solutions associated with constructing a heat pipe as an integral part of the thrust chamber. The feasibility of fabricating heat-pipe-cooled thrust chambers was demonstrated by the fabrication and operation of a non-optimized design.

B. CONFIGURATION

The regeneratively cooled concept described in Section V,A was chosen for the fabrication experiment thrust chamber. The basic configuration of the fabrication experiment thrust chamber is shown in Figures 14 and 15. The design consists of an annular, sodium/nickel heat pipe with the contoured inner surface forming at once the evaporator wall and the thrust chamber wall. A regeneratively cooled condenser is located on the outer cylindrical surface. Sodium vapor flows radially from the evaporator to the condenser and liquid sodium returns to the evaporator through radial return disks which are oriented perpendicular to the axis of the thrust chamber. Each feed disk contains holes for vapor communication and for the positioning of axial support rods. The condenser is designed for convective cooling with water or kerosene at a heat throughput rate of 19 Btu/sec (20 kw). The condenser wall includes a thermal resistance annulus in which stagnant argon or helium (or mixtures thereof) may be placed. The aft closure of the fabrication experiment thrust chamber is corrugated to accommodate the difference in thermal expansion between the evaporator and condenser walls.

V, B, Configuration (cont.)

The evaporator wick, condenser wick, and liquid return passages were fabricated from nickel screen. More detailed descriptions of these components are tabulated below.

Component	Description
Evaporator Wick	5 layers of 120 mesh screen, spot welded in place
Liquid Return Passages (Disks)	6 layers of 60 mesh screen, covered on each side by one layer of 120 mesh screen, all 8 layers spot welded together
Condenser Wick	5 layers of 60 mesh screen covered by 4 layers of 120 mesh screen, spot welded together

The fabrication experiment thrust chamber assembly was designed to mate with the OF_2/B_2H_6 injector designed and fabricated by Aerojet on Contract NAS 7-713. The internal thrust chamber contour consists essentially of two conical surfaces and is the same as that used in tests on the Contract NAS 7-713 injector. The nozzle exit plane diameter of 3.64 in. was chosen for optimum expansion to a 13.5 psia back-pressure. The design heat pipe operating temperature is about 1400°F.

Photographs of the fabrication experiment parts and the completed unit are shown in Figures 16 and 17.

The thrust chamber was designed to the evaporator heat flux distribution shown in Figure 18 using the wicking limit criterion. Actual operation at this condition was never intended because of the experimental nature of this fabrication effort. This heat flux distribution is typical of those encountered in a barrier cooled OF_2/B_2H_6 thrust chamber and the maximum heat flux of 2.75 Btu/in.^{2} sec represents the maximum heat flux which had been

V, B, Configuration (cont.)

achieved in a heat pipe (lithium working fluid) at the time the design work was done. The design total heat transfer rate was 150 Btu/sec.

C. ASSEMBLY AND PROCESSING

The fabrication experiment thrust chamber was assembled and processed at RCA. The manufacturing steps and the processing procedure are described in the following two subsections.

1. Fabrication and Assembly

The formation of the various wick sections required extensive tooling to hold the desired geometry. Special circular holding and cutting fixtures were necessary to produce the radial feed wicks. Also, special eyelet draw dies were necessary to produce the vapor passages. A partial display of the tooling required to form the internal wick and eyelet assemblies is shown in Figure 19. The corrugated diaphragm end closure and expansion loop were hydroformed, and the end plates, rocket nozzle, cylinders, etc. were all formed by standard machining techniques.

Figure 16 displays the total collection of parts which went into the formation of the fabrication experiment. The radial wicks are shown as half sections which are made up of six layers of 60 mesh and two layers of 120 mesh. The 120 mesh attached to the evaporator side of the rocket nozzle was formed by cutting the wick into multiple strips and spot welding each to the nozzle in overlapping layers. In this position, five multiple layers of mesh were attached to this surface. This formation may be seen in Figure 20. In a similar fashion, strips of 120 mesh were spot welded in a radial array on both end plates (Figure 20). The assembled wicks and flow passages prior to attachment of the outer cylinder and end closure, are shown in Figure 21.

V, C, Assembly and Processing (cont.)

The radial flow passage was spot welded to an outer circumferential wrap of 120 mesh screen after being spot welded to the evaporator screen. The first outer circumferential screen layer was cut into narrow 3/4 in. wide strips which were spot welded to the flanged sections of wick formed in the outer radial wicks. Second, strips were cut which bridged between adjacent radial sections. These strips were then spot welded. Finally, continuous circumferential layers of wick were spot welded to the encompassed mesh inside. A total of five layers of 120 mesh and four layers of 60 mesh were used to form the condenser wick.

The assembly of the nickel shell parts was accomplished by TIG welding under an argon gas atmosphere. Subassembly welds were heated in vacuum between 700°C (1292°F) and 900°C (1652°F) and re-examined for leaks. In this regard, a great amount of difficulty was experienced in several weld areas. The faults were traced to poor welding gas which contained large amounts of oil, resulting in thermal cracking and forming carbon deposits locally in the welds. Another problem encountered was thermal stress cracking in adjacent welds in the double shell fluid jacket. Repeated thermal cycling and weld repairs were required to produce a leak tight assembly. The final joints between the water shell and the heat pipe portion were made by brazing in a hydrogen furnace using Nioro (950°C) (1742°F) hard solder. It was generally believed that the use of 200 grade nickel for the shell materials added to the difficulty in welding and future materials should be 270 grade nickel which is better controlled and contains lower impurities.

2. Loading and Processing

A photograph of the pressurized sodium loading system used to fill the heat pipe is shown in Figure 22. The system contained a sodium charge pot heating unit and argon tank with pressure regulator. Before

V, C, Assembly and Processing (cont.)

injecting the liquid sodium, the entire heat pipe assembly was baked under vacuum at 700°C for 24 hours to remove dissolved hydrogen from the metal.

A computed value of 1692 cm^3 (103.5 $in.^3$) of wick material is contained in the heat pipe. Assuming a (0.67) void volume and a sodium density of (0.97 grams/cm^3), the required sodium fill was 1099 grams (2.43 lb). Increasing this quantity for processing losses yielded a value of 1550 grams of sodium (2.55 lb) to be transferred from the charge pot. The entire loading system was contained under argon gas. The heat pipe, charge pot and piping were maintained at approximately 200°C (392°F) during the pressurized liquid sodium transfer.

After cooling to room temperature the heat pipe was removed and installed in a large vacuum processing bell. The heat pipe thrust chamber is shown installed in the vacuum bell in Figure 23. The multistranded tungsten radiation heater shown in Figure 24, was suspended within the thrust chamber.

The system was evacuated to a pressure of 7×10^{-7} torr before application of power to the heater. Processing commenced by slowly increasing the heater power to 6.60 kilowatts at which time the temperature profile tabulated below was recorded. (The thermocouple locations are shown in Figure 15.)

V, C, Assembly and Processing (cont.)

Temperature Profile During Processing

T_1 °C	T_2 °C	T_3 °C	T_4 °C	T_5 °C	T_6 °C	T_7 °C	T_8 °C	T_9 °C	System Pressure, Torr
805	806	805	799	817	751	753	623	787	1.8×10^{-5}
Retest after seal-off									
804	816*	802	797	787	750	704*	622	790	4.3×10^{-6}

*Denotes loose thermocouple

This temperature data indicates that the thrust chamber functioned as a heat pipe since the unit was nearly isothermal. A photograph of the heat pipe rocket nozzle taken during the processing operation is shown in Figure 25.

VI. CYLINDRICAL HEAT PIPE TESTS

A. GENERAL

The basic objective of the cylindrical heat pipe tests was to evaluate the maximum heat flux capabilities of high performance wick designs. Tests were conducted on seven evaporator wick configurations using a cylindrical heat pipe test device. The working fluid was sodium in each test and the heat pipe components were fabricated from 200 series nickel. The following wick types were evaluated: multi-layered screen, felt-type metal, screen covered slots, and sintered nickel powder. The maximum test heat flux was 5 Btu/in.^{2} sec and was achieved with a 0.070 in. thick sintered nickel powder wick (Heat Pipe No. 7). The cylindrical heat pipes were designed, fabricated and tested at RCA.

Originally it was planned to also conduct tests on a few lithium and silver heat pipes; however, these additional tests were not conducted due to funding limitations. This does not compromise the near-term application of heat pipe technology to thrust chamber cooling because the required container materials for lithium and silver heat pipes (TZM molybdenum and Ta-5w) are not generally compatible with the OF_2/B_2H_6 propellant system at the required heat pipe operating temperatures.

The following sections contain descriptions of the test apparatus used and the wicks which were tested and discussions of the results which were obtained.

B. TEST APPARATUS

Two types of cylindrical test devices were used to evaluate the heat flux capabilities of sodium heat pipe evaporator wicks. The majority of the testing (Heat Pipes No. 1 through No. 6) was done with the configuration shown in Figures 26 and 27. This device consists of a 1-1/2 in. dia

VI, B, Test Apparatus (cont.)

cylindrical heat pipe with the evaporator wick positioned on one of the circular ends of the cylinder. Heating was produced by the planar electron bombardment heater filament shown in Figure 28. The heater was positioned parallel to the evaporator wall. The condenser was water-cooled and was located on the cylindrical walls of the heat pipe. Liquid condensed on and returned to the evaporator in the condenser-liquid return wick composed of 6 layers of 50 mesh nickel screen which lined the cylindrical walls.

Heat Pipe No. 7 differed from the others in that a non-condensible gas was used to control the sodium vapor pressure. This design is shown in Figure 29. The heater and evaporator wall details were identical to the previously tested heat pipes.

In both configurations the wick to be evaluated was attached to the upper surface of a 0.092-in.-thick nickel disk which formed the circular end of the heat pipe. The disk was made an electrically positive electrode with respect to the filamentary heater, thus forming an equivalent of a vacuum electronic diode. The electron bombardment power supplied to the test wick surface was adjusted by varying the voltage across the electrodes.

The heat flux capabilities of each wick were evaluated using the following test procedure:

1. Pre-heat test device using radiation from filament and low level electron bombardment until device attains 200°C.

2. Increase electron bombardment of test surface to power level of 100 watts/cm^2 (0.61 Btu/$in.^2$ sec) heat flux. Start water cooling of outer coils.

VI, B, Test Apparatus (cont.)

3. Maintain power density until device attains 800°C (1475°F) temperature.

4. Increase power density in increments of 25 watts/cm^2 until sharp inflection is recorded in thermocouples embedded in test surface. Adjust water flow to inner coaxial water coils to maintain heat pipe temperature below 850°C (1560°F).

The heater characteristics were evaluated to determine the area that was actively heated. Since the area subjected to heating is vital to determining input power density, an accurate determination was required. The first method of evaluation employed a 20:1 scale electrostatic field plot of the electrode configuration. The consequent flux lines which intersect the equipotential lines at right angles are plotted in Figure 30. Since at low electron densities the electrons will follow flux lines, the area heated will be encompassed by the outermost flux lines. The diameter of the bombarded surface was determined to be 2.79 cm (1.100 in.). The second method of heated area determination used the transient heating pattern displayed on a heated disk. A molybdenum disk of 0.025 in. thickness was supported from a concentric ring by four 0.060 in. dia wires. The disk was spaced approximately 0.125 in. from the heater-cathode to simulate diode performance. A potential was applied between the electrodes and several amperes of electron current were drawn to the disk. Color photographs of the bombarded surface were simultaneously taken and used to determine the diameter of the heated area. These photographs showed the heated diameter to be 1.13 in. which is in close agreement with the field plot result.

VI, B, Test Apparatus (cont.)

Chromel-alumel thermocouples were used for measurement of the vapor temperature and the heat pipe temperature profile. The thermocouple locations are shown in Figure 26. Eight thermocouples were recorded. Two thermocouples were inserted into radially drilled holes 0.030 in. from the heated surface and 0.062 in. below the wick surface. One thermocouple (T3) was inserted to the center of the 1-1/2 in. dia disk, the second (T2) was inserted 3/8 in. radially from the edge. These thermocouples served to record the radial temperature profile of the evaporator surface. Thermocouples Nos. 1, 4, 5, 6 and 7 were spot welded to the outer heat pipe wall. Thermocouple No. 8 was a sealed jacketed version for measuring vapor temperature and projected into the vapor space just below the water load. The jacket was brazed to the top disk of the heat pipe to provide a hermetic seal. The entire test device was installed in a large vacuum bell jar and evacuated to 1×10^{-6} torr before testing. The thermocouple outputs from the test device were fed to a 24-position, Honeywell Electronick 16 Type K T/C recorder. A photo of the entire test stand with a sodium-nickel test device in position is shown in Figure 31.

Figure 32 shows the test device which was planned for testing with lithium working fluid. This test device is constructed from molybdenum and is somewhat smaller than the sodium design in order to limit the total power through-put to a convenient level. The water cooled load was also modified to include a gas interface between the heat pipe and water cooling jacket. A greater degree of load variation can be achieved for the lithium study by using this configuration. A similar test device would be utilized in tests with the tantalum/silver heat pipes.

VI, Cylindrical Heat Pipe Tests (cont.)

C. TEST RESULTS

The results obtained during the cylindrical heat pipe tests are summarized in this section. The wick configurations tested are listed in Table 2. Pertinent test data are tabulated in Table 3.

1. Heat Pipe No. 1

The evaporator wick of heat pipe No. 1 consisted of five layers of 120 x 120 nickel mesh which were pressed against the evaporator wall, but not sintered. Testing was done with the heat pipe oriented vertically (evaporator horizontal). The test results indicated thermal runaway[1] when the heat flux was 0.73 Btu/in.^{2}-sec (120 watts/cm^2). Testing was terminated at this level due to a temperature gradient across the evaporator as shown in the following sketch. (The temperature Tl is approximately equal to the heat pipe temperature.)

Heat Pipe No. 1
Vertical Position

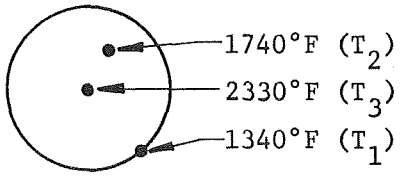

Posttest X-ray photographs and subsequent disassembly showed that the wick had bowed away from the evaporator wall into a dome-shaped geometry (1/8 in. maximum deflection). Thus, thermal contact between the wick and wall was lost and this resulted in loss of local fluid inventory and in thermal runaway. A cross-section view of the evaporator in posttest condition is shown in Figure 33.

1 Thermal runaway was evidenced by a rapid increase in evaporator wall temperature at a fixed input power level. This is indicative of a degradation in the heat pipe mechanism.

VI, C, Test Results (cont.)

2. Heat Pipe No. 2

The second sodium/nickel heat pipe contained a nickel felt type metal (FM-1205 Huyck Metal Co.) evaporator wick. An electron scan photograph of this material is shown in Figure 34. Initial testing on this unit was done with the heat pipe in a vertical position. A heat flux of 1.85 Btu/in.^{2}-sec (304 watts/cm^2) was achieved before excessively high wall temperatures occurred. The temperature profile of the evaporator at maximum heat flux for the vertical position is shown below.

Heat Pipe No. 2
Vertical Position

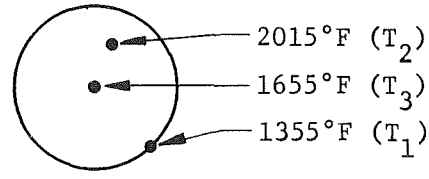

The feltmetal material was sintered to the evaporator end-cap to prevent bowing during thermal cycling. However, due to the dendritic structure of the feltmetal, positive sintering at all locations could not be assured. While X-ray analysis did not verify that the feltmetal pulled away from the evaporator end-cap in the area of maximum temperature, it is believed that this condition may have occurred.

A 58% higher heat flux was achieved when the No. 2 heat pipe was tested in the horizontal position. The maximum heat flux was 3.18 Btu/in.^{2}-sec. The temperature profile measured during the horizontal test showed a thermal gradient similar to the results obtained when tested in the vertical position. The horizontal test temperature profile at maximum heat flux is shown below.

VI, C, Test Results (cont.)

Heat Pipe No. 2
Horizontal Position

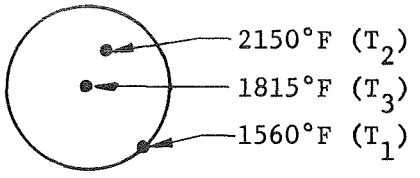

The radial temperature gradient of device No. 2 was evident at the start of testing (low heat flux) and increased in direct proportion to the increasing heat input. It is important to note however, that thermal runaway never occurred in this device. It is also possible that non-uniform flow characteristics caused the temperature at the center of the evaporator to be lower than the temperature of the evaporator nearer the outer diameter.

3. Heat Pipe No. 3

The third sodium/nickel heat pipe contained an evaporator wick which consisted of a composite screen structure. One layer of 50 x 50 mesh was spot welded to form intimate contact with the evaporator wall, and two layers of 120 x 120 mesh were spot welded over the top. Total evaporator wick thickness was approximately 0.032 in. An edge view of this wick is shown in Figure 35. Testing in the vertical position was conducted to a heat flux of 1.48 Btu/in.^{2}-sec (242 watt/cm^2). The test was terminated due to apparent incipience of a wall temperature excursion. Similar behavior was observed when testing in the horizontal position at a heat flux of 2.26 Btu/in.^{2}-sec (371 watt/cm^2). In both cases the heat pipe operating temperature (the vapor temperature) was about 1450°F.

4. Heat Pipe No. 4

Heat Pipe No. 4 employed a cross-channel evaporator wick design. The channels were 0.042 in. wide and 0.028-in. deep and covered with three layers of 320 x 320 screen mesh spot-welded to the channel lands as

VI, C, Test Results (cont.)

shown in Figures 36 and 37. The unit was tested in a horizontal position. A heat flux of 1.5 Btu/in.^{2}-sec (246 watts/cm^2) was achieved at a heat pipe temperature of 1650°F before thermal runaway became apparent. A temperature gradient of approximately 360°F was observed in the condenser area of the heat pipe thereby indicating that a high gas content was trapped within the pipe. This trapped gas does not appear to have influenced the operation of the wick but did produce a relatively high heat pipe temperature. Examination of the unit showed that the evaporator had bowed outward approximately 0.060-in.

5. Heat Pipe No. 5

Heat Pipe No. 5 contained a 0.041 in. thick sintered nickel powder evaporator wick structure. An electron-scan microscope photograph of this wick material appears in Figure 38. Figure 39 is a photograph of the Heat Pipe No. 5 wick sintered to the evaporative wick surface. The wick was sintered in place on the evaporator wall which was then welded in place on the end of the heat pipe.

The design of the test device was modified for the No. 5 heat pipe (and subsequently the No. 6 and No. 7 heat pipes) to include a fluid return wick structure consisting of eight layers of 120 mesh screen instead of the 6 layers of 50 mesh screen utilized on heat pipes 1, 2, 3 and 4. This change was made as an aid to fluid retention in the vertical position. In addition, the processing procedure was modified to include a wet hydrogen (approximately 100 ppm H_2O) firing of the nickel heat pipe components. This procedure was added to decarburize the nickel components to aid welding. Weld leak problems were encountered during testing of Heat Pipes Nos. 2, 3, and 4 due to residual carbon content in the grade "A" nickel used for the heat pipe components.

VI, C, Test Results (cont.)

The maximum heat fluxes achieved with this sintered nickel powder wick were 2.27 Btu/in.^{2}-sec and 3.96 Btu/in.^{2}-sec in the vertical and horizontal positions respectively. Evidence of a thermal runaway was seen at both of these heat flux levels. The temperature profile of the evaporator at maximum heat flux is shown below.

Heat Pipe No. 5
Horizontal Position

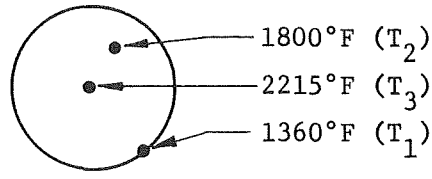

Tests to evaluate startup characteristics were also conducted on heat pipe No. 5. In these tests, a step input heat flux was applied to the evaporator and the evaporator wall temperature response was recorded. Successful startups were achieved at heat fluxes up to 60% of the maximum steady-state heat flux, i.e., up to 2.4 Btu/in.^{2}-sec heat flux, when the sodium was initially liquid at about 210°F. A thermal runaway occurred at the 75% heat flux level (3 Btu/in.^{2}-sec). A similar test was conducted with the sodium initially solid and a thermal runaway occurred at a 10% heat flux level (0.4 Btu/in.^{2}-sec). These startup results are considered qualitative only since the cylindrical heat pipe test device was not designed for transient operation.

6. Heat Pipe No. 6

Heat Pipe No. 6 contained a composite type evaporator wick which consisted of small channels machined into the evaporator wall and covered with a 0.025 in. thick prefabricated sintered nickel powder overlay. The overlay was sintered to the channel lands. The wick is shown in Figures 40 and 41. The substrate channels were 0.005 in. deep, 0.010 in. wide with a 0.010 in. spacing between channels. This heat pipe was tested in the

VI, C, Test Results (cont.)

horizontal position and the maximum heat flux obtained was 1.6 Btu/in.^{2}-sec (262 watts/cm^2). This result is about the same as that obtained with heat pipe No. 4 which contained larger channels covered by a fine pore screen. Neither device approached the values obtained with the isotropic wick forms used in heat pipe No. 2 and heat pipe No. 5. The power limitation was not believed to be due to excessive pressure loss in the channel, but rather the formation of a vapor pocket in the channel.

7. Heat Pipe No. 7

The relatively high heat flux results obtained with the sintered nickel powder wick on Heat Pipe No. 5 prompted further testing with this wick material. Observations and analyses tended to indicate the limiting factor of this particular wick structure was fluid flow; therefore, the wick thickness was increased to 0.070 in. to promote increased fluid flow. The heat pipe No. 7 configuration was different from that utilized previously in that a non-condensible gas (argon) was used to control the sodium vapor pressure (this "gas-loaded" design is illustrated in Figure 29).

One other major difference distinguished heat pipe No. 7 from heat pipe No. 5 and this was the manner in which the wick was installed on the evaporator wall. On heat pipe No. 7, the wick was sintered in place after the evaporator wall (the end cap) had been welded into the cylindrical heat pipe body and the return wick had been installed. Heat pipe No. 5 was assembled by sintering the wick onto the end cap and then welding the end cap - evaporator wick assembly to the cylindrical body - return wick assembly.

Heat pipe No. 7 was tested in the horizontal position and the highest evaporator heat flux tested on this program was achieved. An average

VI, C, Test Results (cont.)

heat flux of 4.94 Btu/in.^{2}-sec was reached at a heat pipe temperature of 1100°F. The evaporator temperature distribution at this heat flux level is sketched below.

Heat Pipe No. 7
Horizontal Position

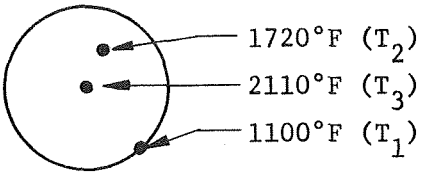

Attempts to increase the heat flux beyond this point were unsuccessful as a very rapid temperature excursion developed which produced burnout of the evaporator wall as shown in Figure 42.

D. DISCUSSION OF RESULTS

1. Wick Design Evaluation

Examination of the maximum heat flux data obtained, summarized in Table 4, reveals that the highest heat fluxes were achieved with sintered nickel powder evaporator wicks (Heat Pipe No. 7 - 4.94 Btu/in.^{2}-sec heat flux, Heat Pipe No. 5 - 3.95 Btu/in.^{2}-sec heat flux). This type of design therefore appears the most promising for future work and will be emphasized in the following discussions of this section.

The experimental study reported here does not eliminate the other wicks tested for future applications in high heat flux heat pipes. The objective of this program is to apply heat pipe technology to thrust chamber cooling on a relatively near-term basis and therefore the obvious choice for further work is the wick design in which maximum performance has been obtained. Future work in which alternate fabrication methods and design

VI, D, Discussion of Results (cont.)

improvements are developed for the other wick types tested may ultimately show that they can perform as well as the sintered nickel powder.

2. Vertical vs Horizontal Operation

Heat Pipes No. 2, 3, 4 and 5 were tested with the cylindrical heat pipe body in a horizontal (evaporator wick vertical) and vertical (evaporator wick horizontal) orientation. The maximum heat fluxes in the horizontal position were significantly higher than in the vertical position. This is believed to be the result of "pooling" of excess sodium on top of the evaporator wick due to the influence of gravity. The vertical results are therefore considered invalid. This pooling phenomenon is not a problem for a heat pipe thrust chamber due to the annular geometry and any "pooling" would occur only on the condenser wick.

3. Wall Temperature Distributions

The measured wall temperature distributions tend to be somewhat erratic and this is believed due to, in most cases, inadequate thermal contact between the evaporator wall and wick. The high wall temperatures measured on Heat Pipes No. 5 and No. 7 are of particular interest since these units contained the sintered nickel powder wicks which appear attractive for future application.

Consequently, a heat transfer analysis of the evaporator region of cylindrical Heat Pipes No. 5 and No. 7 was performed. The analysis was conducted using a two-dimensional conduction network which was solved utilizing the SINDA-3G (32) computer program. Evaporator wall temperature distributions were obtained for heat fluxes in the range of 1 - 5 Btu/in.^{2} sec. The heat flux distribution calculated from heater calibration test data taken

VI, D, Discussion of Results (cont.)

at RCA was assumed. This distribution is shown on Figure 43. The node network which was utilized is shown in Figure 44. The analysis was performed by considering conduction effects (within the nickel walls and the sodium working fluid) and the radially inward heat convection by the liquid sodium. The temperature of the working fluid and wick were assumed equal at all points.

Temperature distributions calculated for Heat Pipes No. 7 and No. 5 at the maximum heat flux condition are shown as Figures 45 and 46. The measured wall temperature are compared to the predictions in Figures 47 and 48. Temperatures calculated for the evaporator midpoint (T3) and 1/2 way between the midpoint and the outer edge of the wall (T2) at a distance of 0.030 in. into the wall are compared to thermocouple data obtained at these points. For Heat Pipe No. 7, the agreement between calculated and measured temperatures is considered good. The T2 values are somewhat lower than calculated and this is probably due to the water cooling close to the evaporator wall which was not considered in the analysis. The beginning of a wall temperature excursion is apparent at the maximum heat flux.

The Heat Pipe No. 5 data indicate that the evaporator midpoint temperature was about 250°F higher than calculated at the maximum heat flux of 4 Btu/in.^{2}-sec. Analyses were performed with and without the sodium convection effects and the calculated wall temperatures agreed within 1°F at the evaporator midpoint. Therefore, the high wall temperatures do not appear attributable to sodium convection effects. A conservative estimate of the possible measurements errors due to two-dimensional conduction effects around the thermocouple and due to placement of the junction was made and the estimate is also shown in Figure 48. A maximum possible error of 100°F was estimated at the maximum heat flux (about 4 Btu/in.^{2}-sec) and this is not sufficient to explain the high wall temperatures.

VI, D, Discussion of Results (cont.)

It is therefore concluded that the high wall temperatures measured on Heat Pipe No. 5 were not the result of normal conduction or convection effects, or due to thermocouple error. Other possible causes of the high temperatures are irregular liquid return flow from the return wick, and locally poor thermal contact between the wick and the evaporator wall.

4. Heat Flux Limits - Sintered Powder Nickel Wicks

Two different types of heat flux limits may have been encountered with the sintered nickel powder wicks in Heat Pipes No. 5 and No. 7. This is indicated by wicking limit or dryout calculations (see Sections III,B and III,D,1) and by comparing the maximum sodium superheat calculated for each test to the incipient boiling superheat predicted by the Holtz model (see Section III,D,4).

The results of wicking limit calculations are shown in Table 4. For the maximum heat flux condition of Heat Pipe No. 5 the calculated system pressure losses are approximately equal to the maximum available pumping pressure due to capillary action. These results therefore indicate that a wicking limit was encountered in the testing of Heat Pipe No. 5.

The wicking limit calculations also indicate that a dryout condition was approached and possibly occurred with Heat Pipe No. 7. The calculated pressure drop for the maximum heat flux condition is about 83% of the maximum available pumping pressure. However, the much more rapid temperature excursion and the rather localized wall burnout suggest that a different limiting mechanism may have been encountered. Burnouts of this type are common in boiling heat transfer tests and, therefore, it seems possible that a boiling limit was achieved with Heat Pipe No. 7. This possibility is also indicated by the fact that the maximum calculated superheat (500°F) compares

VI, D, Discussion of Results (cont.)

well with the prediction for incipient boiling superheat from the Holtz model as shown in Figure 3. (The prediction depends on heat pipe temperature and the maximum previous system pressure. The maximum processing temperature for Heat Pipes No. 5 and No. 7 was about 835°C and this corresponds to a pressure of 0.62 atm.) However, comparison of the maximum superheat to the Holtz model prediction does not appear to uniquely characterize the Heat Pipe No. 7 result as a boiling limit because the maximum superheat for Heat Pipe No. 5 also compares reasonably well with the prediction (Figure 3).

VII. PRELIMINARY THRUST CHAMBER DESIGN ANALYSIS

This section contains the preliminary design analysis results which are considered tentative and are subject to change based on the results of future work.

A. CONCEPT FOR THE WORKING MODEL DESIGN

A sodium/nickel heat pipe thrust chamber with a condenser that is regeneratively cooled by propellants was chosen as the working model design concept. Detailed design and fabrication are planned as future work. It is anticipated that the general configuration will be similar to the fabrication experiment, with a cylindrical cooling jacket surrounding an annular heat pipe. The internal thrust chamber contour is shown in Figure 49 (Reference: JPL Drawing 10022109), and the design operating conditions are summarized in Table 6. The design will incorporate an auxiliary heater for preheating the heat pipe to its operating temperature.

The final evaporator wick configuration has not been chosen; however, a sintered nickel powder wick has been recommended by RCA and this type of design will probably be utilized. It is possible that the heat pipe design will include a combination of this wick structure and the type of liquid return passages developed recently at Aerojet on an IR&D test program.

B. BOUNDARY COOLING

Boundary cooling may be desirable for reducing the thrust chamber heat flux levels and application of this auxiliary cooling technique will be considered to the extent that performance considerations allow. A 92% c* performance level is desired. The utilization of boundary cooling produces a mixture ratio distribution loss (MRDL). This loss was estimated for the OF_2/B_2H_6 engine and is shown in Figure 50. The MRDL must be added to the

VII, B, Boundary Cooling (cont.)

energy release loss (ERL) associated with the injector. A 2% ERL is believed achievable; therefore, the boundary cooling conditions for 6% MRDL loss, tabulated below, are considered to represent the allowable boundary cooling conditions.

Boundary Coolant MR	Allowable Flow Rate, % of Total Flow Rate
0	10 (40% of the fuel flow rate)
0.5	19
1.0	28

Barrier cooling (boundary coolant MR > 0) is currently preferred over fuel film cooling (boundary MR = 0) for the heat-pipe-cooled thrust chamber because it has been used more frequently and more successfully than film cooling in OF_2/B_2H_6 systems. A disadvantage is that wall deposits have been observed in low MR barrier flows and these deposits can produce undesirable injector characteristics. However, wall deposits may also be obtained with fuel film cooling. Data obtained in previous laboratory and hot firing tests (Ref 31) have indicated that B_2H_6 is an acceptable film coolant if sufficient wall coverage is maintained, but the lab tests also showed that decomposition occurs and boron deposits begin to form at wall temperatures greater than 1000°F. Wall temperatures greater than 1000°F are expected in the evaporator section of a film cooled sodium heat pipe thrust chamber.

C. GAS SIDE HEAT TRANSFER ANALYSIS

Local heat flux values were estimated for the working model design thrust chamber operating at the following conditions: (1) no barrier cooling, (2) 28% barrier cooling flow at barrier MR = 1.0, and (3) 19% barrier cooling flow at barrier MR = 0.5. The heat fluxes were calculated from the usual convection relationship, shown as Equation 24.

VII, C, Gas Side Heat Transfer Analysis (cont.)

$$q/A = h_g (T_{aw} - T_w) \qquad \text{Eq 24}$$

For the no-barrier-cooling case, the adiabatic wall temperature, T_{aw}, was assumed equal to 98% of the theoretical combustion temperature. Adiabatic wall temperature values with barrier cooling were estimated using the entrainment model for gas film cooling developed at Aerojet by R. L. Ewen (Ref 31). Heat transfer coefficients, h_g, were calculated from the simplified correlation described in Appendix B. The modified form which accounts for the increased mass velocity in the barrier flow stream was used for the barrier cooled cases. The h_g and T_{aw} values are shown in Figure 51.

Heat flux distributions calculated for an 1800°F wall temperature are also shown in Figure 51. The maximum heat fluxes are 6.1 Btu/in.^{2} sec for no barrier cooling, 5.2 Btu/in.^{2} sec for 28% barrier cooling at MR = 1.0, and 4.3 Btu/in.^{2} sec for 19% barrier cooling at MR = 0.5. The indicated total heat transfer rates range from 650 Btu/sec (no barrier cooling) to 430 Btu/sec (0.5 MR barrier cooling). It was further estimated that maximum heat flux can be decreased to about 3.7 Btu/in.^{2} sec (but no lower) with 0.5 MR barrier cooling by increasing the barrier flow rate to the 25-30% range. However, barrier flow rates greater than 19% will degrade performance below the desired level.

D. CHOICE OF COOLANT AND INJECTOR TYPE

The choice of condenser coolant and injector type are interrelated because the thrust chamber heat load is sufficient to produce vaporization of the propellant. This is demonstrated in Table 7 which shows coolant outlet temperature and the required injector type for various cooling cycles with no barrier cooling and with 0.5 MR barrier cooling.

VII, D, Choice of Coolant and Injector Type (cont.)

The Table 7 results show that fuel cooling is not feasible if the thrust chamber is not barrier cooled because the 905°F outlet temperature is sufficiently high that chemical decomposition is possible. Oxidizer cooling is feasible but the relatively high outlet temperature (865°F) tends to complicate the condenser design due to the small temperature difference from heat pipe to condenser coolant near the coolant outlet. A gas/liquid injector is required in this case. Condenser cooling with both propellants is preferred for the thrust chamber with no barrier cooling. Condenser cooling could be accomplished with the total flow rates (210°F outlet temperature), or a portion of each flow rate down to about 80% (425°F outlet temperature). A gas/gas or gas/gas + liquid/liquid injector would be required.

For the 0.5 MR barrier cooled case, the total or core oxidizer flows or the total fuel flow could be utilized as coolants and a gas/liquid injector would be required. Two phase flow may be difficult to avoid if both the total oxidizer and fuel flow rates are used for condenser cooling. An acceptable alternate scheme is cooling with the core oxidizer and fuel flows and utilizing a gas/gas + liquid/liquid injector.

E. CONDENSER DESIGN

1. Design Approach

Coolant side heat transfer in a cooling system where a complete change in phase occurs can be quite complex. The propellant cooled condenser of the heat pipe thrust chamber will operate in this manner, with subcooled liquid entering at the inlet and superheated vapor leaving at the outlet. This type of operation is termed the "once-through" problem in the literature (Ref 33), and some experimental work has been done in this area (Ref 34). Three regimes of convective heat transfer will be encountered and

VII, E, Condenser Design (cont.)

a total of seven mechanisms are believed possible. Furthermore, it is felt that these mechanisms are inter-related as shown schematically in Figure 52.

In a purely regenerative cooled thrust chamber with OF_2/B_2H_6 propellants, all of the possible mechanisms should be considered in designing the coolant passage because the heat fluxes are high and the local coolant side heat transfer coefficient is the major parameter controlling local wall temperature. The coolant passage design in a heat pipe thrust chamber is not so dependent on local coolant side heat transfer coefficient for the following reasons:

(1) the wall thermal resistance in the heat pipe condenser tends to be larger in proportion to the total coolant jacket thermal resistance than in a conventional regeneratively cooled system. The effect of variations in coolant side heat transfer coefficient on local heat flux are therefore reduced.

(2) Locally excessive wall temperature problems cannot be encountered in the cooling jacket since the maximum possible cooling jacket temperature is the heat pipe temperature regardless of the local coolant heat transfer coefficient value. (The heat pipe temperature is controlled by the overall condenser thermal resistance and the coolant bulk temperature).

(3) The relatively low cooling jacket heat fluxes are conducive to the utilization of two-dimensional wall conduction effects. Through proper design, these effects can provide a further reduction in the heat flux transmitted to the coolant and consequently a lower coolant side heat transfer coefficient can be accommodated.

VII, E, Condenser Design (cont.)

Significant amounts of liquid forced convection or nucleate boiling are not expected to occur in the cooling jacket since the peak nucleate boiling heat flux of both propellants is estimated to be relatively low. Therefore, it is believed that an adequate cooling passage design can be established by assuming that film boiling occurs in the liquid and two phase regions. The coolant passage design would then be based on film boiling and gaseous convection heat transfer coefficients.

Film boiling heat transfer coefficients can be estimated from one of the correlations developed for hydrogen (Ref 35), such as Equation 25, and gaseous convection can be described with the more standard turbulent convection correlation, Equation 26.

$$\frac{Nu}{Nu_{calc,\ v,\ s.p.}} = f(\chi) \qquad \text{Eq 25}$$

where:

$$Nu_{calc} = 0.026\ Re_{v,\ s.p.}^{0.8}\ Pr_{v}^{0.33}\ \left(\frac{\mu_v}{\mu_w}\right)^{0.14}$$

$$f(\chi) = \exp(-0.185 - 0.251\ \ln \chi - 0.00767\ (\ln \chi)^2)$$

$$Nu_b = 0.023\ Re_b^{0.8}\ Pr_b^{0.4} \qquad \text{Eq 26}$$

2. Design Concept

Preliminary design analyses have been performed for an OF_2 (or FLOX) cooled condenser assuming 19% barrier cooling at 0.5 MR. These analyses indicate that mass fluxes in the range of 1-4 lb/sec in.^{2} will be required within the coolant channels. This requirement yields relatively small

VII, E, Condenser Design (cont.)

flow areas; therefore, helical coolant channels which spiral around the condenser from the aft to the forward end appear appropriate. However, a constant area channel is not desirable because the mass fluxes required to provide adequate cooling in the liquid and low quality regions produce excessively high vapor velocities near the cooling jacket outlet. It appears that this problem can be alleviated by employing a variable area channel such as that shown in Figure 53. In this particular design the helical coolant channel is machined into a copper ring. A nickel ring attached to the inside diameter of the copper ring provides the desired wall thermal resistance. The coolant flows in three parallel passages when it is liquid and in the low quality 2-phase state. The lands between the channels act as cooling fins. As the gaseous state is approached, the channel is expanded by removing the two inner copper lands. The wall fin effect is reduced but this is compensated for by a higher coolant heat transfer coefficient (compared to the low quality region) due to the increased velocity.

F. COLD START DESIGN CONCEPT

One of the more significant problems to be faced in designing a flight type heat-pipe-cooled rocket engine is that of startup. Ideally, the engine should be able to start in space without requiring preheating or some sort of pilot burn to thaw the working fluid and bring the pipe to operating temperature. In this section, a heat pipe design concept will be discussed which appears capable of operating in this manner.

For the purposes of this discussion, it will be assumed that the heat-pipe-cooled rocket engine consists of a sodium/nickel heat pipe chamber and nozzle with a propellant-cooled heat pipe condenser. Furthermore, it will be assumed that the heat pipe will be in a frozen condition (i.e., at temperatures below the sodium melting temperature of 208°F) prior to ignition.

VII, F, Cold Start Design Concept (cont.)

1. Failure Modes

There exist two readily identified modes of failure which can occur in the rapid startup of a frozen, high flux heat pipe. The first is evaporator wick dryout resulting from only partial thawing of the heat pipe. Immediately following ignition, the incident heat produces very rapid melting and evaporation of the sodium in the evaporator wick. With high flux heat pipes, thin evaporator wicks are required and consequently the initial charge of sodium in the evaporator wick is small and probably insufficient to thaw the remainder of the pipe. If the remainder of the pipe stays frozen, no sodium is able to return to the evaporator to replace that which has vaporized and the evaporator overheats and burns out.

The second failure mode is somewhat more complex and can be encountered with a fully thawed heat pipe. The problem is encountered when the heat pipe is below its operating temperature, and the low temperature liquid sodium in the evaporator is subjected to high heat fluxes. As discussed previously, heat pipe operation can be limited by sonic vapor flow at low temperatures (see Section III,D). In addition, a limit due to evaporation kinetics may also be encountered. The calculations of Reiss and Schretzmann indicate that for sodium the kinetics limit is more severe than the sonic limit as shown in Figure 54 (Ref 25).

Consequently, at low temperatures it is possible for the incident heat flux to exceed the ability of the wick to dissipate it by evaporation. This, of itself, does not result directly in burnout, as the stored heat [(incident heat) - (heat leaving by evaporation and conduction) = (stored heat)] goes into raising the evaporator temperature and this temperature will increase until the point is reached at which the evaporation rate is sufficient to accommodate the incoming heat transfer rate. However, the

VII, F, Cold Start Design Concept (cont.)

high flux part of the evaporator can be driven to a temperature above that of the remainder of the heat pipe. As a result, the superheat of the sodium in the hot part of the evaporator can become excessive and boiling and burnout are likely to occur.

The design concept which appears capable of overcoming the startup problem consists of a noncondensible gas loaded heat pipe with special auxiliary rapid thawing capillary structures. A schematic drawing of the concept is shown in Figure 55. This figure shows a cross section of a heat-pipe-cooled rocket engine containing radial condensate return capillaries and an inert gas reservoir. This concept is intended to provide for progressive thawing of the heat pipe under full thermal load while simultaneously maintaining sufficient pressure in the pipe to avoid a film boiling type burnout. Aside from the gas loading, the feature which makes this concept function is the capillary structure attached to the exterior of the radial condensate return capillaries. This capillary structure, which will be called the startup reservoir, has a greater capillary diameter than the evaporator and has a gradation in capillary size going from the free surface down into the reservoir. If, for example, the evaporator wick were to consist of two layers of 200-mesh screen, then the capillary on the side of the radial feeders might be two layers of 100-mesh screen covered with a layer of 75-mesh screen. The startup reservoir is not in "capillary contact" with the radial feeder capillaries; that is, an impervious surface separates the startup reservoir from the radial feeder capillaries. When the heat pipe is charged, sufficient sodium should be placed in it to completely fill the capillary structure.

At the time the rocket engine is started, the entire startup reservoir is filled with solid sodium and the insert gas fills the vapor flow area. After ignition, the heat coming into the evaporator thaws the sodium in the evaporator wick and then begins to evaporate it. The sodium vapor

VII, F, Cold Start Design Concept (cont.)

which is generated is restricted by the inert gas from immediately flowing throughout the entire chamber and begins condensing on the cold solid sodium in the startup reservoir next to the evaporator wick. The condensing sodium will immediately thaw the solid sodium, as each unit which condenses will thaw approximately 30 times its weight of solid sodium. The molten sodium now present in the reservoir will flow to the evaporator because of the smaller capillary diameter of the evaporator wick, thereby replenishing the evaporator. As the portion of the startup reservoir closest to the evaporator is heated, the evaporator temperature will rise, the sodium vapor pressure will increase, and the sodium vapor cloud will expand, pushing back the inert gas and exposing more of the solid sodium in the reservoir to the hot sodium vapor. This process will continue until all of the reservoir is exposed and melted. At that time, the heat pipe operating temperature will rise to the point at which the noncondensible gas is driven out of the heat pipe into the gas bottle and the condenser is exposed to the sodium vapor. The quantity of sodium available for condensing on and thawing the condenser is now quite large and the condenser should thaw with no difficulty. Once the condenser is thawed, the heat pipe will be in its normal operating mode.

The size of the gas reservoir which must be carried along with the heat pipe is not very large. If, for example, the heat pipe has a steady state operating temperature of 1350°F and it is desired to start operation (i.e., have sodium vapor pressure - inert gas pressure) at 1100°F, then the gas reservoir would require a volume about 1/4 to 1/5 the vapor volume of the heat pipe. For the designs under consideration, this would be approximately a 7-in. diameter spherical, extremely low pressure (1 psia maximum pressure) gas bottle.

It is recognized that the foregoing discussion does not cover all the details of the concept. However, it is thought that this general approach can be applied to flightweight designs to yield a completely passive heat pipe system which may not require a special start sequence.

VIII. CONCLUSIONS AND RECOMMENDATIONS

1. The existing heat pipe technology was reviewed and it was found that the literature is extensive. Certain operating limits of heat pipes have been investigated experimentally and analytically; however, the evaporator boiling limit has not been well established and research in this area is recommended.

2. The major design considerations for heat-pipe-cooled thrust chamber are: (1) choice of working fluid and container material, (2) method of condenser of cooling, (3) allowable heat flux levels, (4) fabrication capabilities, (5) physical size and total heat transfer rate, (6) startup procedure, and (7) acceleration and vibration effects.

3. The sodium (working fluid) and nickel (container material) heat pipe system was chosen for the working model OF_2/B_2H_6 thrust chamber design which will be designed and fabricated on a future program. The sodium/nickel combination has been utilized extensively in the heat pipe field and nickel has been successfully employed in OF_2/B_2H_6 engines. Lithium and silver are also potential working fluids for heat pipe thrust chambers; however, their near-term application is hindered by a lack of demonstrated chemical compatibility between the required container materials and the propellants and combustion gases.

4. Three design concepts for heat-pipe-cooled thrust chambers were established which are characterized by the following condenser cooling techniques: regenerative cooling, radiation cooling, and internal-regenerative cooling. The regeneratively cooled concept was found to be feasible for a sodium/nickel heat pipe thrust chamber operating with OF_2 and B_2H_6 propellants at 3.0 mixture ratio, 100 psia chamber pressure, and 1000 lb thrust. The regeneratively cooled concept was chosen for the working model design.

VIII, Conclusions and Recommendations (cont.)

5. Evaporator heat flux limits had not been investigated extensively prior to this program. A cylindrical heat pipe test device was designed, fabricated, and tested on this program and was found to be a valuable tool for investigating evaporator heat flux limits. With this device the heat flux capability of sodium heat pipes was extended to 5 Btu/in.^{2}sec. This represents a significant advancement in the state-of-the-art of heat pipes; however, more testing is recommended to further extend this capability since a 6 - 8 Btu/in.^{2}sec heat flux limit is desirable for the working model design.

6. The feasibility of fabricating heat-pipe-cooled thrust chambers was demonstrated by the fabrication of an unoptimized sodium/nickel thrust chamber design. This "fabrication experiment" thrust chamber was processed and tested and was found to function as a heat pipe.

7. Additional work is also recommended to investigate transient heat pipe operation and to further evaluate rapid startup designs and procedures.

REFERENCES

1. Riebling, R. W., and Others, "A Survey of the Current Status of Thrust Chamber Technology for Oxygen Difluorine/Diborane Propellants", Paper No. 70-717, presented at AIAA 6th Propulsion Joint Specialist Conference, San Diego, California, 15-19 June 1970.

2. Cheung, H., A Critical Review of Heat Pipe Theory and Applications, Lawrence Radiation Laboratory, Livermore, California UCRL 50453, July 1968.

3. Eastman, G. Y., "The Heat Pipe", Scientific American, 38-46, May 1968.

4. Feldman, K. T., and Whiting, G. H., "The Heat Pipe", Mechanical Engineering, Vol. 89, No. 2, 30-33, February 1967.

5. Grover, G. M., and Others, "Structures of Very High Thermal Conductance", J. of Applied Physics, Vol. 35, 1990-1991, June 1964.

6. Cotter, T. P., Theory of Heat Pipes, Contract W-7405-ENG-36, Los Alamos Scientific Laboratory, Los Alamos, New Mexico, Report AED LA-3246-MS.

7. Cotter, T. P., "Heat Pipe Startup Dynamics", Thermionic Conversion Specialist Conference (IEEE), Palo Alto, California, October 1967 344-348, LA-DC-9026, (STAR N68-28359).

8. Kemme, J. E., Heat Pipe Capability Experiments, Los Alamos Scientific Laboratory, Los Alamos, New Mexico, Report LA-3585-MS, October 1966.

9. Kemme, J. E., High Performance Heat Pipes, Los Alamos Scientific Laboratory, Los Alamos, New Mexico, LA-DC-9027, October 1967.

10. Kemme, J. E., "Ultimate Heat Pipe Performance", Thermionic Conversion Specialist Conference (IEEE), Framingham, Massachusetts, October 1968.

11. Stephanou, S. E., and Others, "Application of Heat Pipe Technology to Rocket Engine Cooling", Paper No. 69-582, AIAA 5th Propulsion Joint Specialist Conference, Colorado Springs, Colo. (1969).

12. Bromberg, R., and Others, Method of and Means for Cooling the Throat Wall of Rocket Engine Nozzle, U.S. Patent 3,493,177; 3 February 1970.

13. Cosgrove, J. H. Engineering Design of a Heat Pipe, Ph.D. Thesis, North Carolina State University, 1966, (STAR:N68-29703).

14. Haskin, W. L., Cryogenic Heat Pipe, Flight Dynamics Lab, Wright-Patterson AFB, Dayton, Ohio, Report AFFDL-TR-66-228, June 1967. AD-657-025.

REFERENCES (cont.)

15. Schlapbach, M. E., Survey of Heat Pipes, Boeing Company, Huntsville, Alabama Report No. D5-13432, February 1968, AD-838 675L.

16. Feldman, K. T., Heat Pipe Analysis, Design, and Experiments, Scott-Engineering Sciences, Pompano Beach, Florida, Publication No. 9068, December 1968.

17. Kemme, J. E., Heat Pipe Design Considerations, LA-4221-MS, Los Alamos Scientific Laboratory, Los Alamos, New Mexico, 1 August 1969.

18. Vennard, J. K., Elementary Fluid Mechanics, 3rd Edition; John Wiley and Sons, New York, New York

19. Levy, E. K., "Theoretical Investigation of Heat Pipes Operating at Low Vapor Pressures," ASME Trans., Vol. 90B, No. 4, 547-552, November 1968.

20. Deverall, J. E., and Others, High Thermal Conductance Devices Utilizing the Boiling of Lithium or Silver, University of California Los Alamos, New Mexico, LA-3211, October 1964.

21. Schwartz, J., The Heat Pipe and Its Operation, Jet Propulsion Laboratory Pasadena, California, Report 701-21, January 1969.

22. Heat-Pipe Design Manual, Martin-Marietta Corporation, Baltimore, Maryland Nuclear Report AEC MND-3288, February 1967 (NEA:2268).

23. Marto, P. J. and Rohsenow, W. M., "Effects of Surface Conditions on Nucleate Pool Boiling of Sodium", Trans of ASME, Vol. 88C, 196-204, May 1966.

24. Edwards, J. A., and Hoffman, H. W., "Superheat with Boiling Alkali Metals", Proc. Conf. Appl. of High Temperature Instrumentation to Liquid Metal Experiments, AEC Res. and Dev. Report ANL-7100, September 1965.

25. Holtz, R. E., Effects of Pressure - Temperature History Upon Incipient Boiling Superheats in Liquid Metals, Argonne National Laboratory, ANL-7184, June 1966.

26. Chen, J. E., "Incipient Boiling Superheats in Liquid Metals", J. Heat Transfer, 90(3), 303-12, 1968.

27. Reiss, F., and Schretzmann, K., "Pressure Balance and Maximum Power Density at the Evaporation Gained from Heat Pipe Experiments", Int. Conf. Thermionic Electrical Power Generation, Stresa, Itlay, 1968.

REFERENCES (cont.)

28. Deverall, J. E., The Effect of Vibration on Heat Pipe Performance, Los Alamos Scientific Laboratory, Los Alamos, New Mexico, Report AEC LA-3798, 4 October 1967.

29. Advanced Injectors for Space Storable Propellants, Final Report on Contract NAS 8-713, Aerojet-General Corporation Report 713-F, 3 October 1969.

30. Whittick, J. S. and Others, Physical Properties of Liquid Oxygen Difluoride and Liquid Diborane: A Critical Review, Stanford Research Institute Report No. 951581-4, 1 July 1967.

31. Stull, D. R. and Others, JANAF Thermochemical Tables, Dow Chemical Co., Midland, Michigan, 30 June 1966.

32. Reid, R. C., and Sherwood, T. K., The Properties of Gases and Liquids, Their Estimation and Correlation, 2nd Edition, McGraw Hill, 1966.

33. FLOX-Diborane Technology - Boundary Reactions, Final Report on Contract NAS 7-659, Aerojet-General Corporation Report 659-F, September 1969.

34. Lewis, D. R., and Others, Chrysler Improved Numerical Differencing Analyzer for 3rd Generation Computers, TN-AP-287, Chrysler Corporation Space Div., New Orleans, La., 20 October 1967.

35. Jordan, D. P., "Film and Transition Boiling", Advances in Heat Transfer, Vol. 5, Academic Press., 99, September 1968.

36. McAdams, W. H., and Others, "Vaporization Inside Horizontal Tubes", Trans. ASME 63, 545 (1941).

37. Giarratano, P. J., and Smith, R. V., "Comparative Study of Forced Convection Boiling Heat Transfer Correlations for Cryogenic Fluids", Advances in Cryogenic Engineering, Vol. 11, 492, (1966).

TABLE 1

REPORTED HEAT PIPE PERFORMANCES

Working Fluid	Wick	Z, Inches	ID, Inches	Q, Btu/sec	Q/A, Btu/sec-in.^{2}	Temp, °F	Attitude (< from H)	Enclosure	Geometry	Source
Nitrogen	Rayon Cloth	33	0.69	0.12	--	-256	H	304 SS	Cyl	Haskin, Wright-Patt. AFB
Ethyl Alcohol	Screen+Artery	47	~1.0	~0.02	--	~104		Glass	Cyl	Katzoff, NASA
Freon	Woven Fiberglass	9	0.42	0.10	--	200		Glass	Cyl	RCA
Naphthalene	Al Screen	26	0.40	0.106	0.02	374	10° Incline	Al	Cyl	RCA
Water	Sintered Copper	4	1.75	1.27	0.3604	234	H	Cu	Re-entrant	RCA
Water	Fiberglass	48	0.187	0.095	--	212	H	Copper	Serpentine	RCA
Water	SS Screen	18	0.43	--	--	212	H	304 SS	"Y"	RCA
Water	SS Screen	23	0.43	0.133	0.031	257	H	304 SS	"Y"	RCA
Water	SS Screen	29.6	0.72	0.10	--	199	H	SS	Cyl	LASL
Water	Sintered Copper	15	1.5	0.95	0.76	200		Copper	Cyl	RCA
Water	Monel Beads	16	1.9	1.42*	--	440	12°	Brass	Cyl	Cosgrove, N. C. State
Water	Monel Beads	16	1.9	1.09*	--	420	30°	Brass	Cyl	Cosgrove, N. C. State
Water	Monel Beads	16	1.9	0.66*	--	320	V	Brass	Cyl	Cosgrove, N. C. State
Water	Sintered Copper	10	--	15.91	0.34	336	Vertical	Copper	Annular	RCA
Water	Sintered Copper	3.3 Long	3.8-4.9	11.84	0.31	374	Vertical	Copper	Re-entrant	RCA
Mercury	SS Screen	10	0.375	0.38	0.15	644	H	304 SS	Cyl	RCA
Cesium	Wire Screen	~3.5	~0.6	0.31	--	1560		Niobium	Cyl	Brosens (IECEC, 1967)
Potassium	Slots+Tight Screen	12	0.3	1.19	--	1350		Nickel	Cyl	LASL
Potassium	Slots+Loose Screen	12	0.3	2.47*	--	1340		Nickel	Cyl	LASL
NaCl	Moly Mesh	10	0.74	0.95	0.12	2550	H+V Cond Up	Alumina/ TZM	Cyl,2-Piece	RCA
LiF	Moly Mesh	18	0.625	0.95	0.18	2192	V Cond Up	Moly	Cyl	RCA
Sodium	Slots	12	0.3	1.42*	--	1540		Nickel	Cyl	LASL
Sodium	Slots+Tight Screen	12	0.3	3.79*	--	1540		Nickel	Cyl	LASL
Sodium	SS Screen	25	0.63	0.95	--	1530	H	304 SS	Cyl	LASL
Sodium	Slots+150 ⌓Screen	33.4	~0.7	5.22*	--	1560	H	?	Cyl	LASL
Sodium	Slots+10 ⌓Screen	33.4	~0.7	9.47	--	1560	H	?	Cyl	LASL
Sodium	Wire Screen	53	0.75	7.59	--	1520	V Cond Up	?	Cyl	LASL
Sodium	SS Screen	14	0.338	0.19	0.06	1320	V Cond Up	Hastelloy X	Cyl	RCA
Sodium	SS Screen	10	0.437	0.38	0.06	1560	H	Nickel	Rt. Angle	RCA
Sodium	Slots	--	0.8 OD	3.5	≥2.5	~1500	V	SS ?	Cyl	Reiss, Schretzmann
Lithium	Moly Mesh	1.5	--	0.95	0.18	2550	V	TZM	Annular	RCA
Lithium	Woven Mesh	24	?	4.27	1.53	2640	H	Moly	Cyl	RCA
Lithium	Wire Screen	15	0.41	1.85*	1.28*	2280	V	Niobium	Cyl	LASL
Silver	Wire Screen	~8	0.41	3.32*	2.51*	3630	H	Ta-5%W	Cyl	LASL

*Limiting.

TABLE 2

EVAPORATOR WICKS TESTED
(Material in each case is Nickel 200)

Heat Pipe	Wick Description
No. 1	Multi-Layer Screen, 0.042 in. thick. 5 layers of 120 x 120 plain weave mesh Layers spring loaded against evaporator wall Butt joint between evaporator and liquid return wicks
No. 2	Fiber Metal, 0.040 in. thick One layer of Huyck Metal Co. FM-1205 Density = 15%, Wick sintered to evaporator wall
No. 3	Composite Screen, 0.032 in. thick 2 layers of 120 x 120 plain weave mesh over 1 layer of 50 x 50 plain weave mesh. Each layer spot welded in place.
No. 4	Screen Covered Channels, 0.038 in. thick. 11 x 11 matrix of channels, each 0.028 in. deep and 0.042 in. wide, covered by 2 layers of 320 x 320 plain weave mesh Screen spot welded to channel lands.
No. 5	Sintered Nickel Powder, 0.041 in. thick 100 mesh nickel powder, Density = 15%, wick sintered to evaporator wall Sleeve joint between evaporator and liquid return wicks
No. 6	Sintered Disk Covered Channels, 0.035 in. thick 64 x 6 matrix of channels, each 0.010 in. deep and 0.005 in. wide, covered by a 0.025 in. thick sintered nickel powder disk.
No. 7	Sintered Nickel Powder, 0.070 in. thick Same material as Heat Pipe No. 5 Wick sintered to evaporator wall and liquid return wick.

TABLE 3

DATA SUMMARY FOR SODIUM-NICKEL TESTS

	Test No.	Power Input: Total Power Watts	Power Input: Q/A W/cm^2	Power Input: Q/A $BTU/in^2 sec.$	Power Transfer Calorimetric Watts	T_8 °C	T_2-T_1 °C	T_3-T_1 °C	T_2-T_3 °C	Test Position	Comments
Test Device #1	7	870	134	0.82	678	401	124	386	262	V	Leaked at lower weld, wick bowed
	8	870	134	0.82	772	405	124	385	261	V	away from evaporator. Sintering
	9	940	145	0.89	762	462	419	563	144	V	to evaporator could help.
	19	940	145	0.89	962	476	6	286	280	V	
	20	948	146	0.90	--	512	11	454	443	V	
Test Device #2	48	765	117	0.72	562	502	98	57	41	V	Leak in lower weld area repaired.
	49	1150	177	1.10	930	586	186	84	102	V	Better Horizontal performance
	50	1620	249	1.53	1305	709	215	92	123	V	due to pool boiling when vertical
	51	1972	304	1.87	1518	808	292	91	201	V	
	52	1972	304	1.87	1542	808	288	92	196	V	
	13	1438	221	1.36	992	642	176	72	104	H	
	14	2040	314	1.93	1458	815	239	71	168	H	
	15	2687	414	2.54	2259	737	324	144	180	H	
	16	2760	425	2.61	2396	754	333	145	188	H	
	20	2912	449	2.75	2548	785	338	174	164	H	
	21	3222	496	3.04	2786	813	348	171	177	H	
	22	3366	519	3.18	3140	831	347	167	180	H	
Test Device #3	24	1317	202	1.24	895	652	173	230	-57	V	
	25	1481	228	1.40	1112	740	218	296	-78	V	Apparent thermal runaway reached
	26	1577	242	1.48	1248	775	256	307	-51	V	
	14	1161	179	1.10	675	673	145	129	16	H	Post analysis showed slight bowing away
	15	1615	249	1.53	997	755	248	134	114	H	of wick structure
	16	1730	266	1.63	1128	789	268	107	161	H	
	17	2200	339	2.08	1947	761	343	176	167	H	Evaporator bowed outward
	*22	1659	256	1.57	1124	798	318	188	130	H	
	24	2103	324	1.99	1789	771	376	266	110	H	
	25	2294	353	2.17	1916	784	393	279	114	H	
	26	2400	370	2.27	2146	794	399	299	100	H	
	27	2406	371	2.28	2247	796	400	334	---	H	

Test Device Position
H - Horizontal
V - Vertical

*New heater

TABLE 3 (cont.)

DATA SUMMARY FOR SODIUM-NICKEL TESTS

	Test No.	Power Input: Total Power Watts	Power Input: Q/A_2 W/cm^2	Power Input: Q/A_2 BTU/in^2 sec.	Power Transfer Calorimetric Watts	T_8 °C	T_2-T_1 °C	T_3-T_1 °C	T_2-T_3 °C	Test Position		Comments
Test Device #4	23	1294	199	1.22	935	843	118	240	-122	V		Appeared to be gas loaded. Evaporator
	30	826	127	.78	419	650	38	44	-6	H		bowed severely.
	31	1248	192	1.18	792	855	46	83	-37	H		
Test Device #5	19	2406	370	2.27	2242	730	162	285	-123	V		Thermal runaway reached
	21	2444	376	2.31	1852	731	119	306	-187	H		
	23	3293	507	3.11	3524	600	150	387	-237	H		Start-up(liquid 100°C) reached 60% of
	24	3630	560	3.44	3933	651	168	458	-290	H		646 w/cm^2, pulsed instant on.
	25	4020	620	3.80	4102	687	197	479	-280	H		
	27	3323	514	3.15	3289	549	194	368	-232	H		Na solid - runaway experienced
	28	4175	644	3.95	4210	709	147	424	-277	H		at 10% max. power
	29	4187	646	3.96		733	240	470	-330	H		
Test Device #6	8	1361	209	1.28	816	774	53	126	-73	H		Overlay bowed away from substrate
	9	1702	262	1.61	858	807	75	171	-96	H		X-rays of evaporator confirmed.
	11	1217	187	1.15	812	485	227	529	-302	H		
	12	1408	217	1.33	1007	522	262	600	-338	H		
						T_1					*	
Test Device #7	18	2412	371	2.27	2257	661	126	172	-46	H	60	
	19	3440	530	3.25	3134	662	175	251	-76	H	60	Testing completed
	20	3850	593	3.64	3372	662	196	338	-142	H	60	
	21	3950	609	3.73	3567	664	196	366	-170	H	60	
	22	4568	704	4.32	3946	663	265	427	-162	H	63	
	24	4825	720	4.42	4165	611	274	439	-165	H	25	Burnout occurred at center
	25	5175	797	4.89	4310	608	310	462	-152	H	25	of evaporator
	27	5223	805	4.94	4415	595	345	558	-213	H	15	

*Gas pressure (mm Hg)

TABLE 4

SUMMARY OF MAXIMUM HEAT FLUX DATA

Heat Pipe No.	Wick Type	Max. Heat Flux Btu/in.^{2}-sec	Limiting Factor	(1) $\frac{\Delta P_{ew}}{10^{-3}}$	(2) $\frac{\Delta P_{lrw}}{10^{-3}}$	(3) $\frac{\Delta P_{vap}}{10^{-3}}$	(4) $\frac{\Delta P_{tot}}{10^{-3}}$	(5) $\frac{\Delta P_{tot}}{\Delta P_{cap}}$
1	Multi-layer Screen	0.89	Mechanical Failure	6.45	10.6	0.075	17.1	0.098*
2	Fiber Metal	3.2	Unexplained High Wall Temperatures	31.6	38.0	0.97	70.6	0.08*
3	Composite Screen	2.26	Unknown	7.22	27.1	0.49	34.8	0.199*
4	Screen Covered Channels	1.50	Mechanical Failure	0.2	14.6	0.14	14.9	0.015*
5	Sintered Nickel Powder	3.95	Wicking Limit	713	157	1.49	871	1.0*
6	Sintered Powder Covered Channels	1.61	Mechanical Failure	16.0	63.9	0.25	80.2	0.093*
7	Sintered Nickel Powder	4.94	Wicking Limit or Boiling Limit	565	221	29.8	816	0.83**

(1) ΔP_{ew} = Calculated Pressure Drop in Evaporator Wick, $lb_f/in.^2$

(2) ΔP_{lrw} = Calculated Pressure Drop in Liquid Return Wick, $lb_f/in.^2$

(3) ΔP_{vap} = Calculated Pressure Drop in Vapor Phase, $lb_f/in.^2$

(4) ΔP_{tot} = Total Pressure Drop, $lb_f/in.^2$

(5) ΔP_{cap} = Capillary Pumping Pressure, $lb_f/in.^2$

* Calculations Based on 800°C Properties

** Calculations Based on 600°C Properties

TABLE 5

MEASURED CHARACTERISTICS OF WICK MATERIALS USED

1. 120 x 120 Mesh

Permeability (k)	=	1.7322×10^{-6} cm^2
	=	1.864×10^{-9} ft^2
Pumping Pore (r_c)	=	0.01909 cm
	=	0.000626 ft

2. 60 x 60 Mesh

Permeability (k)	=	2.38×10^{-6} cm^2
	=	2.56×10^{-9} ft^2
Pumping Pore (r_c)	=	0.0298 cm
	=	0.000977 ft

3. 50 x 50 Mesh

Permeability (k)	=	6.47×10^{-6} cm^2
	=	6.96×10^{-9} ft^2
Pumping Pore (r_c)	=	0.05802 cm
	=	0.001903 ft

4. Sintered Nickel Powder

Permeability (k)	=	7.027×10^{-8} cm^2
	=	7.56×10^{-11} ft^2
Pumping Pore (r_c)	=	0.00387 cm
	=	0.000126 ft

5. Feltmetal FM1205

Permeability (k)	=	1.268×10^{-6} cm^2
	=	1.357×10^{-9} ft^2
Pumping Pore (r_c)	=	0.00379 cm
	=	0.000124 ft

TABLE 6

WORKING MODEL DESIGN OPERATION CONDITIONS

Engine Mixture Ratio	=	3.0 OF_2/B_2H_6
Chamber Pressure	=	100 psia
Vacuum Thrust	=	1000 lb_f
Contraction Ratio	=	1.56:1
Expansion Area Ratio	=	60:1
c* Efficiency	=	92%
Total Flow Rate	=	2.6 lb/sec
Fuel Flow Rate	=	0.65 lb/sec
Oxidizer Flow Rate	=	1.95 lb/sec
Throat Diameter	=	2.60 in.

TABLE 7

CONDENSER COOLING CONSIDERATIONS

Barrier Cooling	Condenser Coolant	Outlet Temperature, °F	Injector Type
None	Oxidizer	865	Gas/Liquid
	Fuel	*905	-
	**Oxidizer + Fuel	210	Gas/Gas
	**80% (Oxidizer + Fuel)	425	Gas/Gas + Liquid/Liquid
19% at MR = 0.5	Oxidizer	365	Gas/Liquid
	Fuel	515	Gas/Liquid
	**Oxidizer + Fuel	*2 Phase	-
	Core Oxidizer	465	Gas/Liquid
	Core Fuel	*1360	-
	**Core Oxidizer + Core Fuel	146	Gas/Gas + Liquid/Liquid

* Denotes unacceptable condition
** Equal outlet temperatures assumed

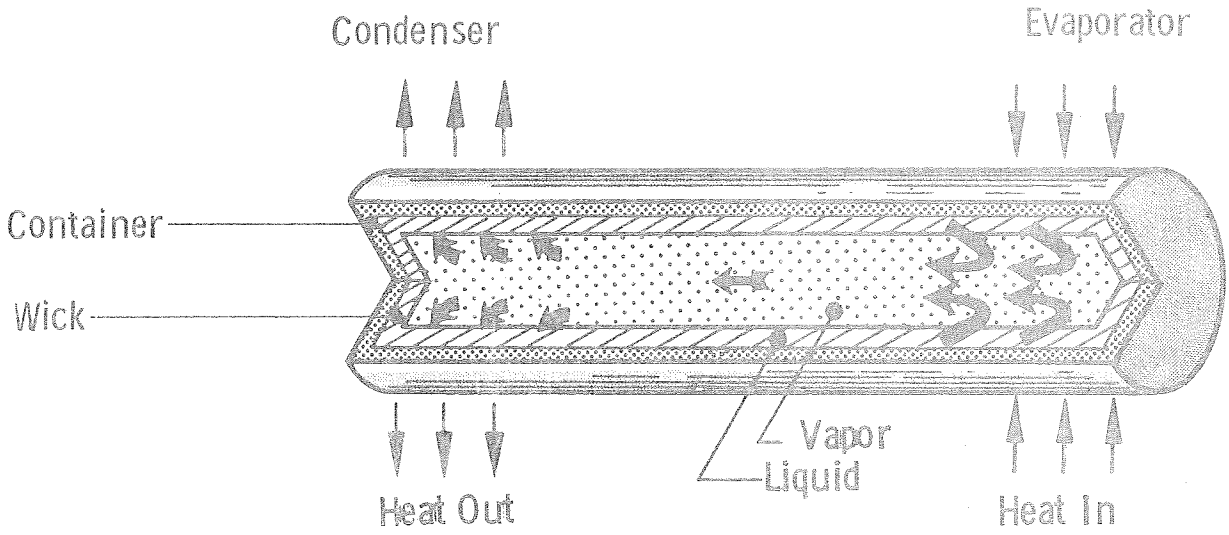

3 BASIC COMPONENTS

1. Container
2. Wick
3. Working Fluid

3 IMPORTANT CHARACTERISTICS

1. Very High Conductance
2. Heat Flux Reduction
3. Heat Flux Averaging

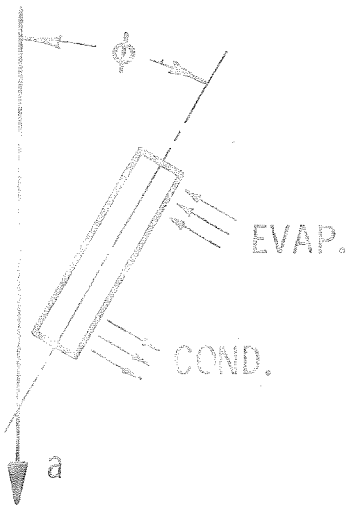

ORIENTATION

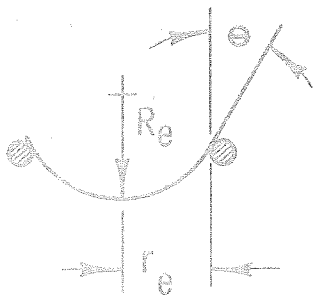

$$\cos\Theta = \frac{r_e}{R_e}$$

MENISCUS DETAIL

Heat Pipe Schematic

Figure 1

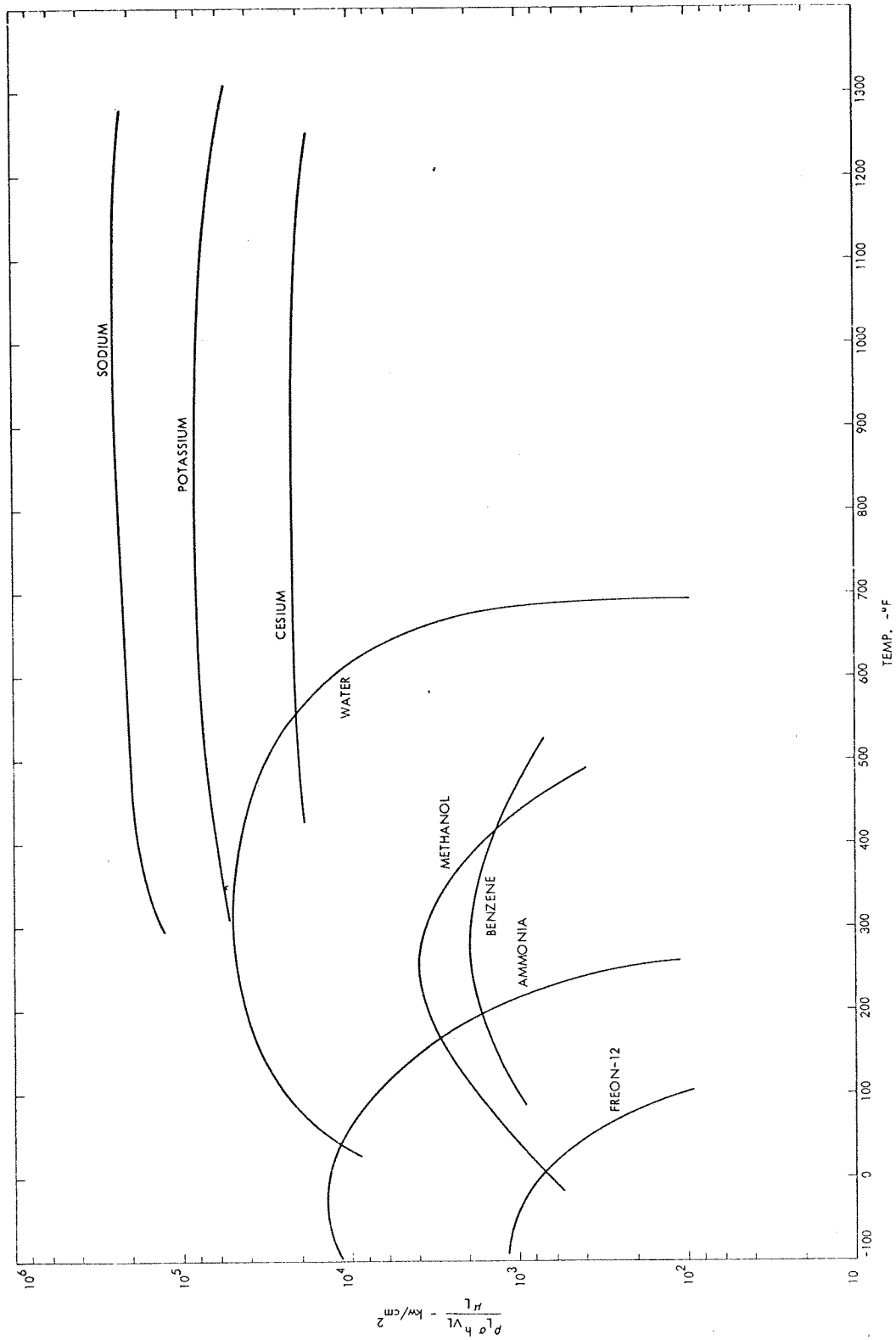

Liquid Transport Factor

Figure 2

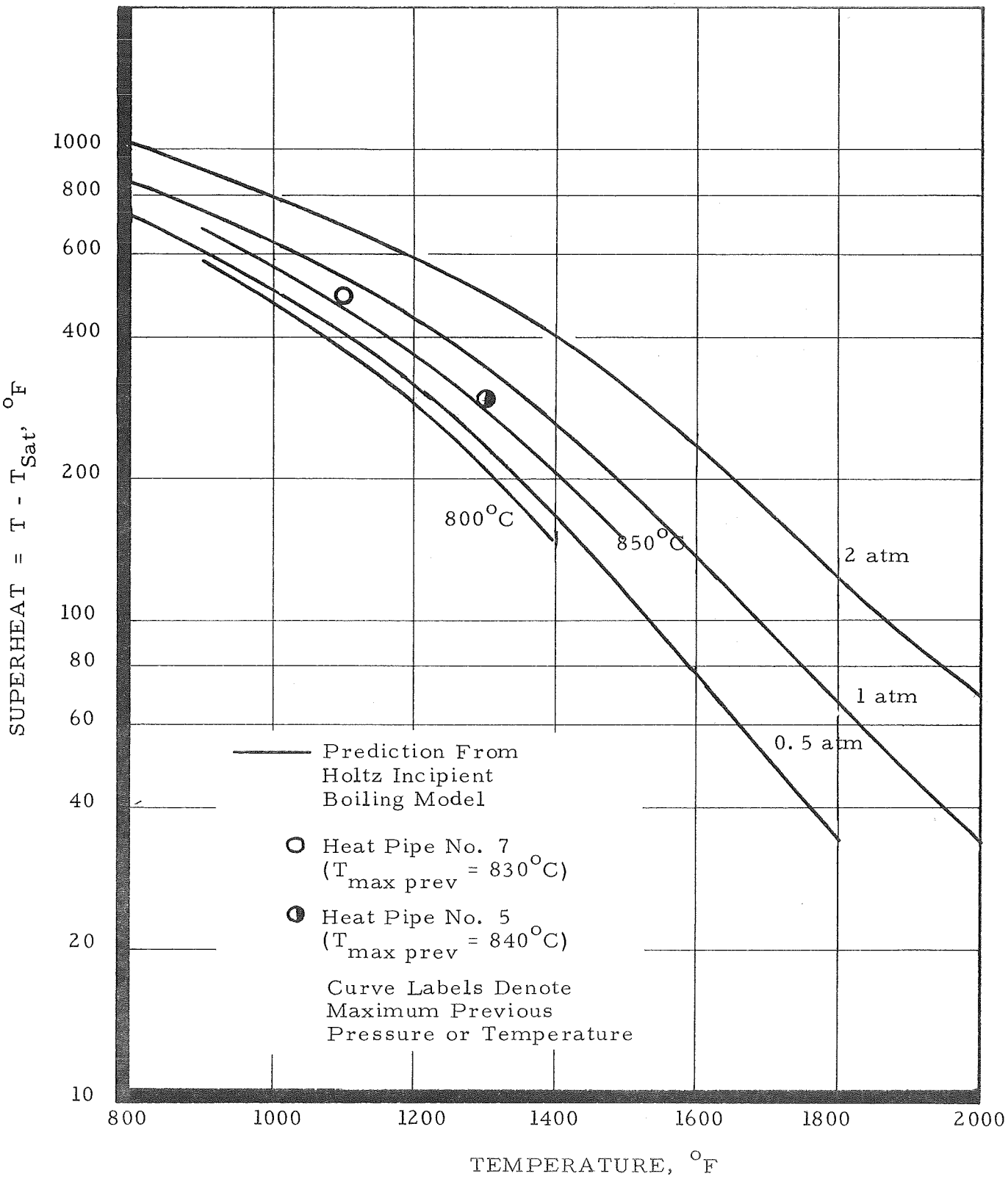

Incipient Boiling Superheats for Sodium

Figure 3

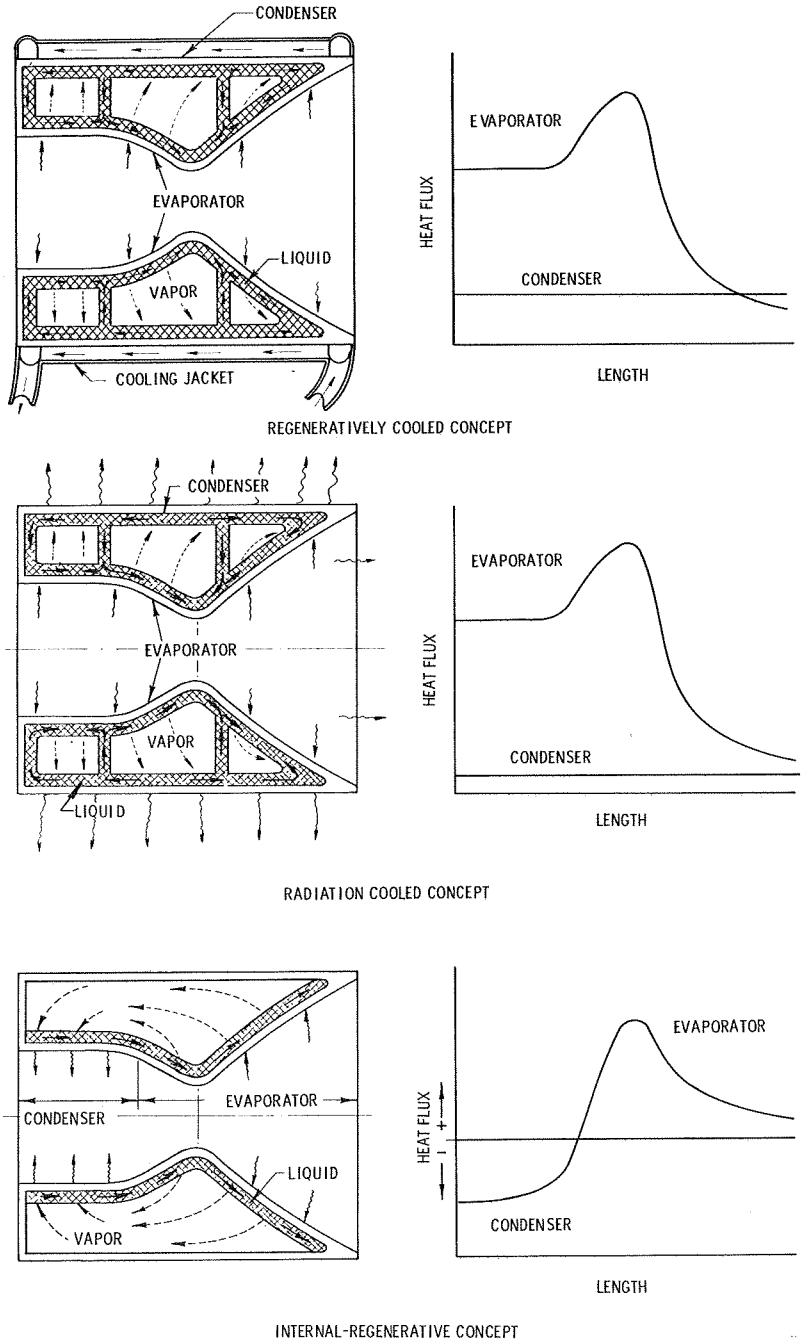

Heat-Pipe-Cooled Thrust Chamber Concepts

Figure 4

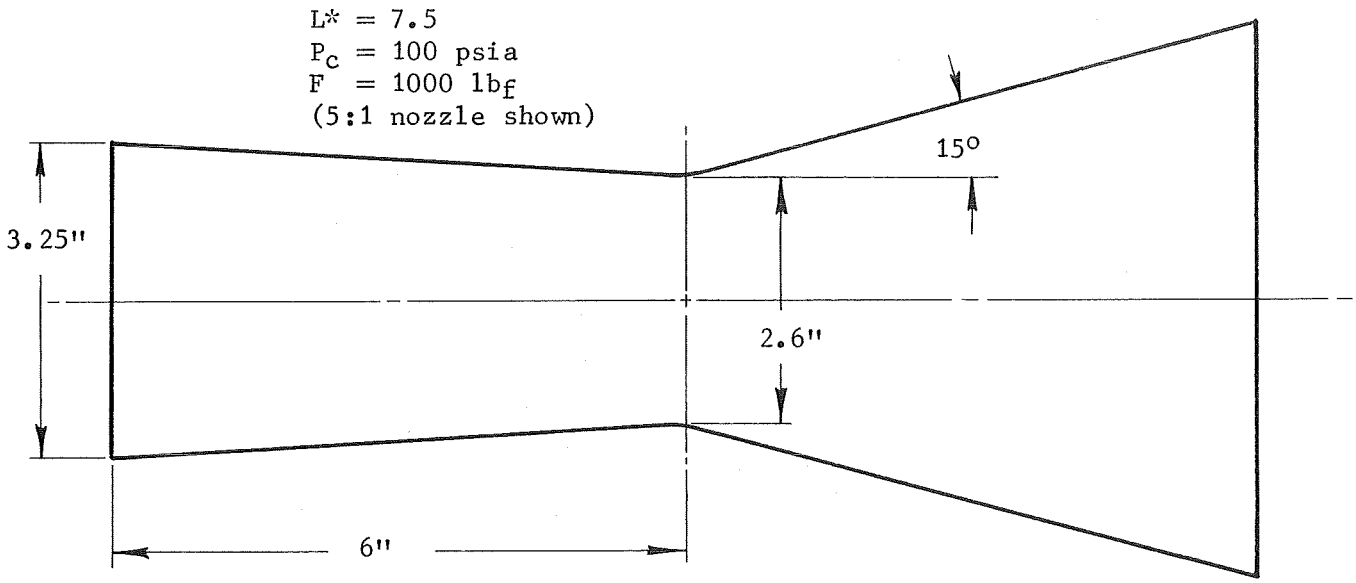

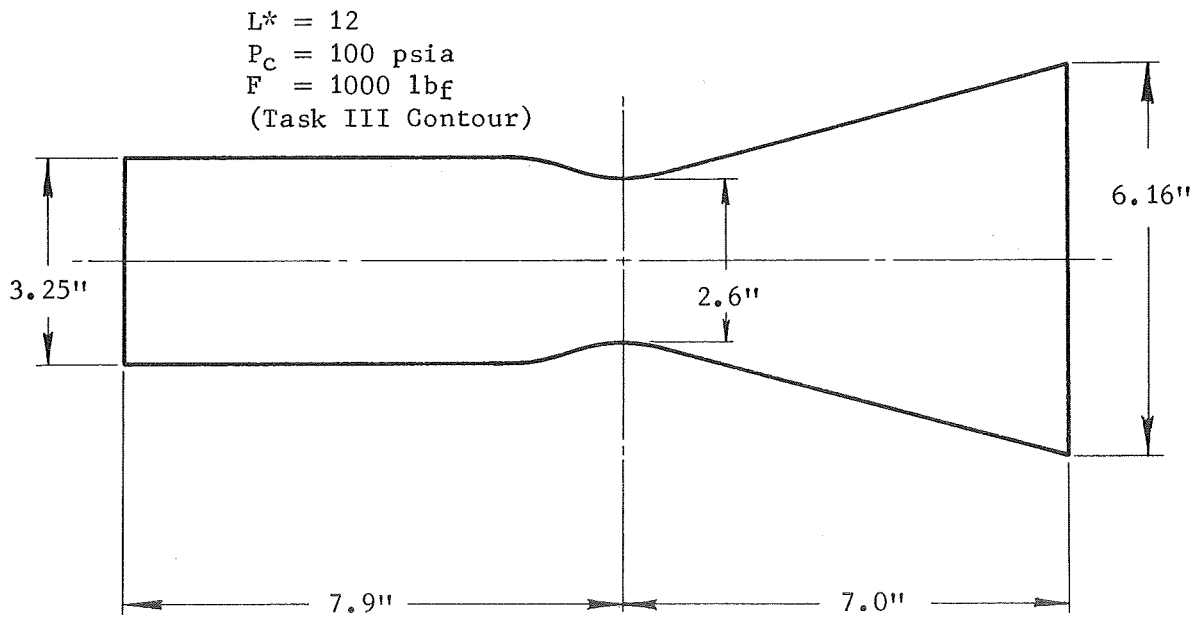

Thrust Chamber Configurations

Figure 5

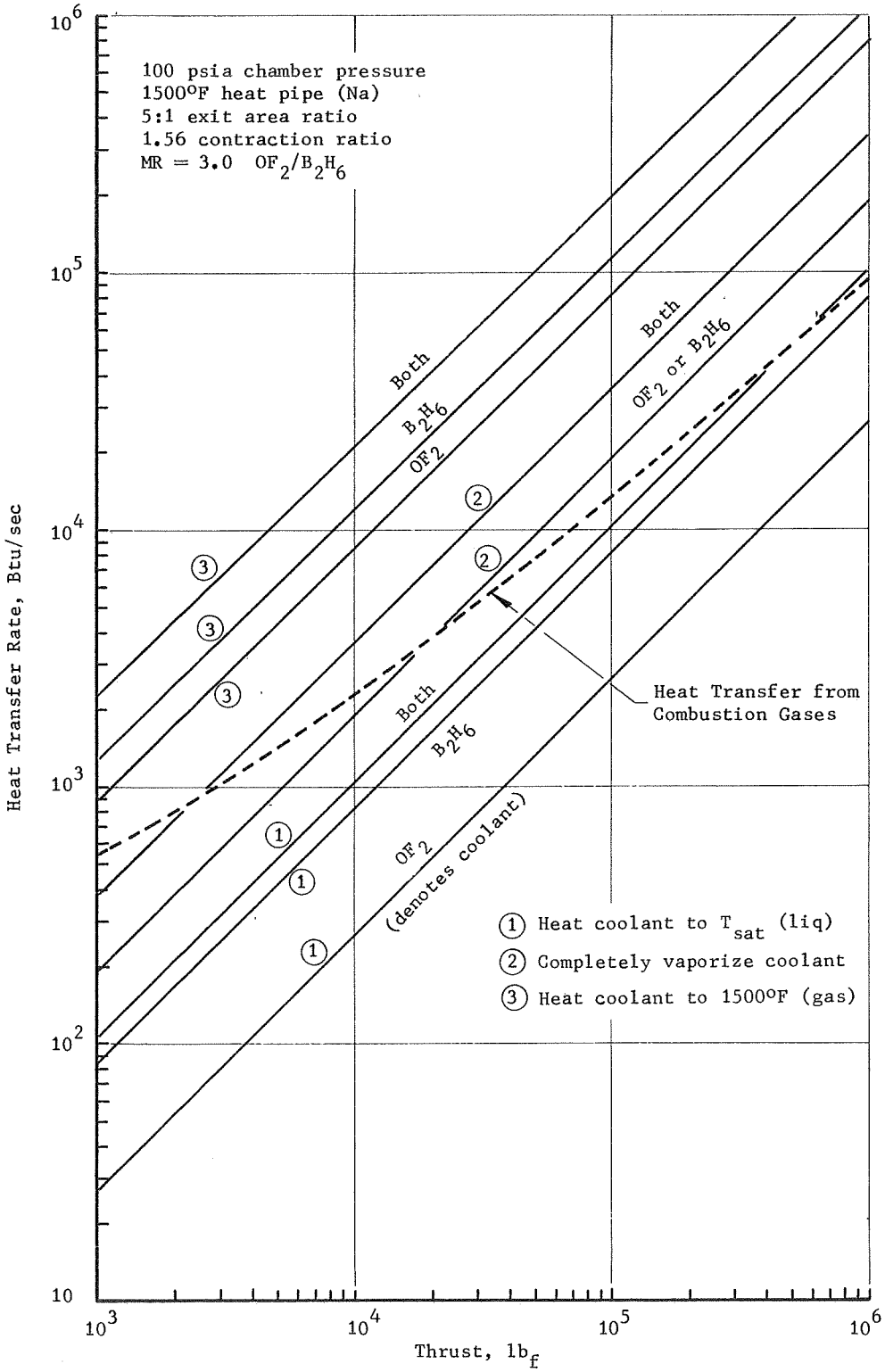

Typical Regenerative Cooling Results

Figure 6

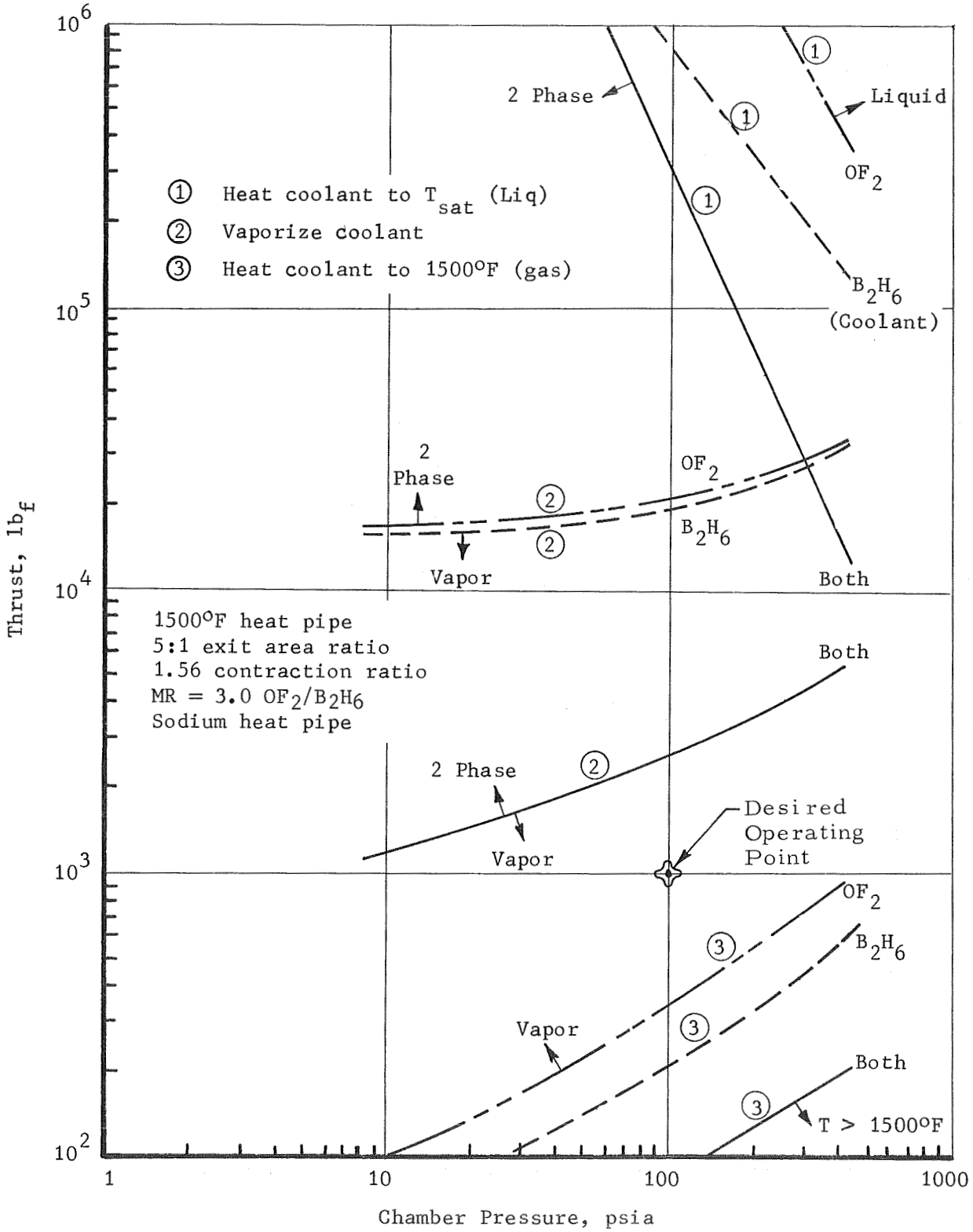

Feasibility Chart for Regeneratively Cooled Condenser Concept

Figure 7

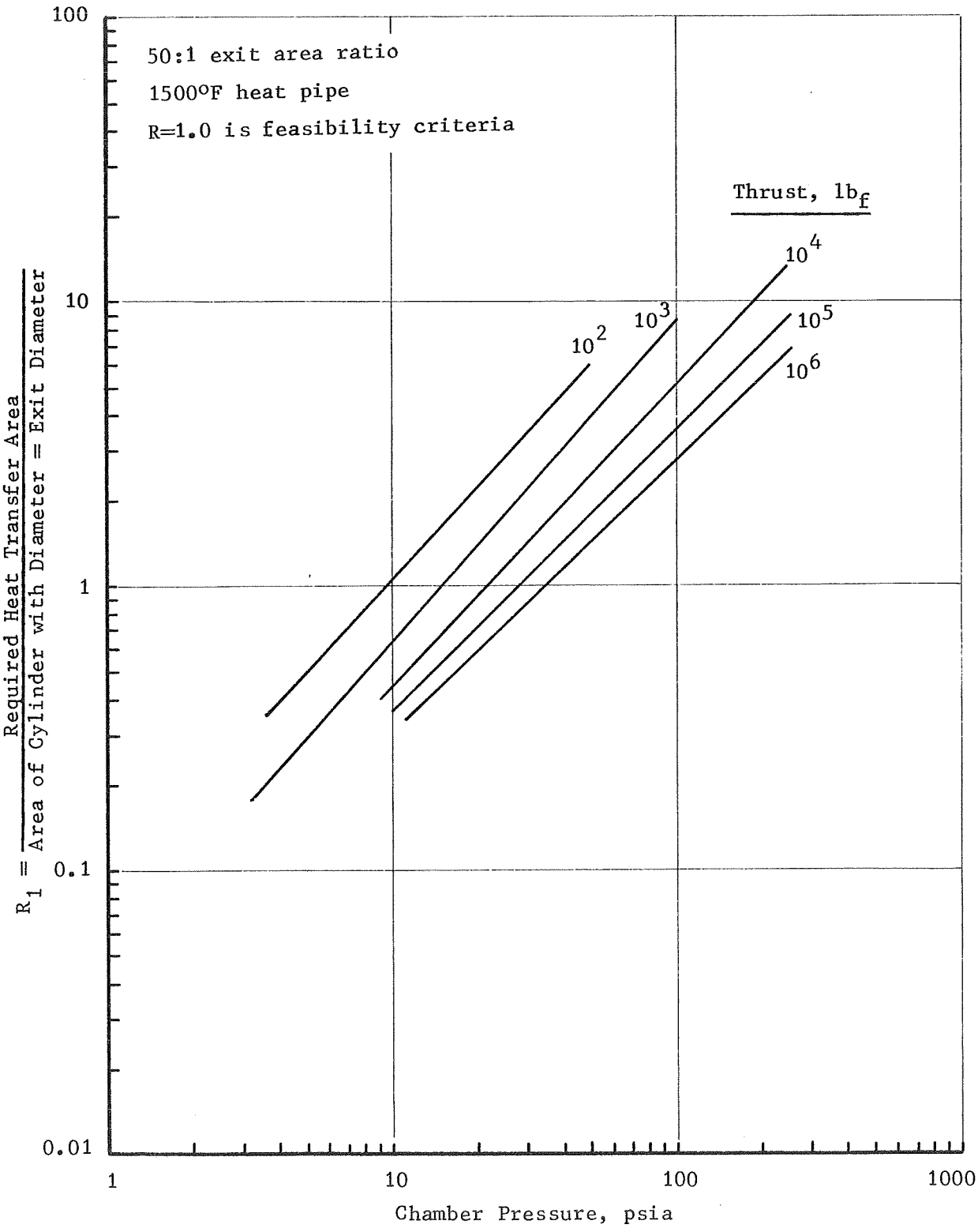

Typical Radiation Cooling Analysis Results

Figure 8

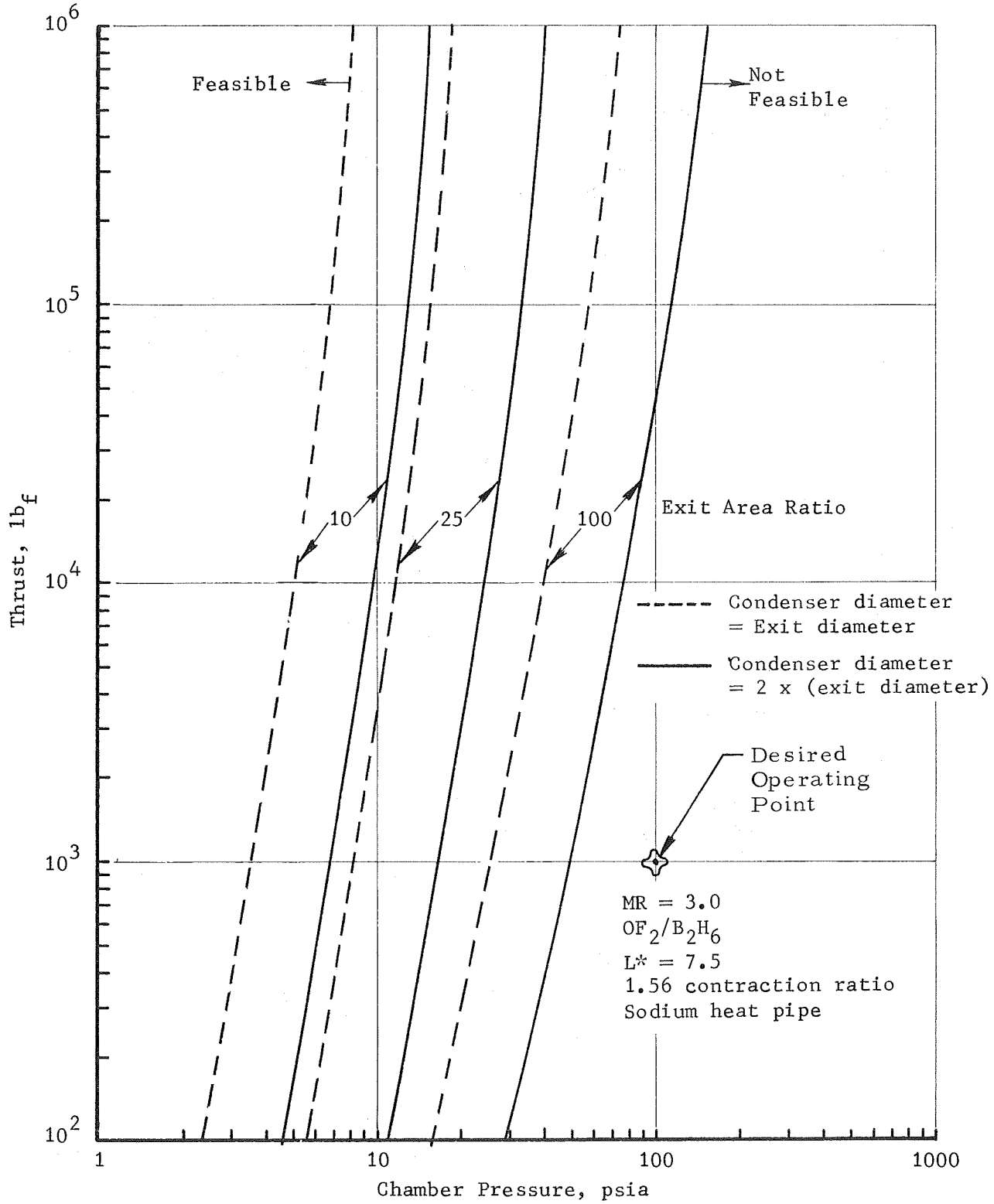

Feasibility Chart for 1500°F Radiation Cooled Heat Pipe Thrust Chamber

Figure 9

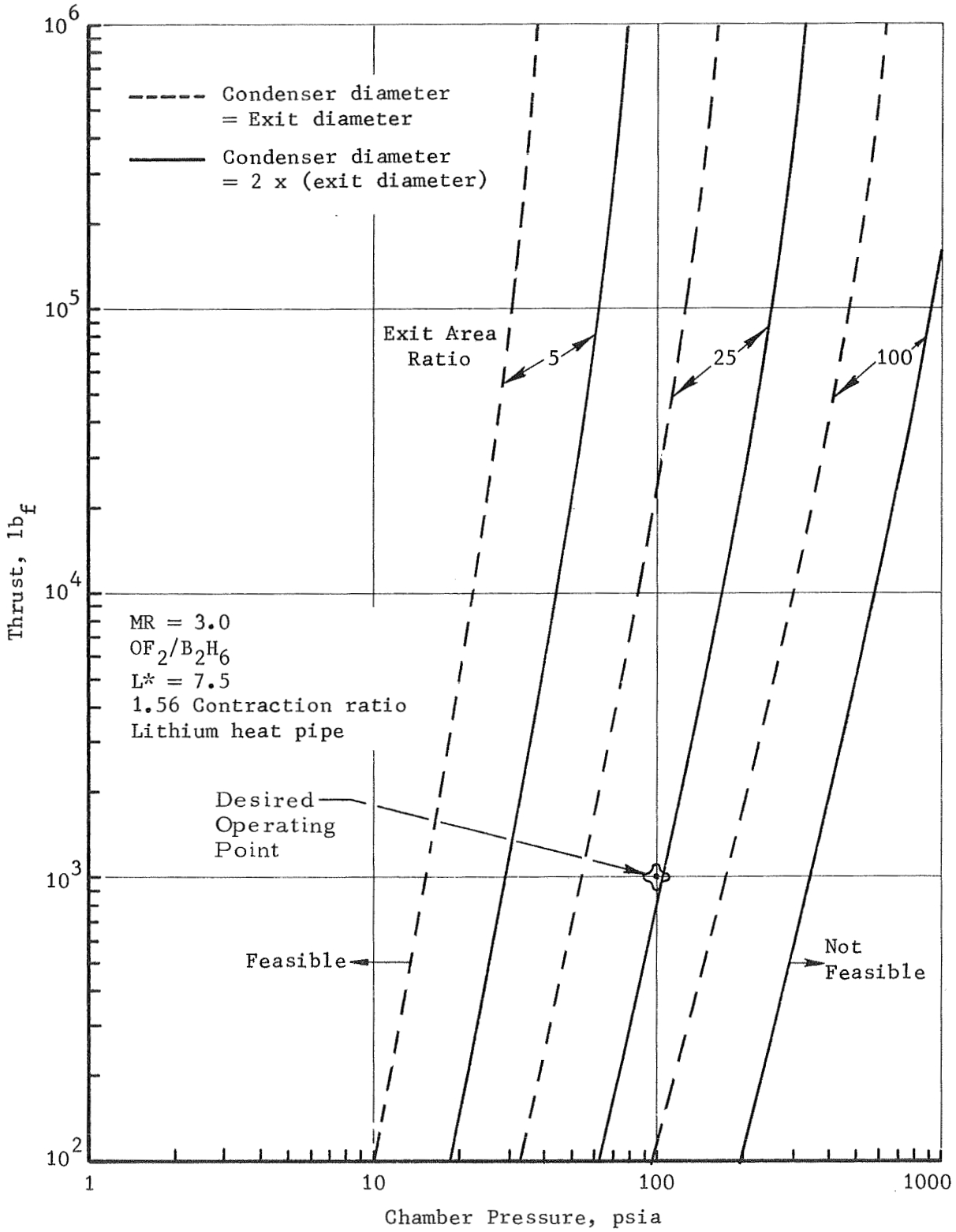

Feasibility Chart for 2500°F Radiation Cooled Heat Pipe
Thrust Chamber

Figure 10

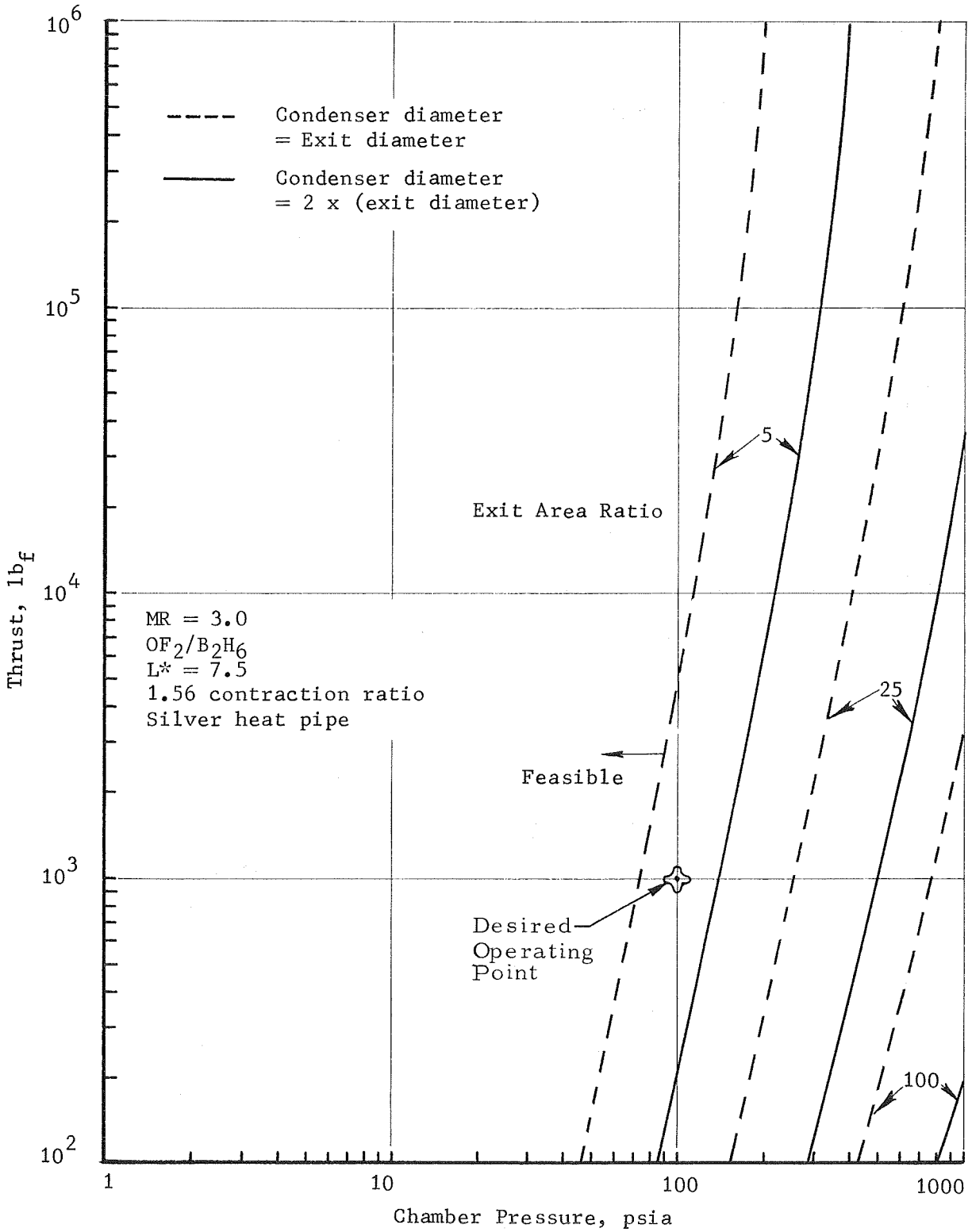

Feasibility Chart for 3500°F Radiation Cooled Heat Pipe Thrust Chamber

Figure 11

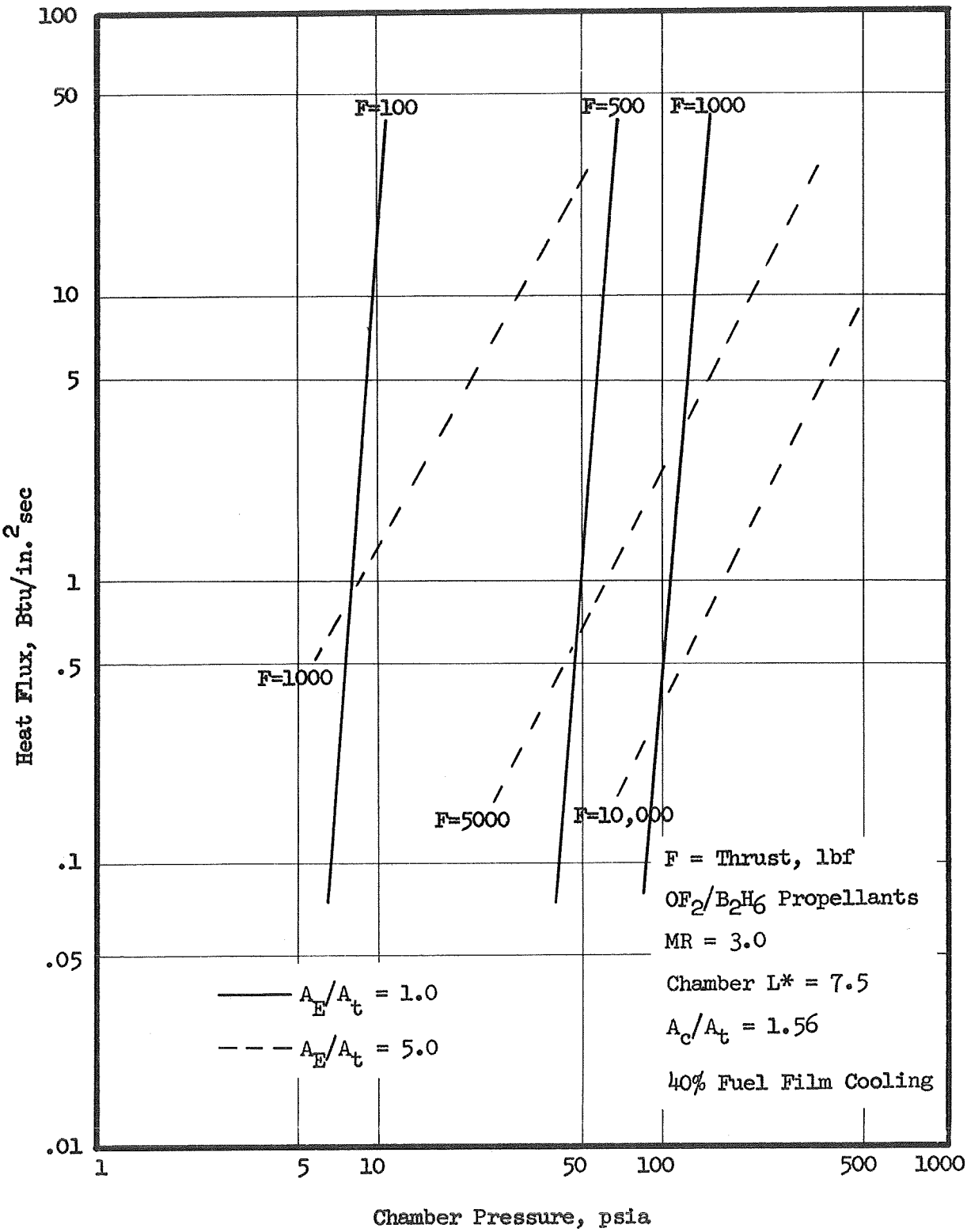

Heat Flux to B_2H_6 Film Coolant in an Internal Regenerative System

Figure 12

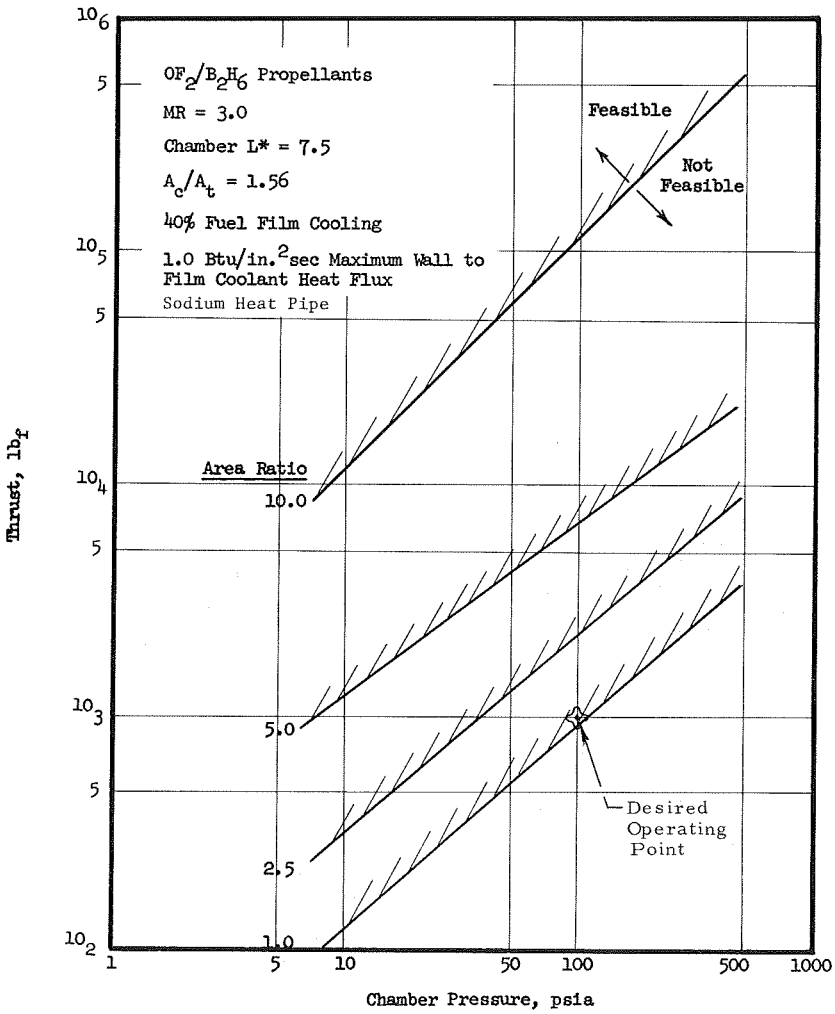

Feasibility Chart for Internal-Regeneratively Cooled Condenser Concept

Figure 13

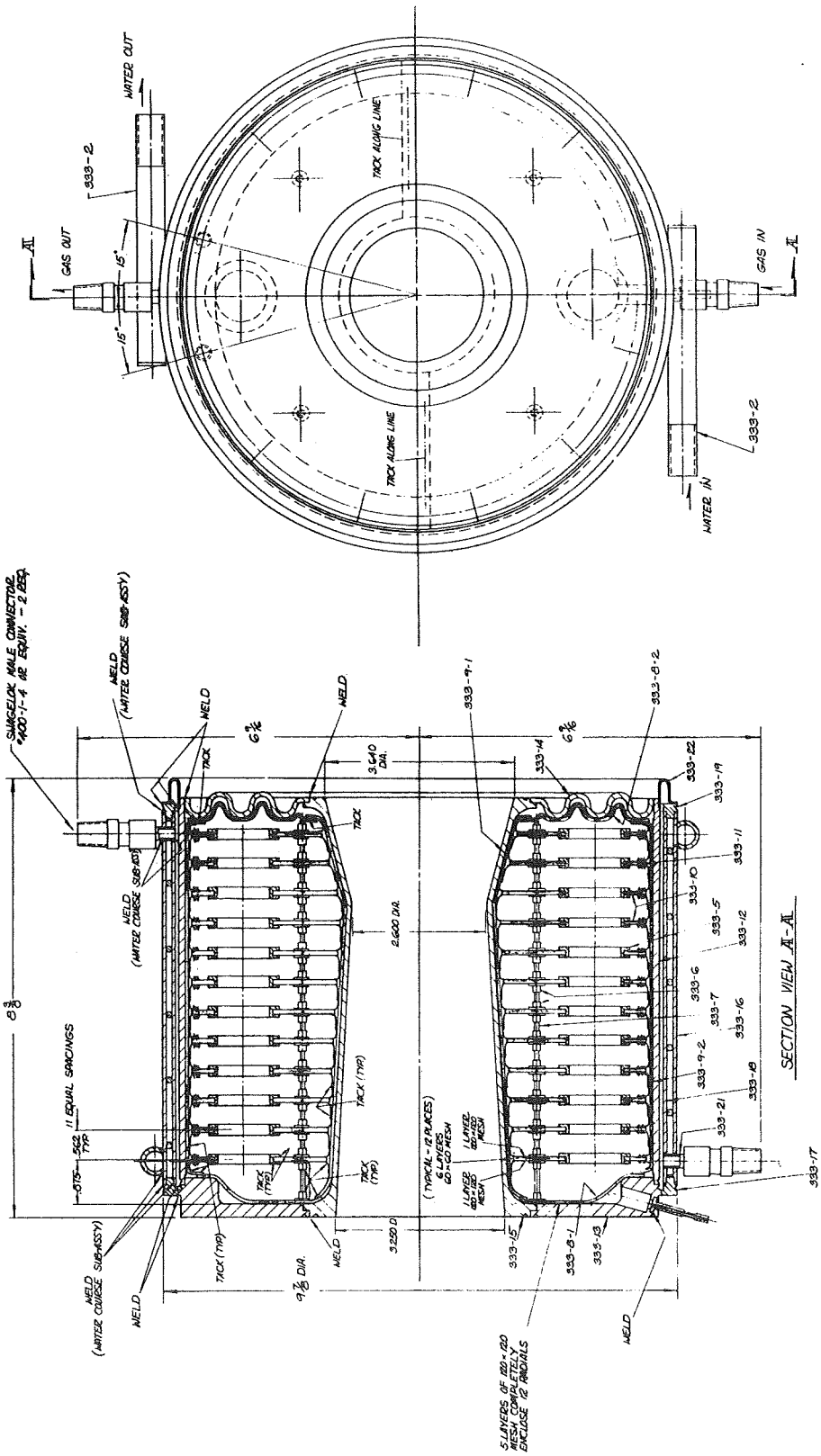

NOTE: Numbers refer to other detail drawings not shown in this report.

Fabrication Experiment Thrust Chamber, Assembly Drawing

Figure 14

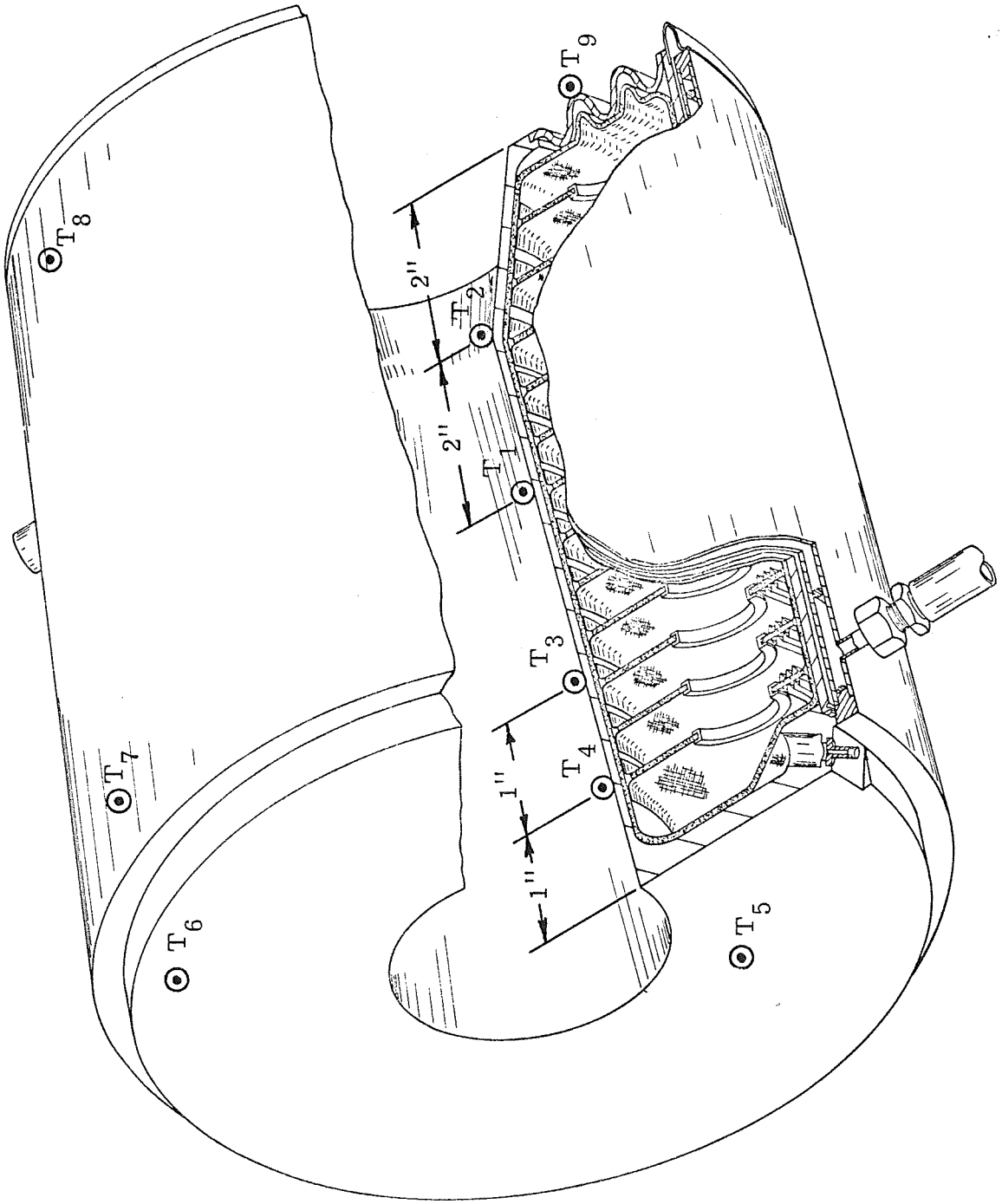

Fabrication Experiment Thrust Chamber, Cutaway View

Figure 15

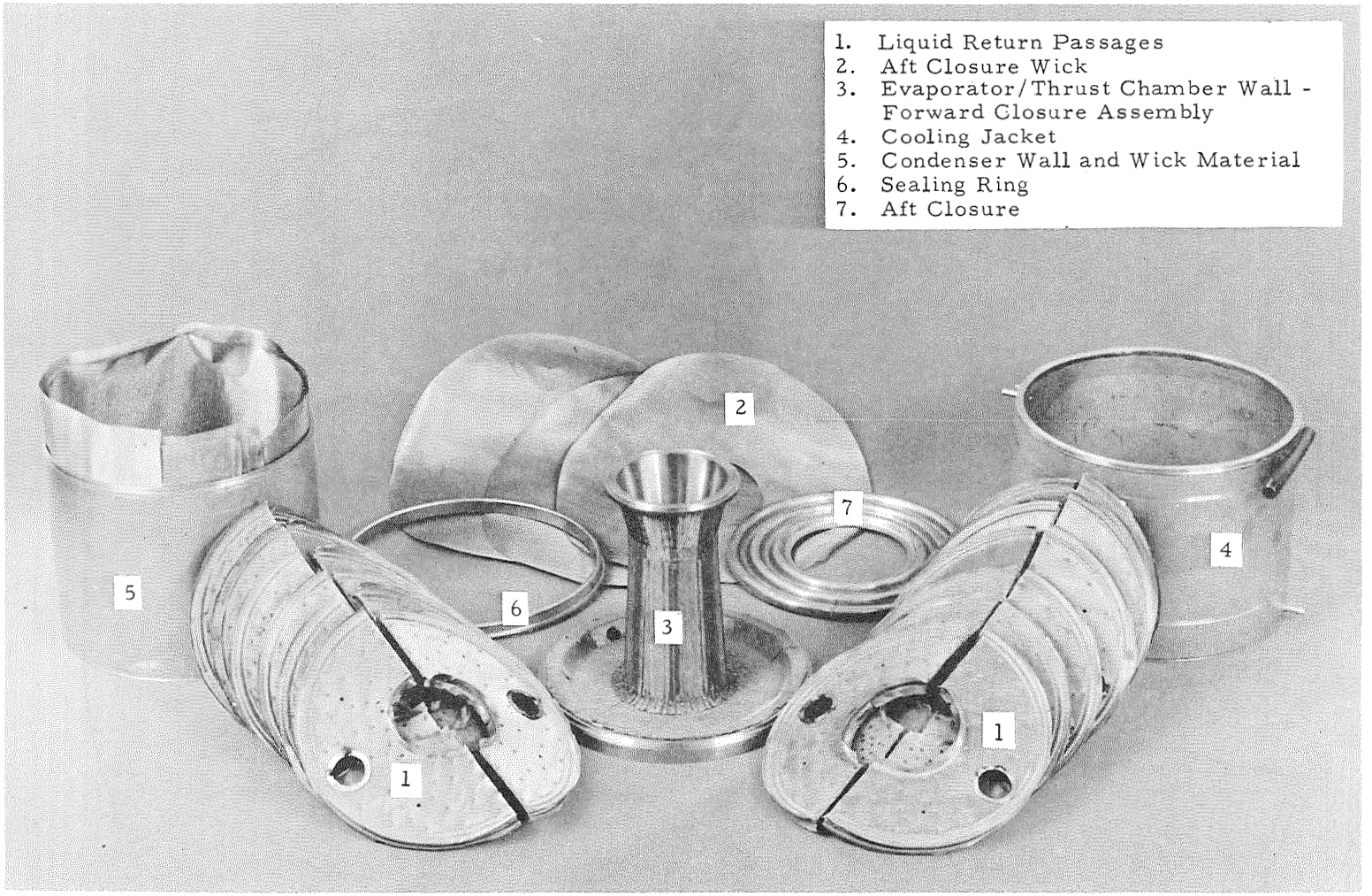

Figure 16

Parts for the Fabrication Experiment Thrust Chamber

Completed Fabrication Experiment Thrust Chamber

Figure 17

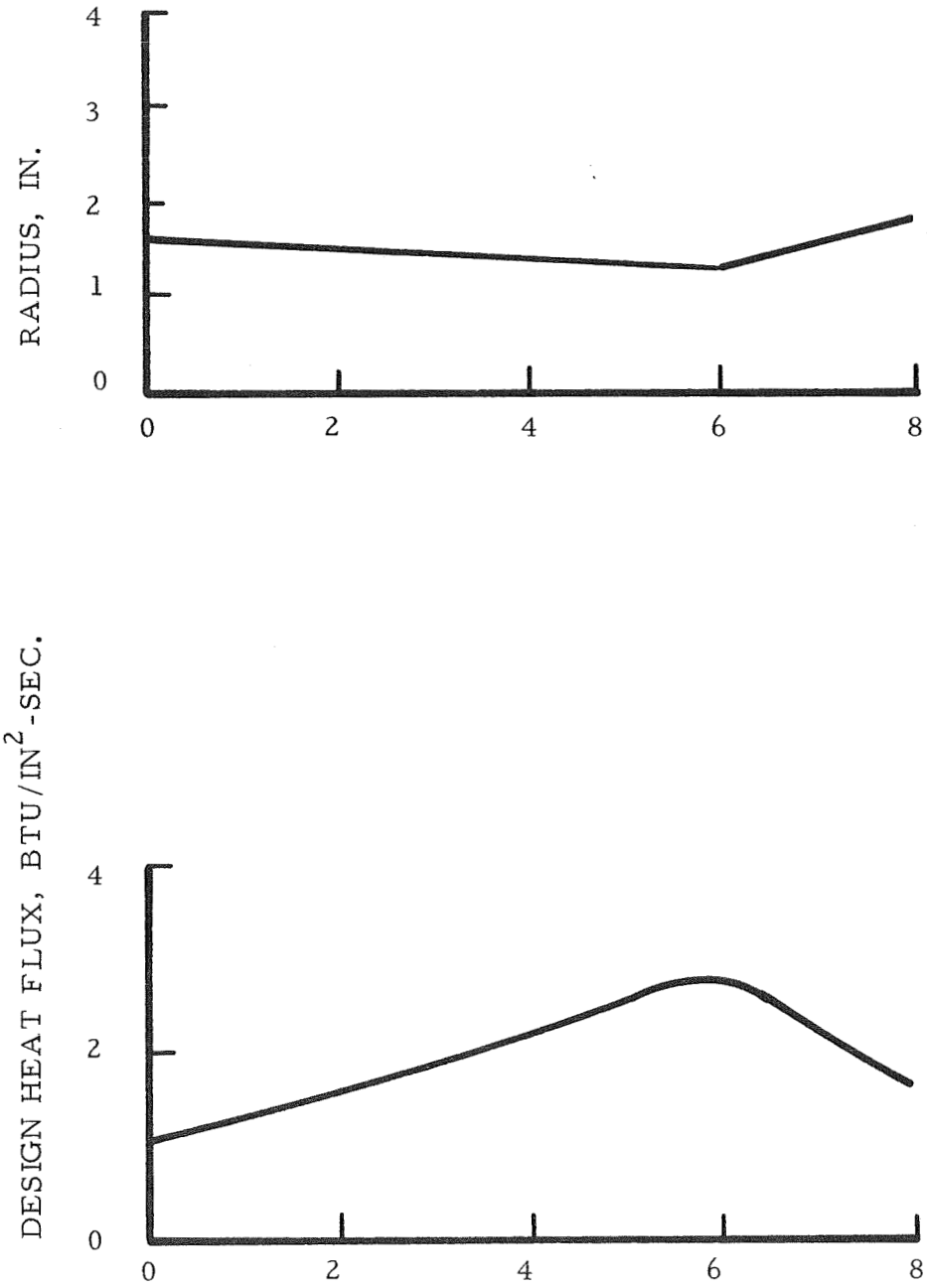

Design Heat Flux Distribution for the Fabrication Experiment Thrust Chamber

Figure 18

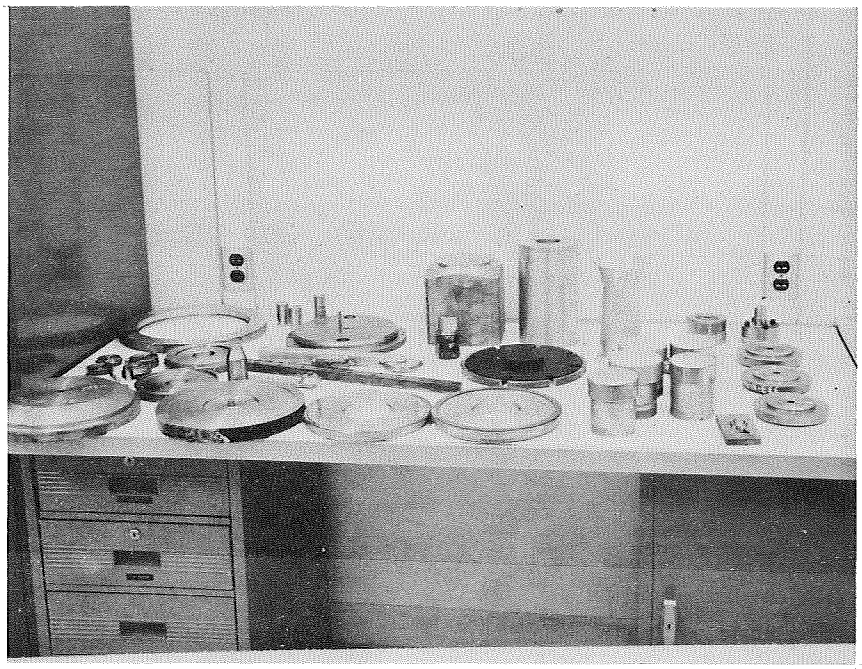

Wick Fabrication Tooling

Figure 19

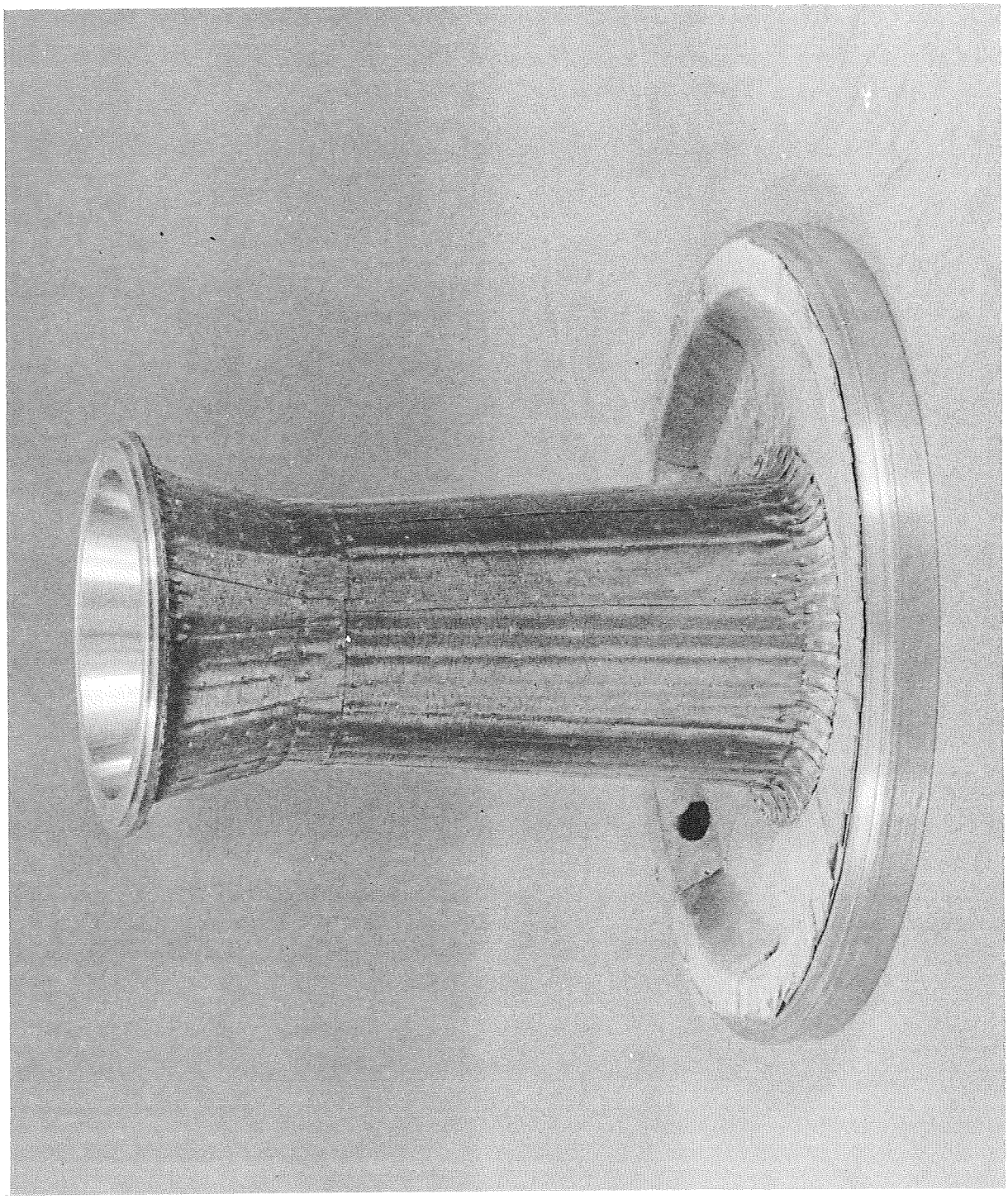

Closeup View of Evaporator Wick

Figure 20

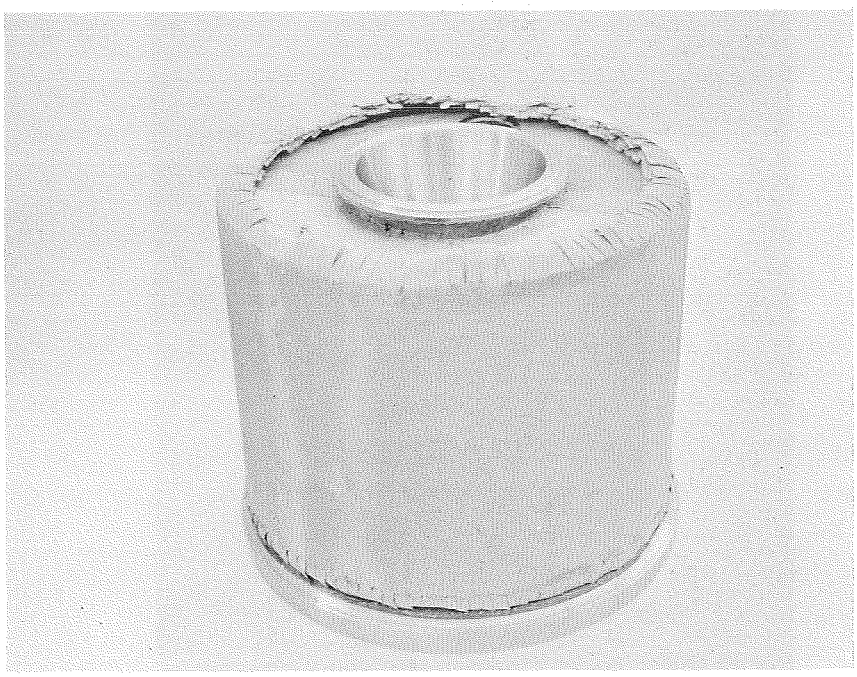

Figure 21. Thrust Chamber after Installation of Wicks and Radial Flow Passages

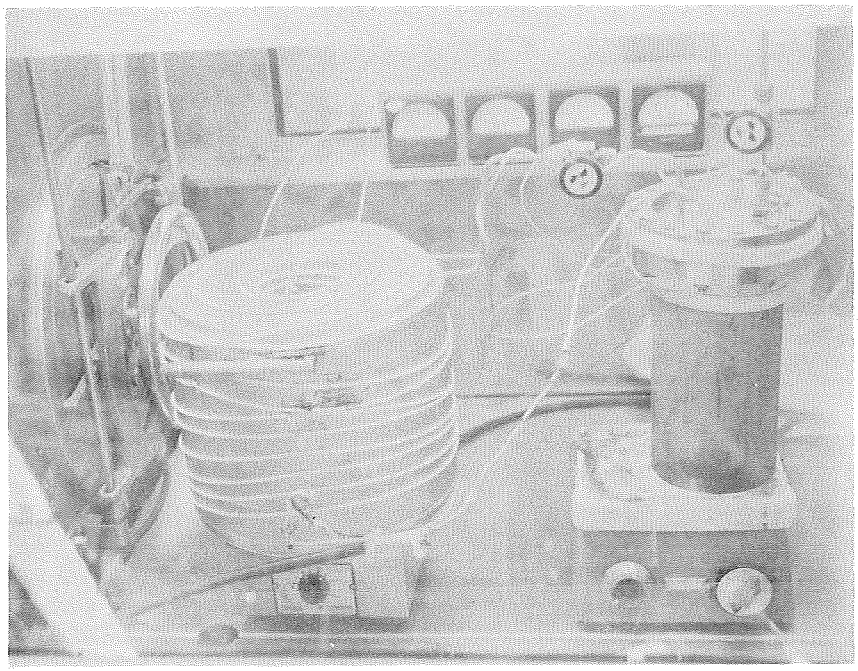

Figure 22. Sodium Loading System

Figures 21 and 22

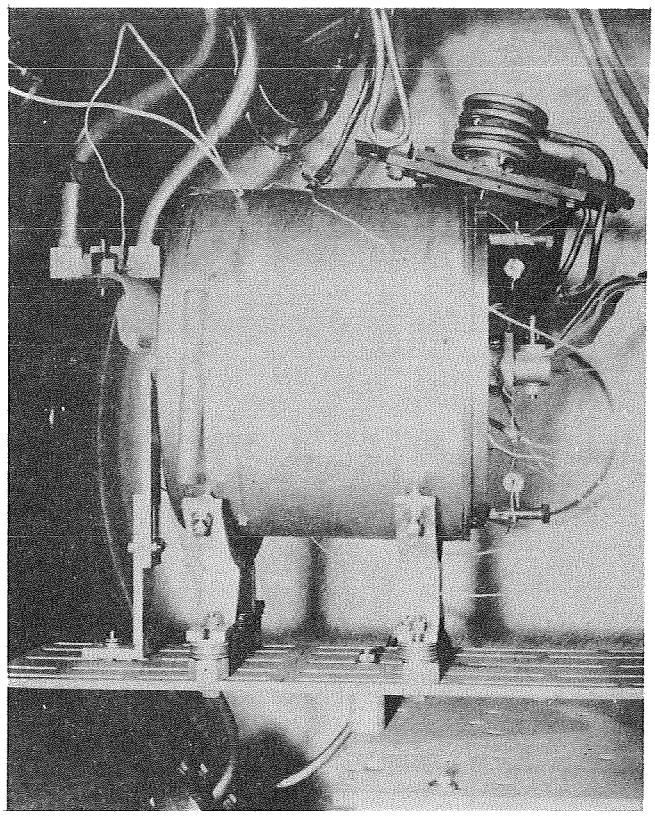

Figure 23. Heat Pipe Thrust Chamber Installed in a Vacuum Bell

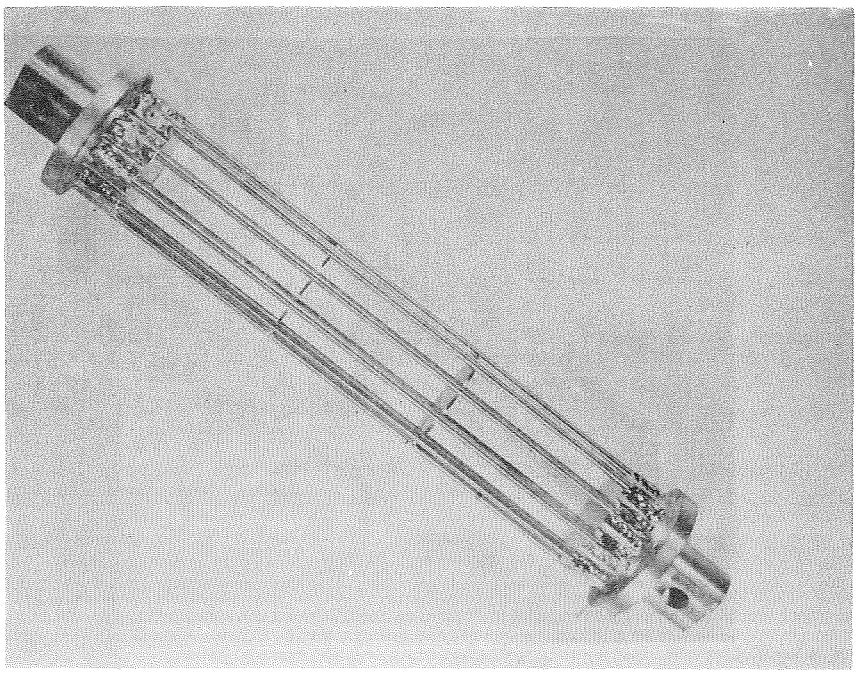

Figure 24. Multi-strand Tungsten Radiation Heater

Figures 23 and 24

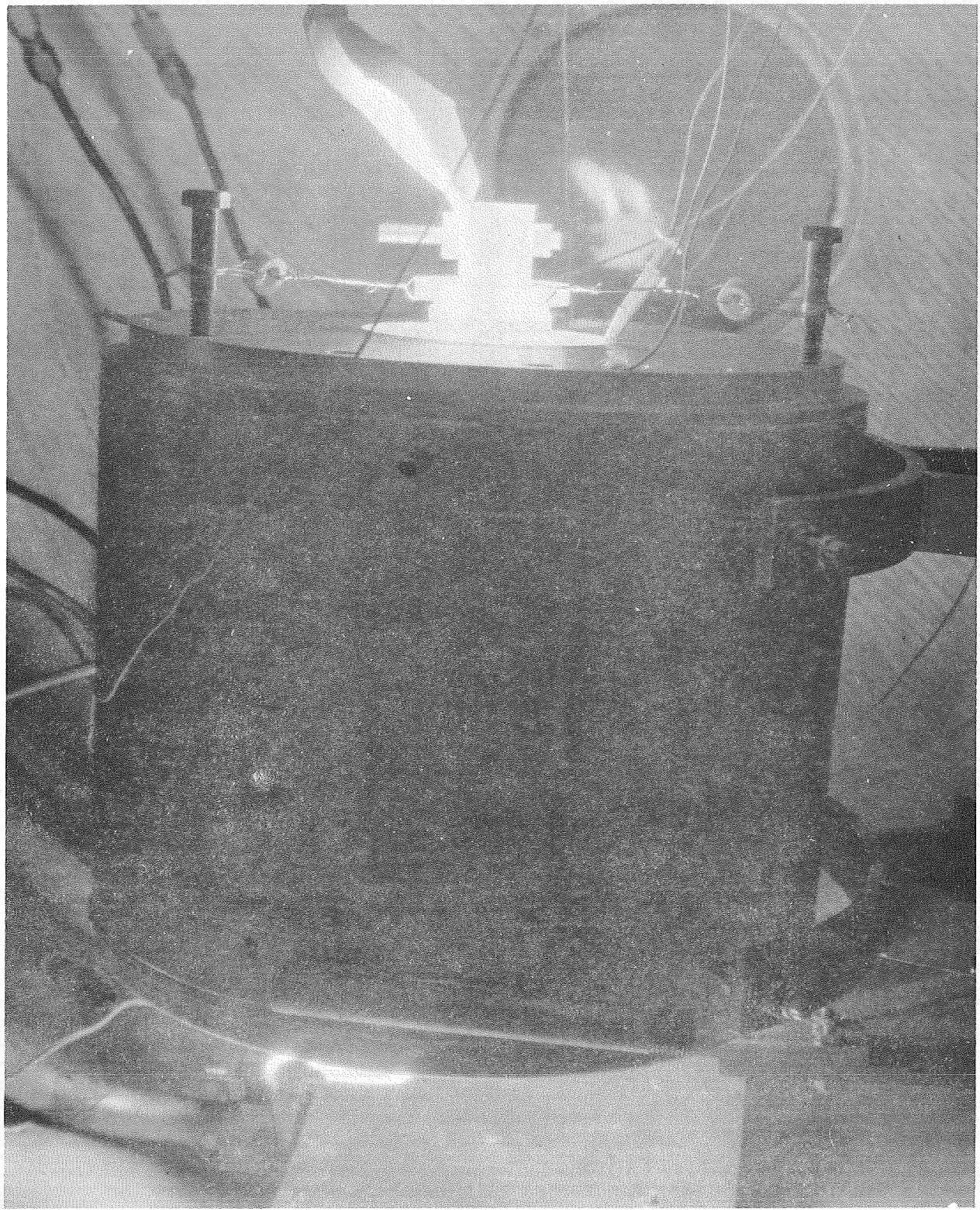

Fabrication Experiment Thrust Chamber Being Processed

Figure 25

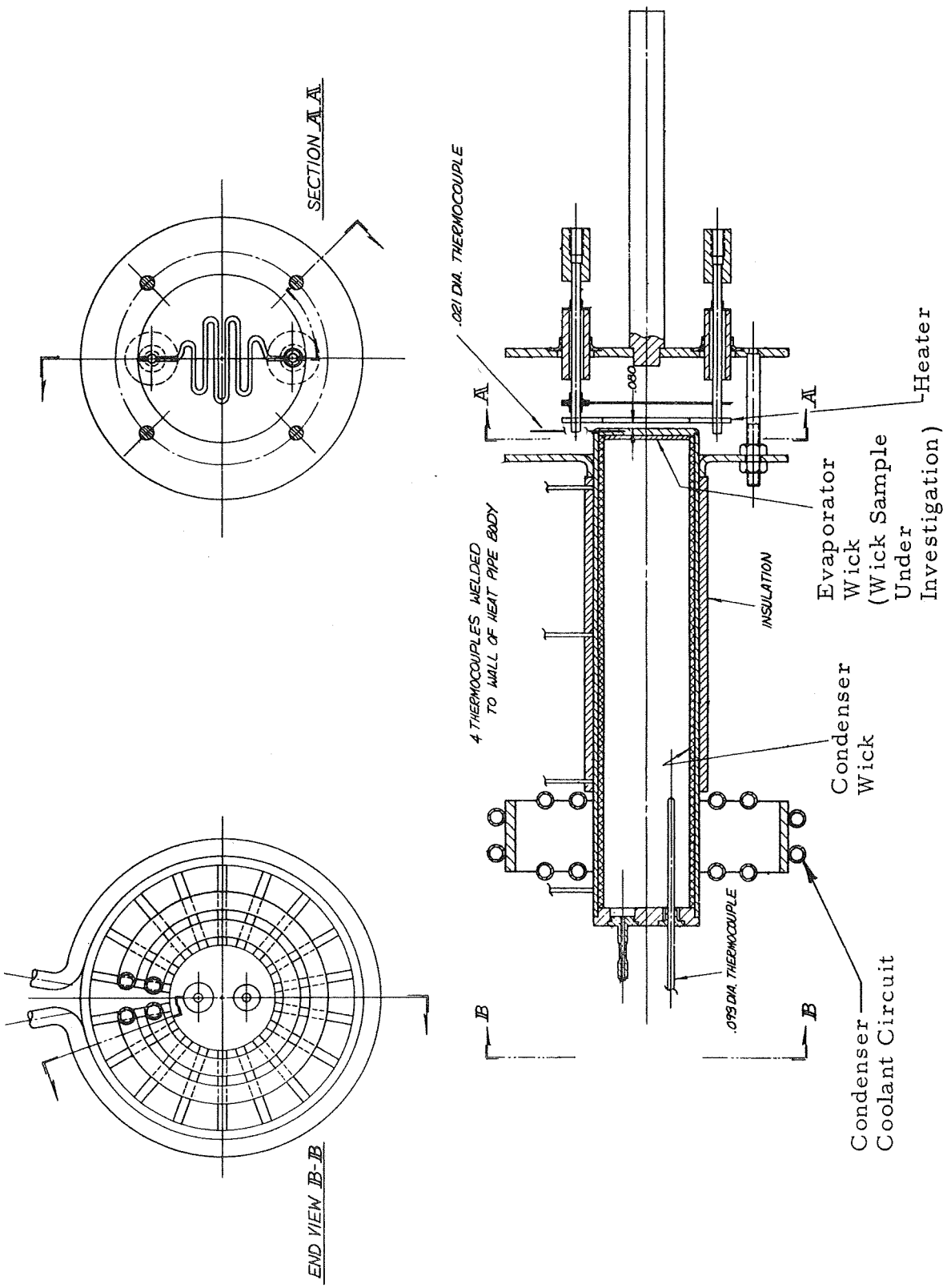

Cylindrical Heat Pipe Test Device, Assembly Drawing

Figure 26

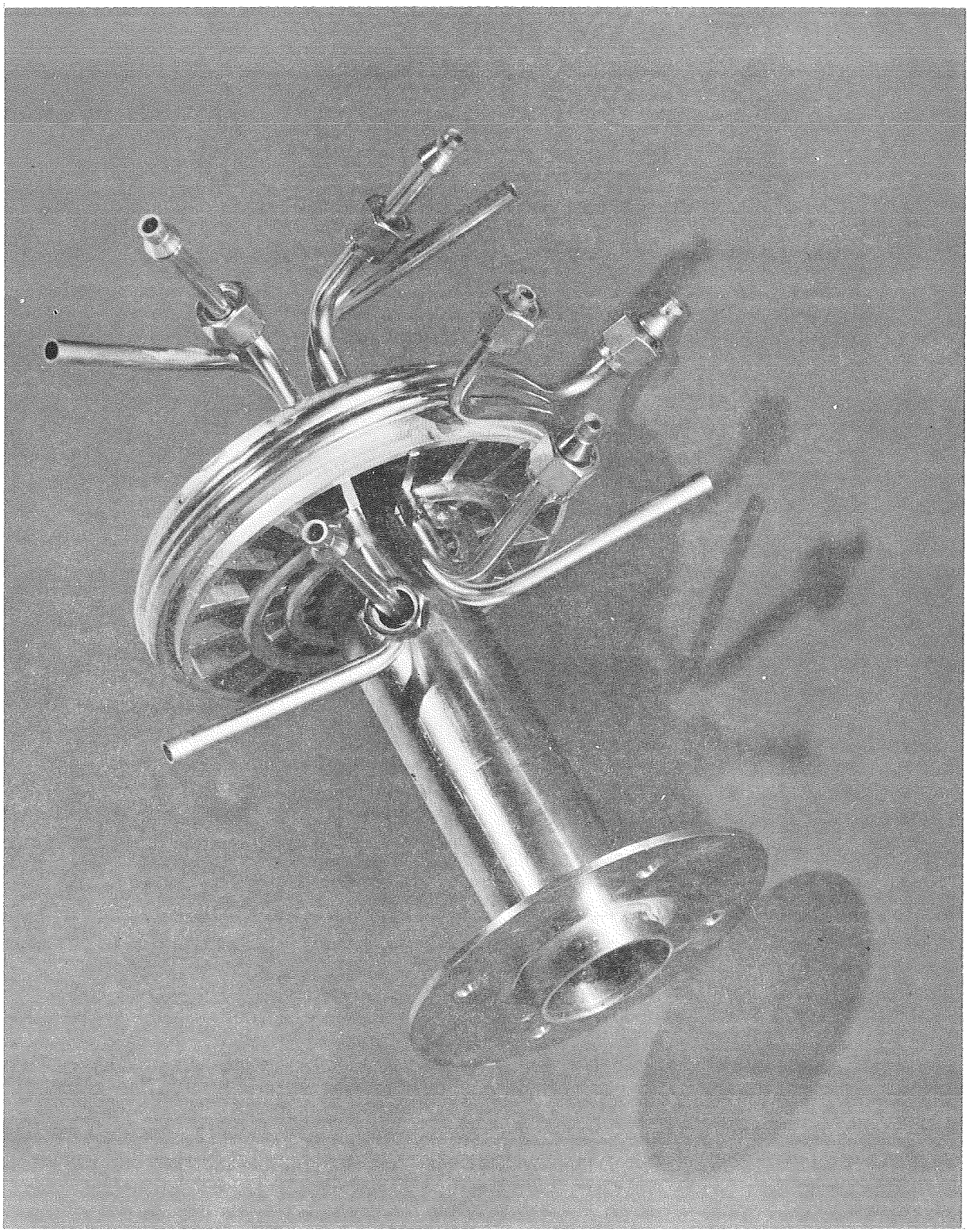

Cylindrical Heat Pipe Test Device (Prior to Installation of Wick Structures and Evaporator Wall)

Figure 27

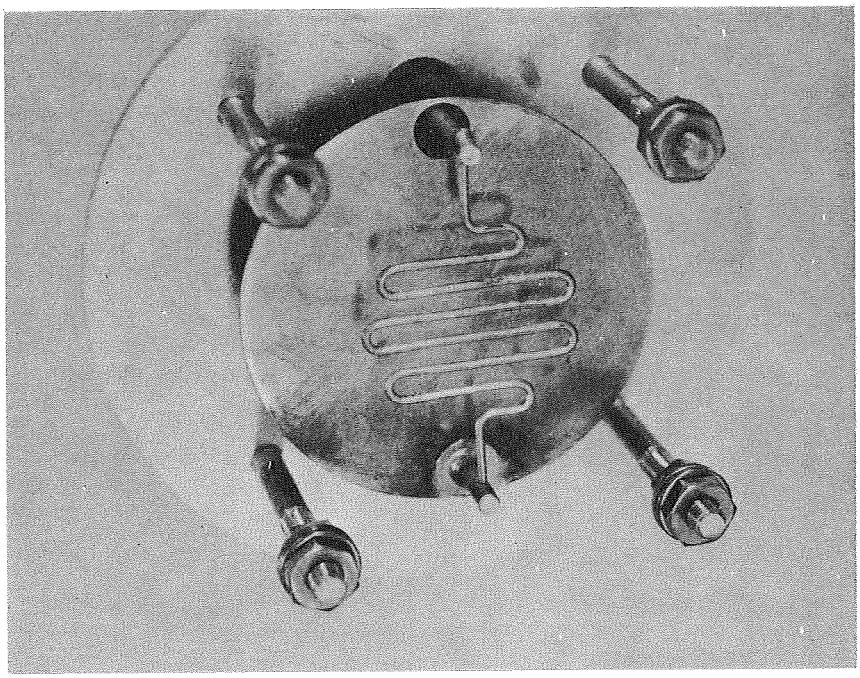

Electron Bombardment Heater

Figure 28

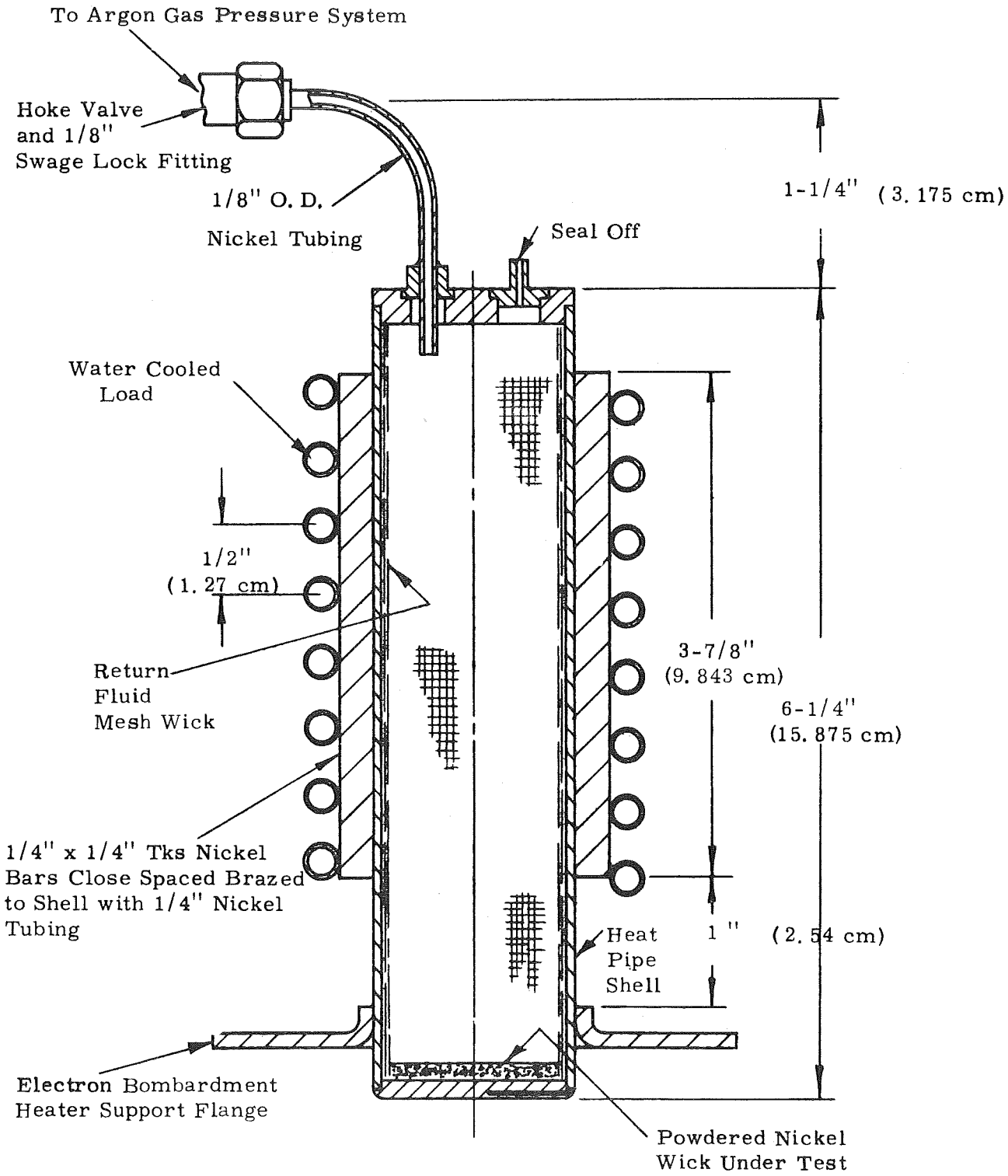

Note: Wick locations same as shown on Figure 26.

Gas-Loaded Cylindrical Heat Pipe Test Device

Figure 29

Filament Geometry - Eight Cells, .396cm spacing, 0.133cm diameter thoriated tungsten 24.56cm length

Filament Characteristics - for thoriated wire with 20% W_2C at 2025° K
Current = 52.5 Amperes
Voltage = 6.10 Volts

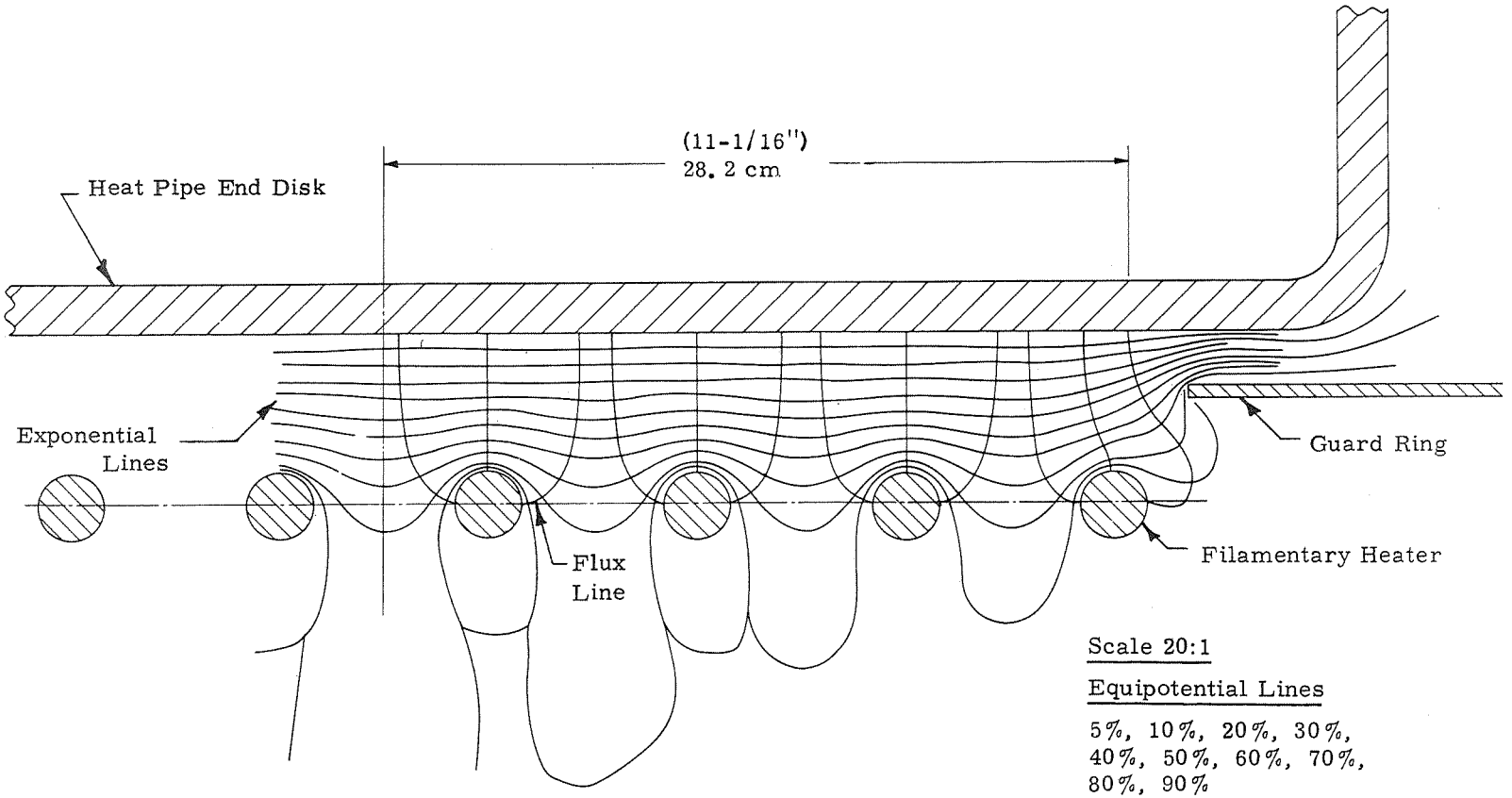

Electrostatic Field Plot of Heating Pattern

Figure 30

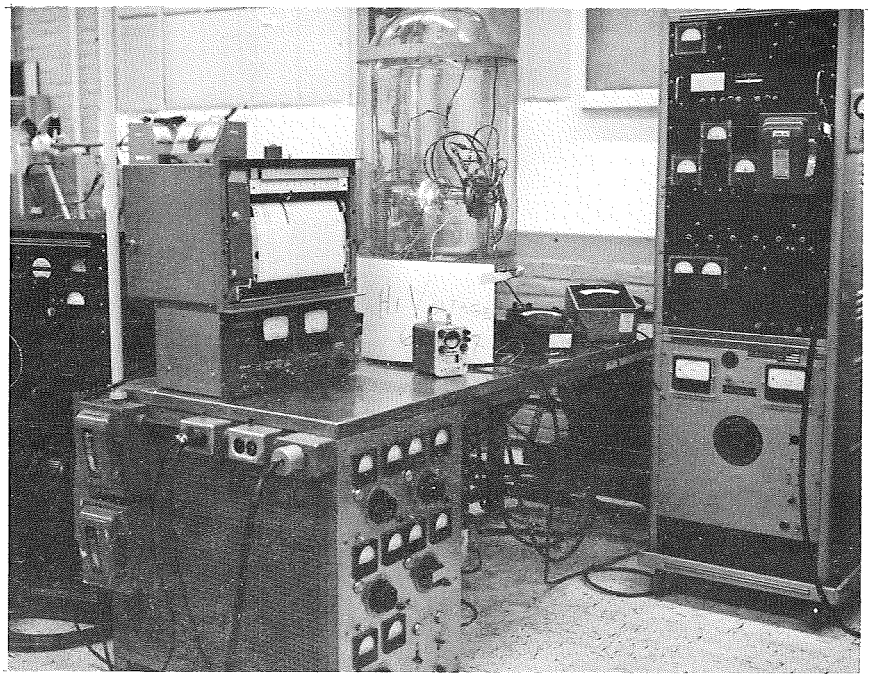

Test Setup

Figure 31

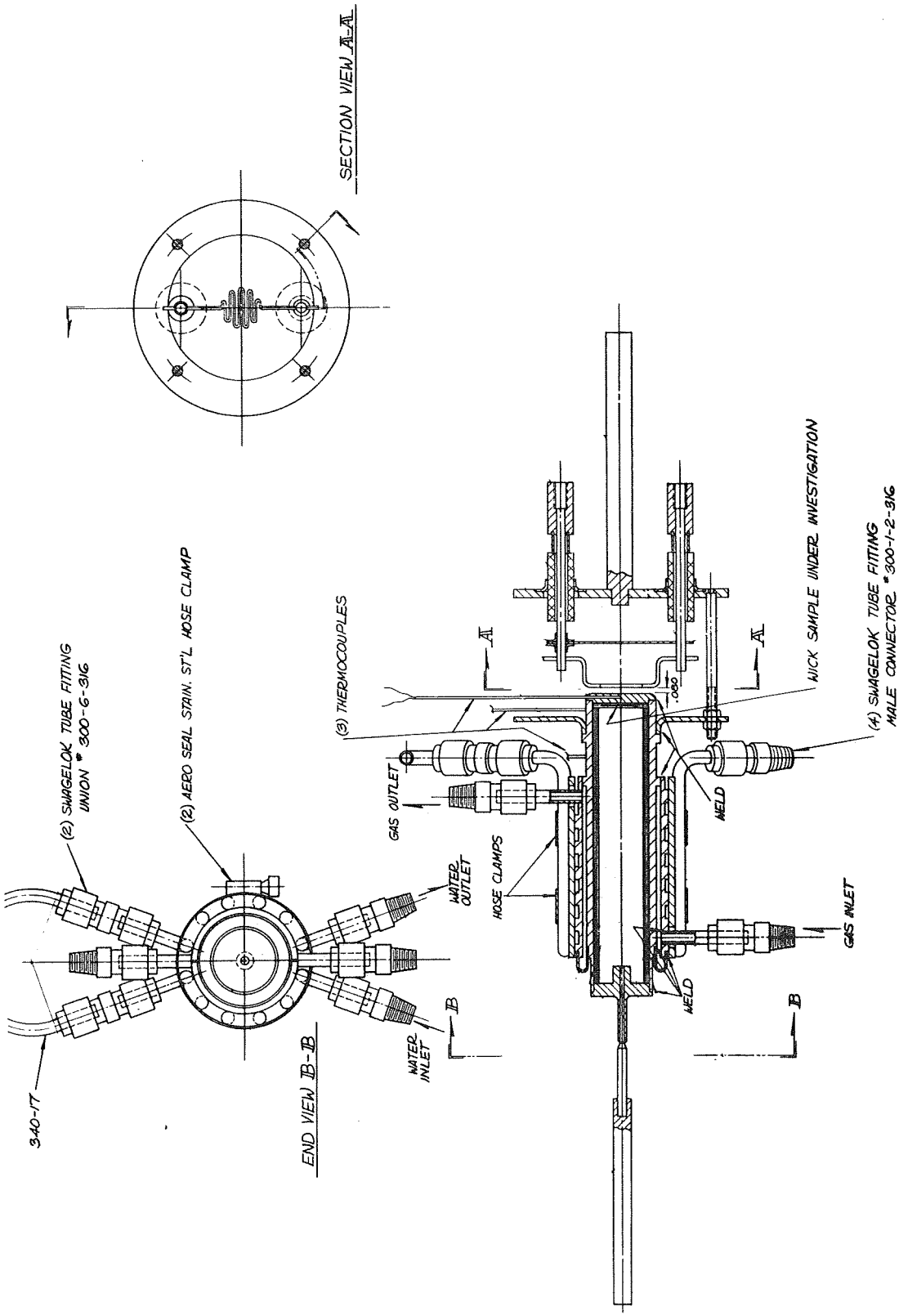

Cylindrical Heat Pipe Test Device for Lithium

Figure 32

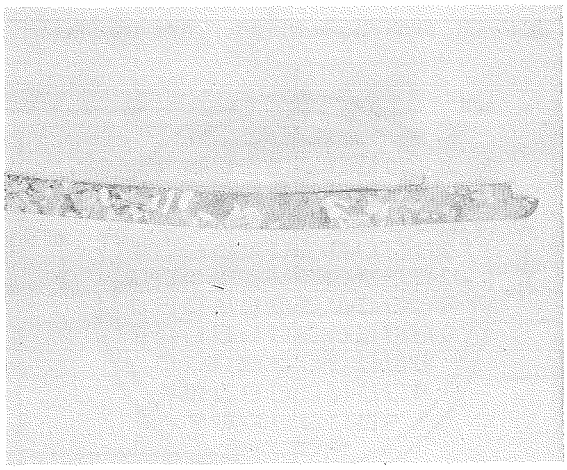

Figure 33. Cross-Section of Heat Pipe No. 1 Evaporator Wall and Wick (Post-Test)

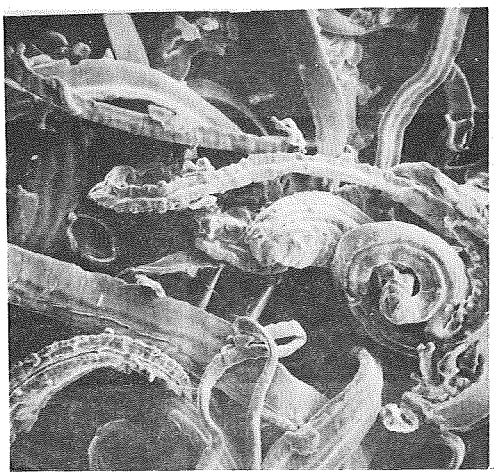

Figure 34. Electron Scan Microscope Photograph of Heat Pipe No. 2 Evaporator Wick Material (Magnification: 500X)

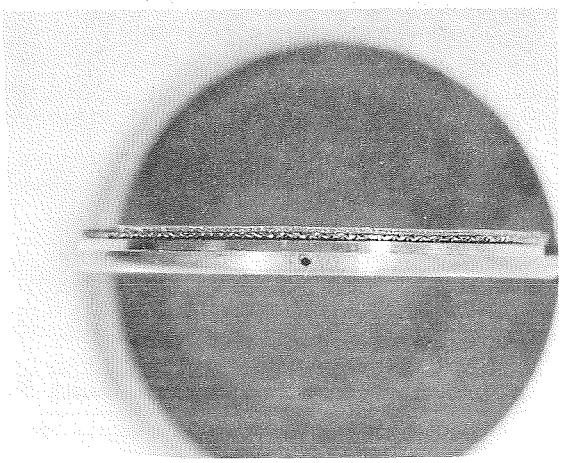

Figure 35. Edge View of Heat Pipe No. 3 Evaporator Wick

Figures 33, 34 and 35

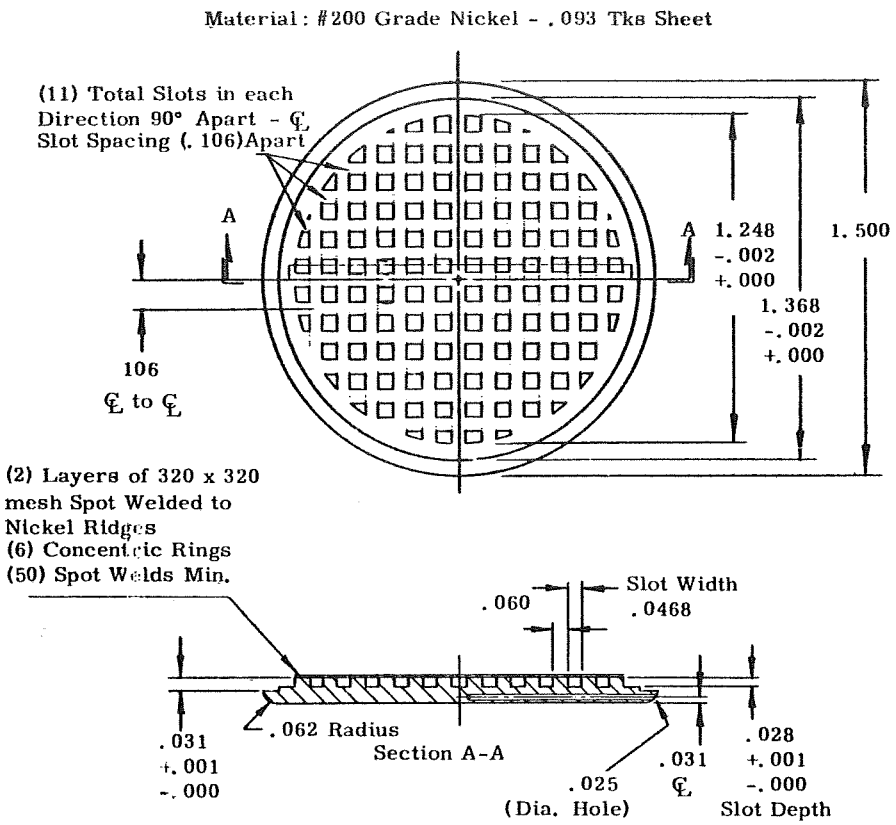

Figure 36. Heat Pipe No. 4 Evaporator Wick

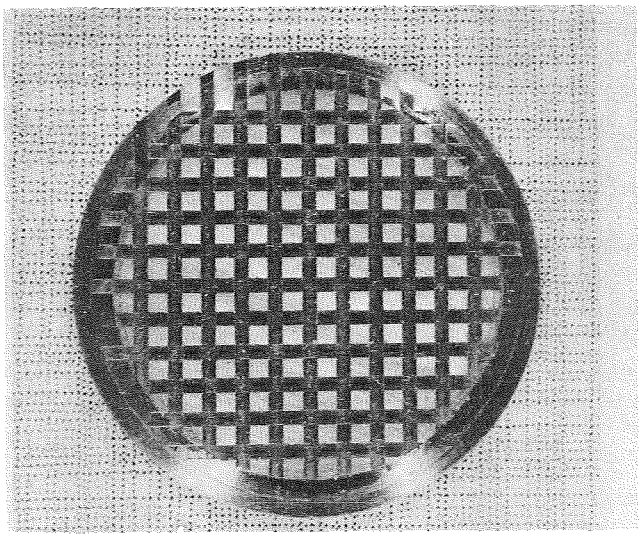

Figure 37. Evaporator Wick Channels, Heat Pipe No. 4

Figure 38. Electron Scan Microscope Photograph of Sintered Nickel Powder Wick Material (Magnification:50X)

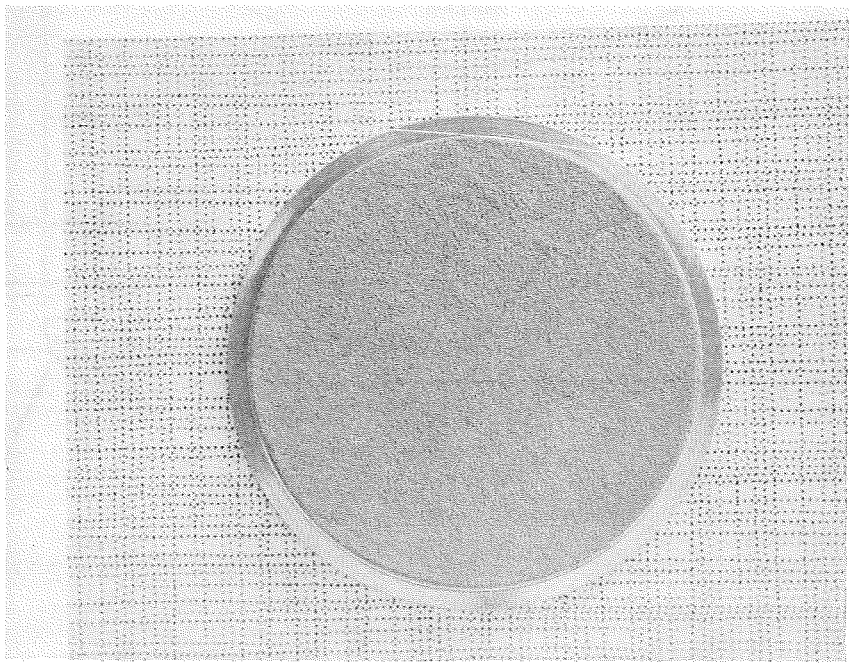

Figure 39. Heat Pipe No. 5 Evaporator Wick (Pre-Test)

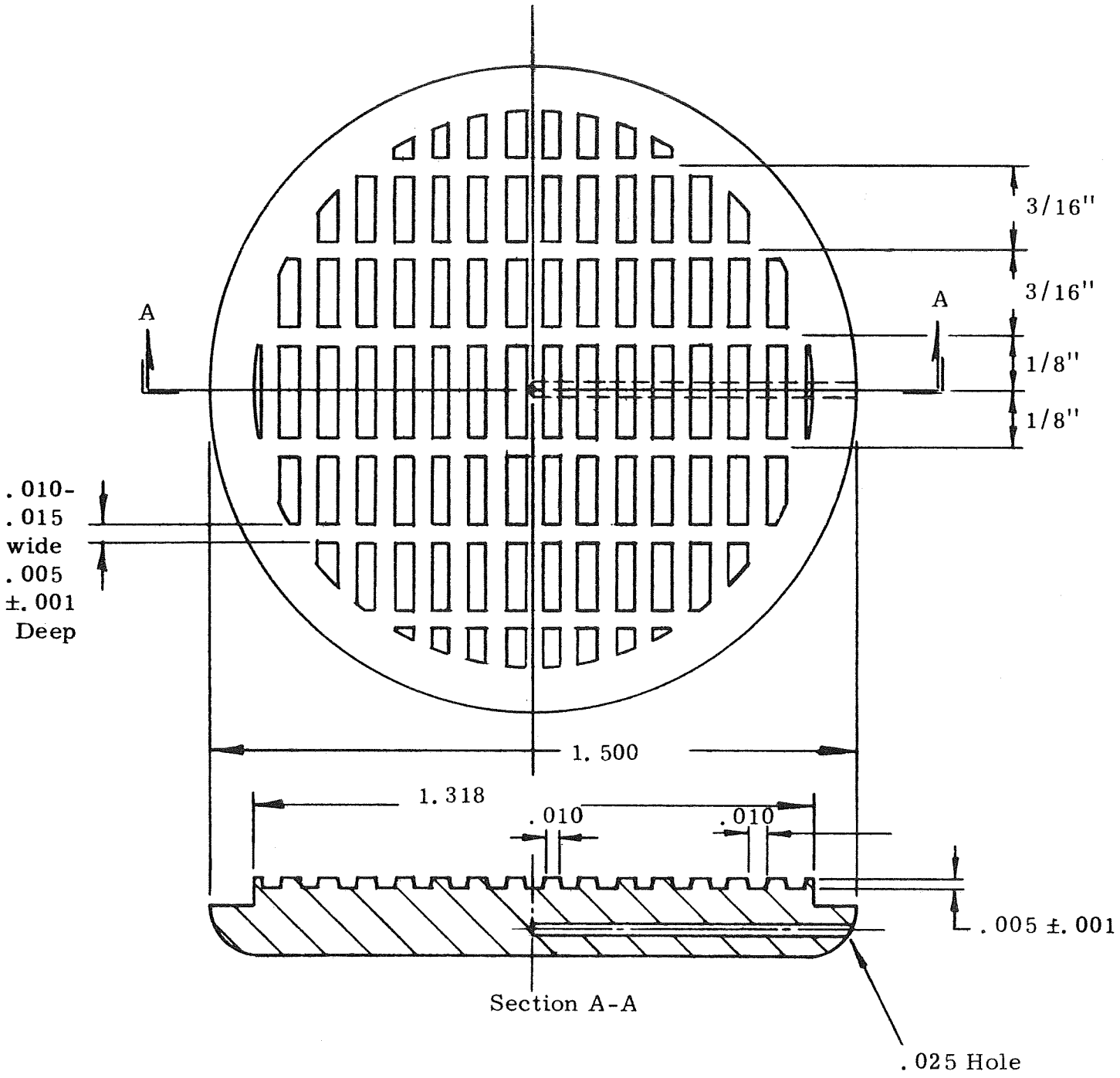

Evaporator Wick Channel Design, Heat Pipe No. 5

Figure 40

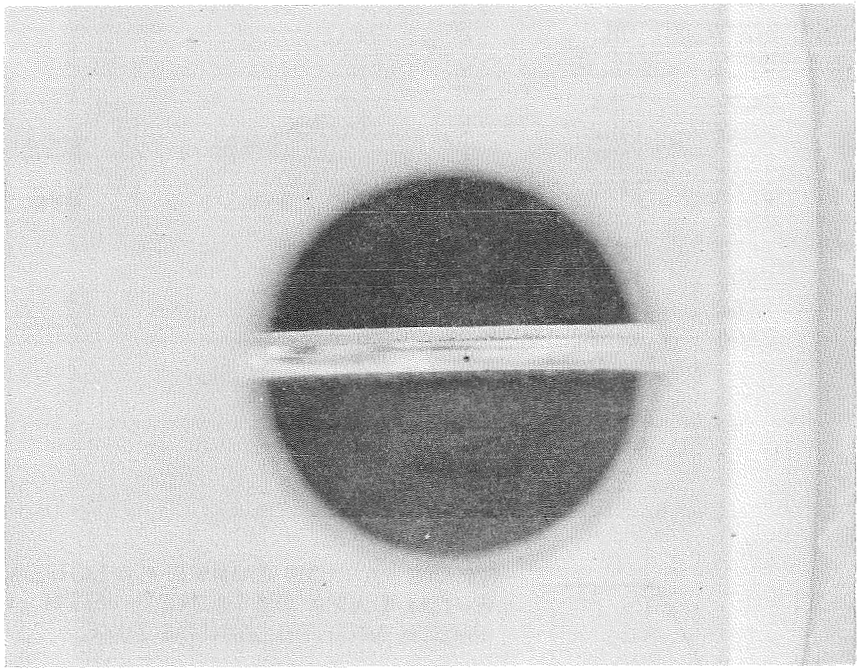

Figure 41. Edge View of Heat Pipe No. 6 Evaporator Wick

Figure 42. Evaporator Wall Burnout, Heat Pipe No. 7

Figures 41 and 42

TEMPERATURE DISTRIBUTION

RADIUS, IN.	TEMP°F	TEMP°C
5/8	2476	1358
1/2	2494	1368
3/8	2536	1391
1/4	2579	1451
0	2611	1433
1/4	2610	1432
3/8	2595	1424
1/2	2556	1402
5/8	2506	1372

$$\frac{(q/A)_{local}}{(q/A)_{ave}} = \frac{(T^4)_{local}}{(T^4)_{ave}}$$

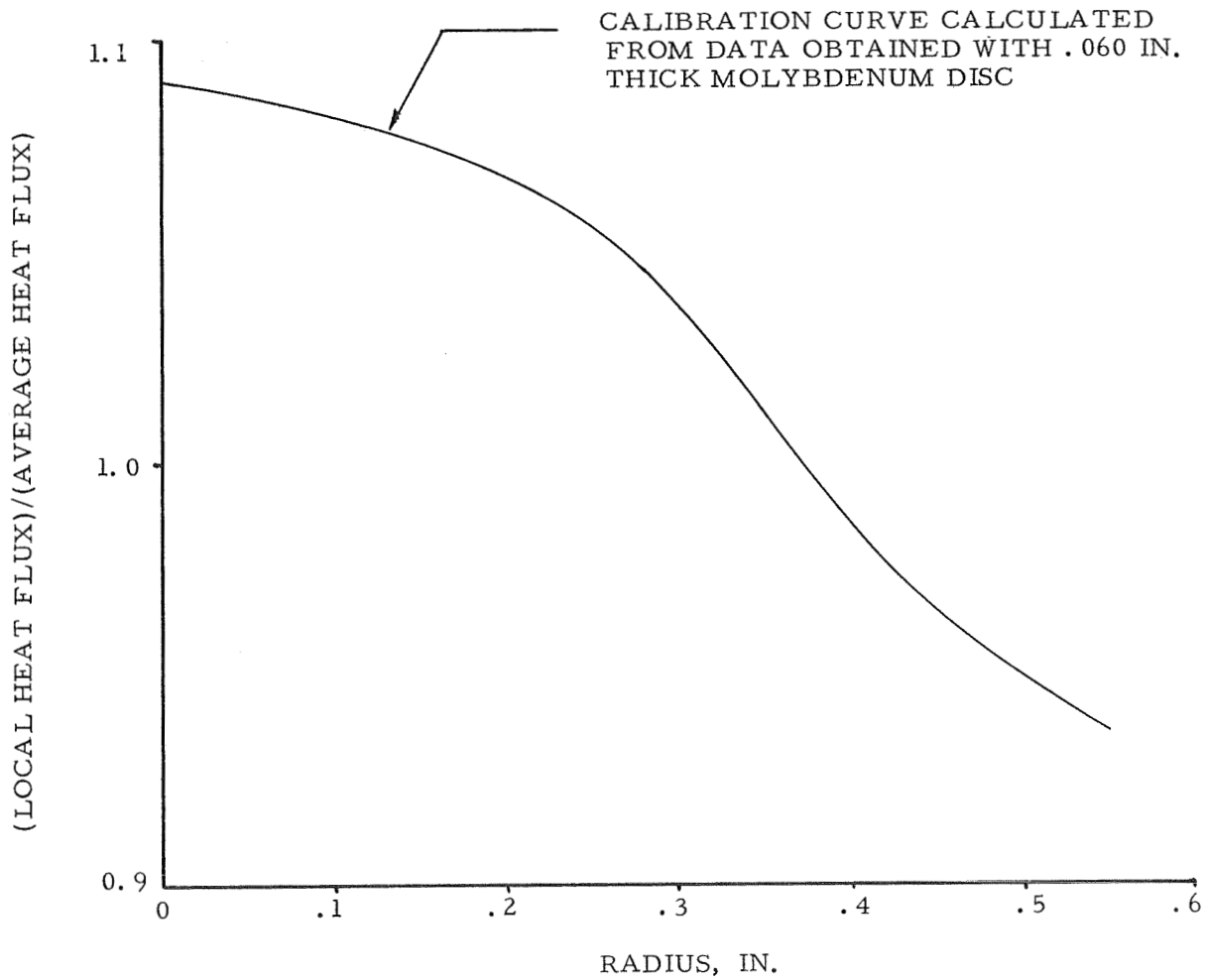

Evaporator Heat Flux Distribution

Figure 43

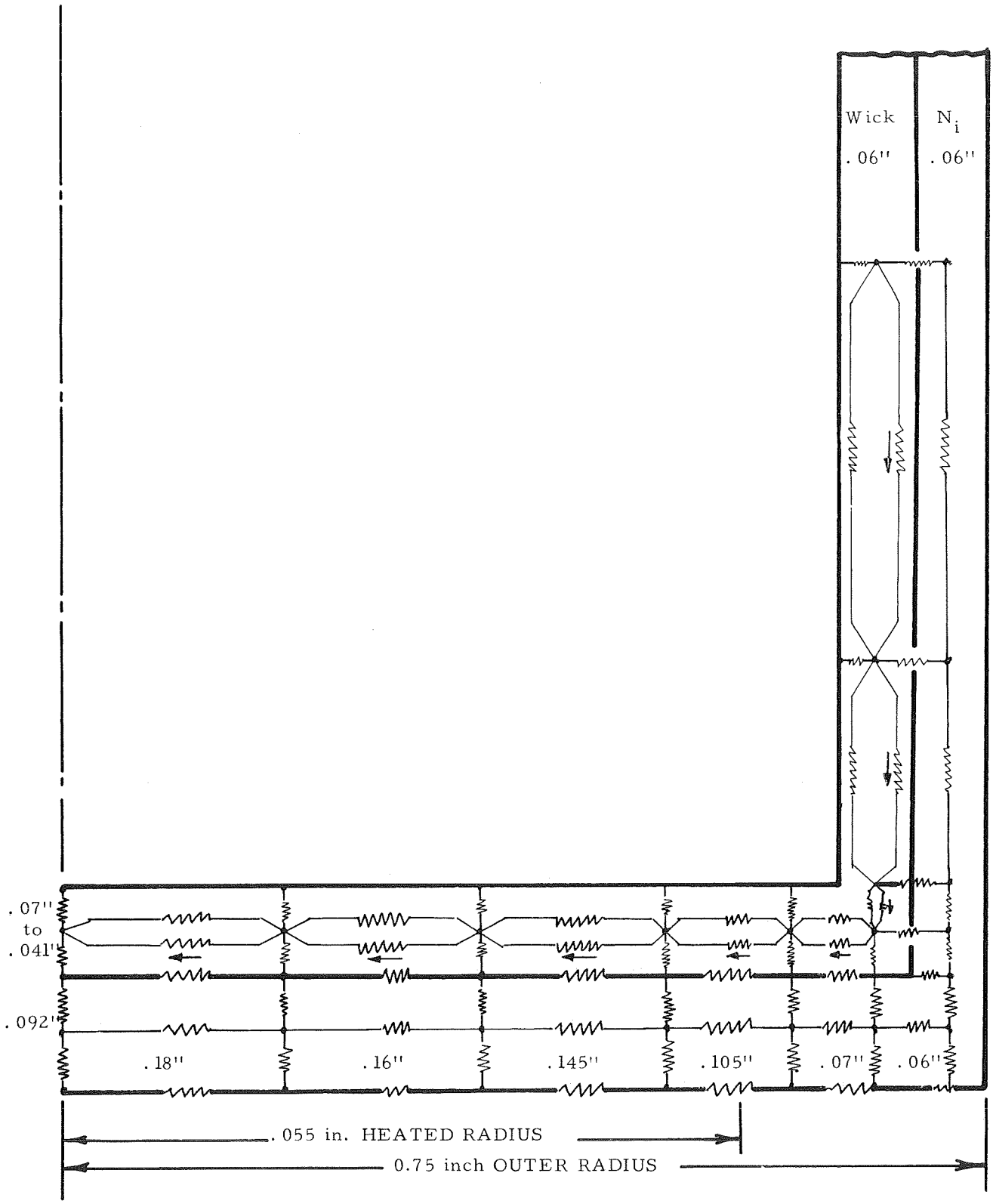

Two-Dimensional Conduction Network

Figure 44

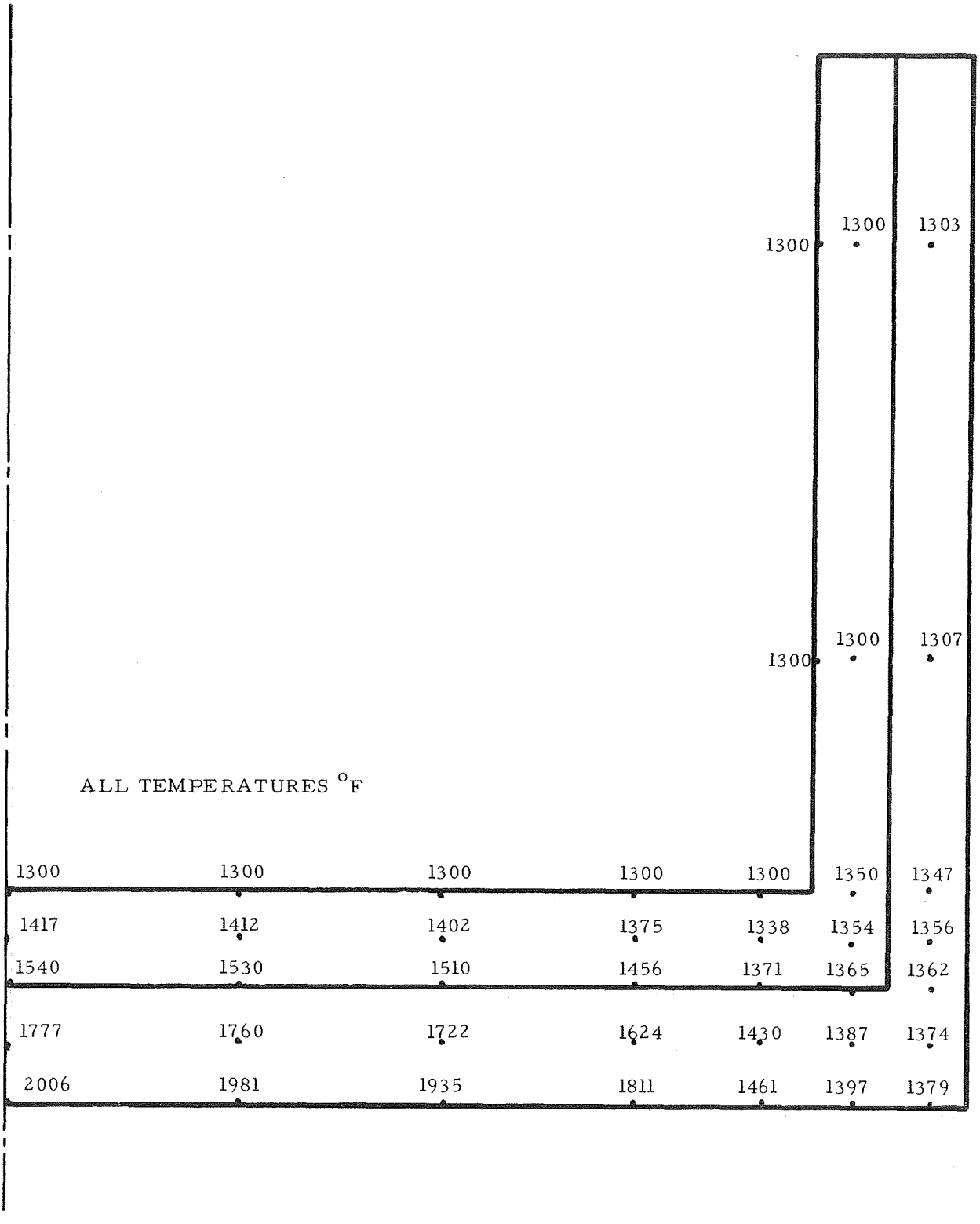

Calculated Temperature Distribution at Maximum Heat Flux,
Heat Pipe No. 5

Figure 45

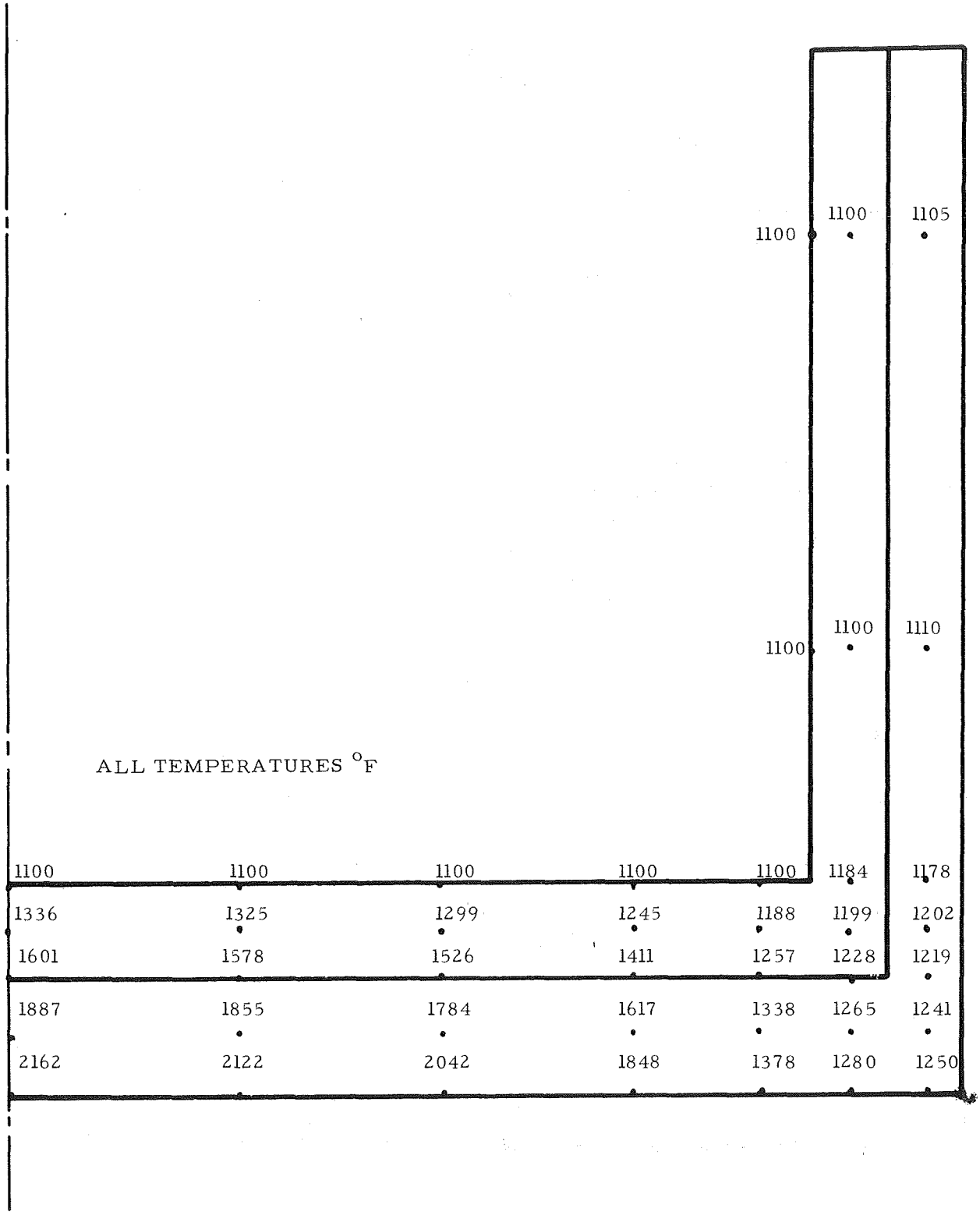

Calculated Temperature Distribution at Maximum Heat Flux,
Heat Pipe No. 7

Figure 46

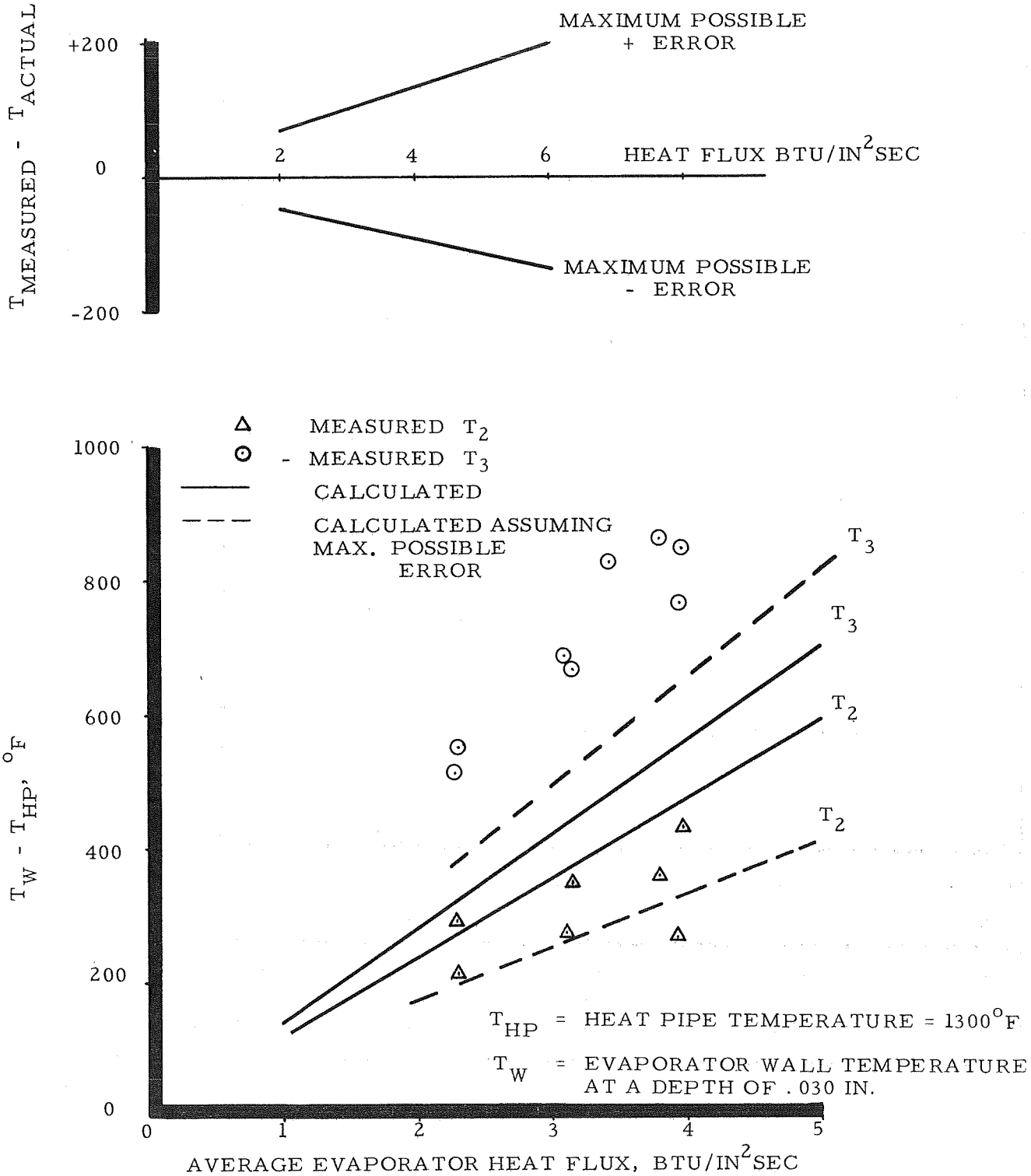

Comparison of Calculated and Measured Wall Temperatures,
Heat Pipe No. 5

Figure 47

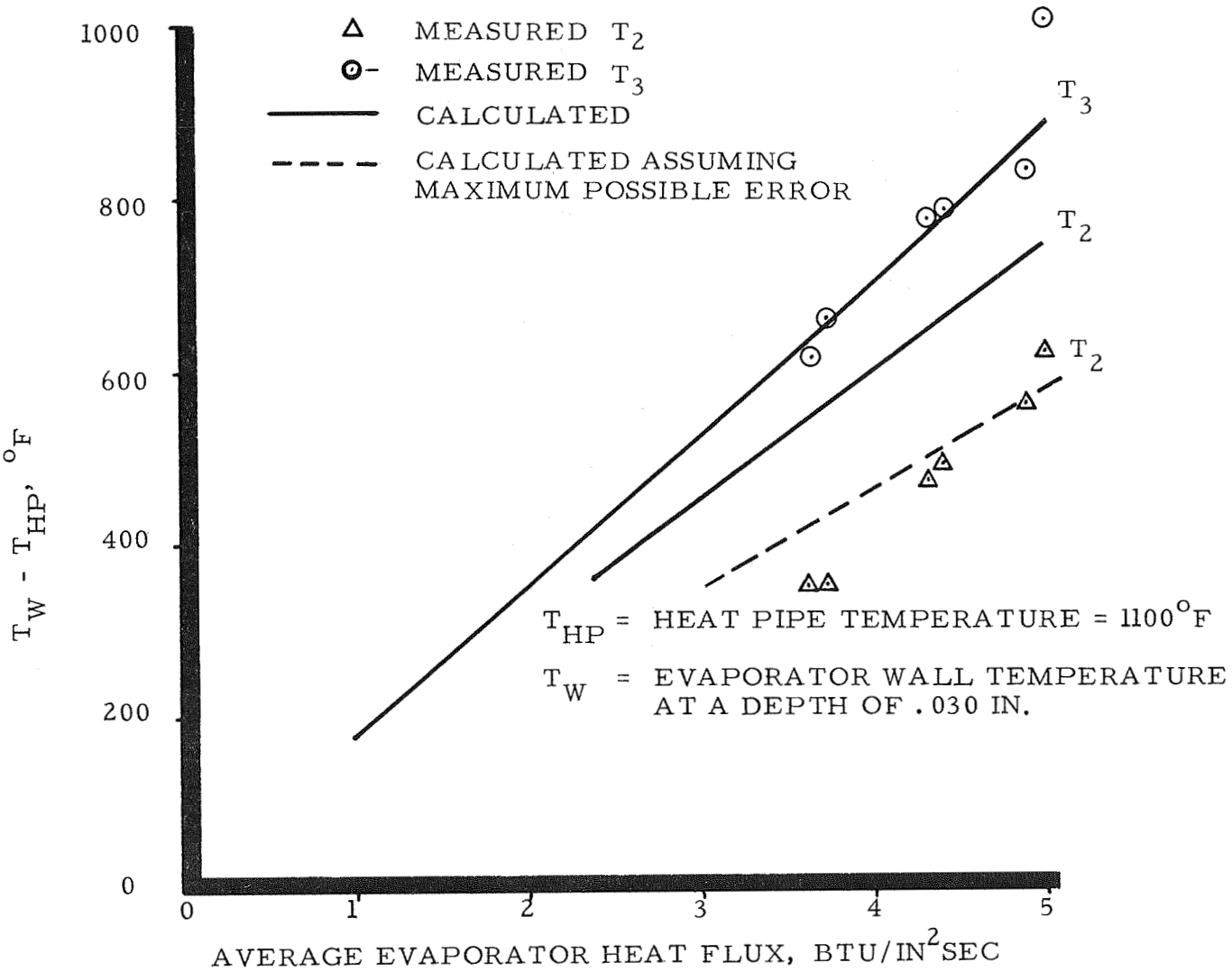

Comparison of Calculated and Measured Wall Temperatures, Heat Pipe No. 7

Figure 48

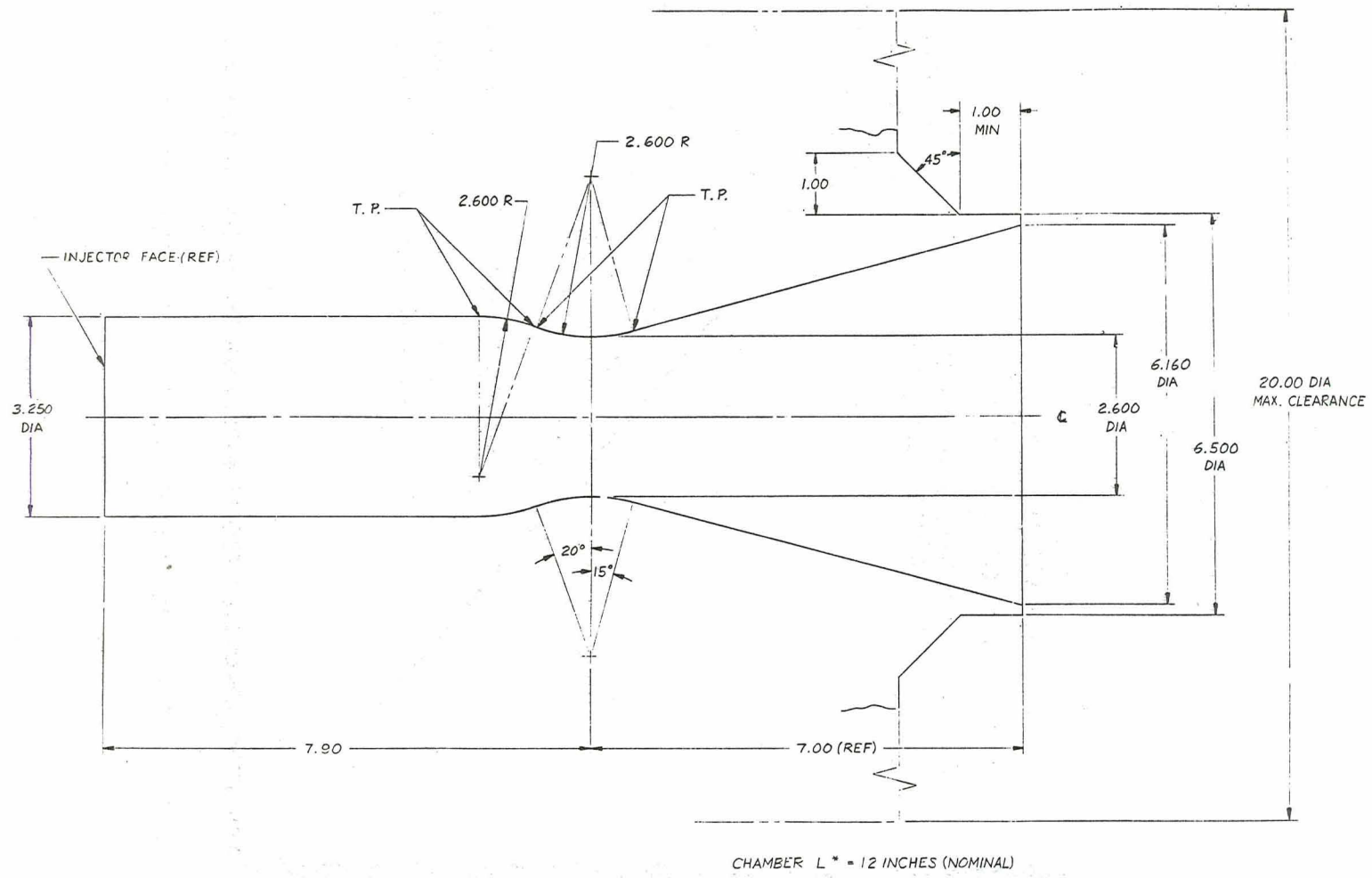

Figure 49

Internal Contour for Working Model Design Thrust Chamber

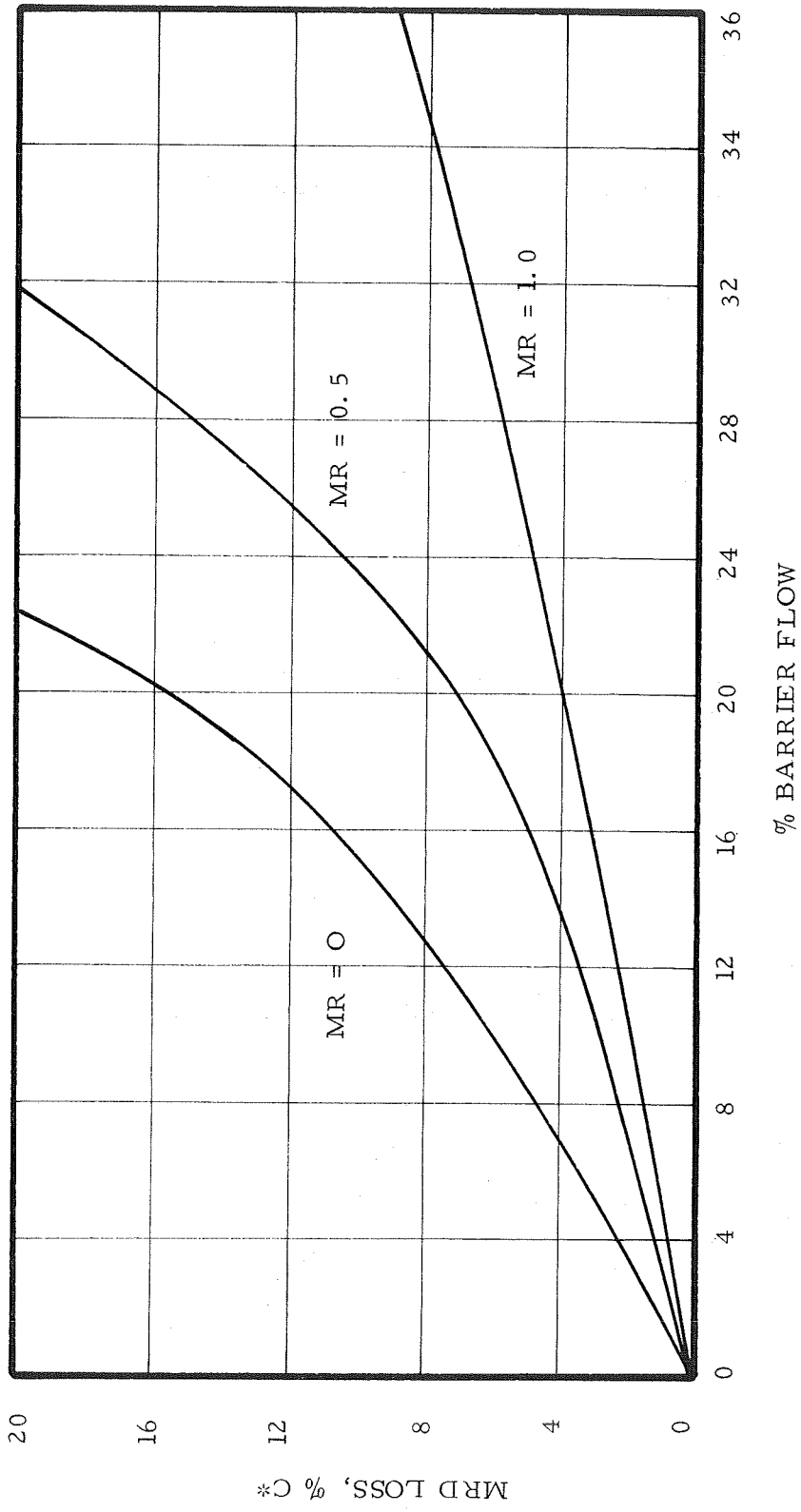

Figure 50

Performance Losses Due to Boundary Cooling

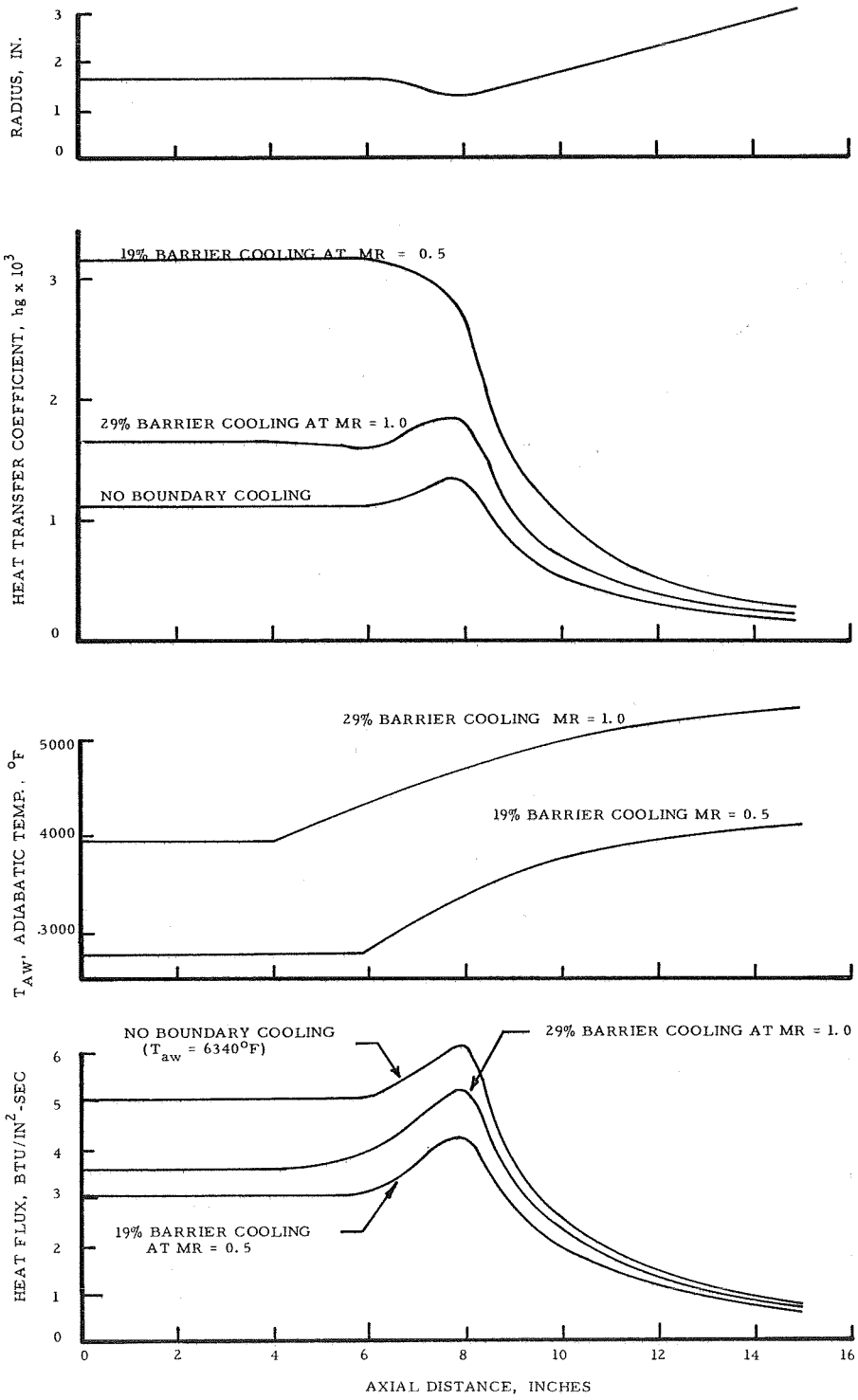

Heat Flux, Heat Transfer Coefficient, and Adiabatic Wall Temperature Distribution

Figure 51

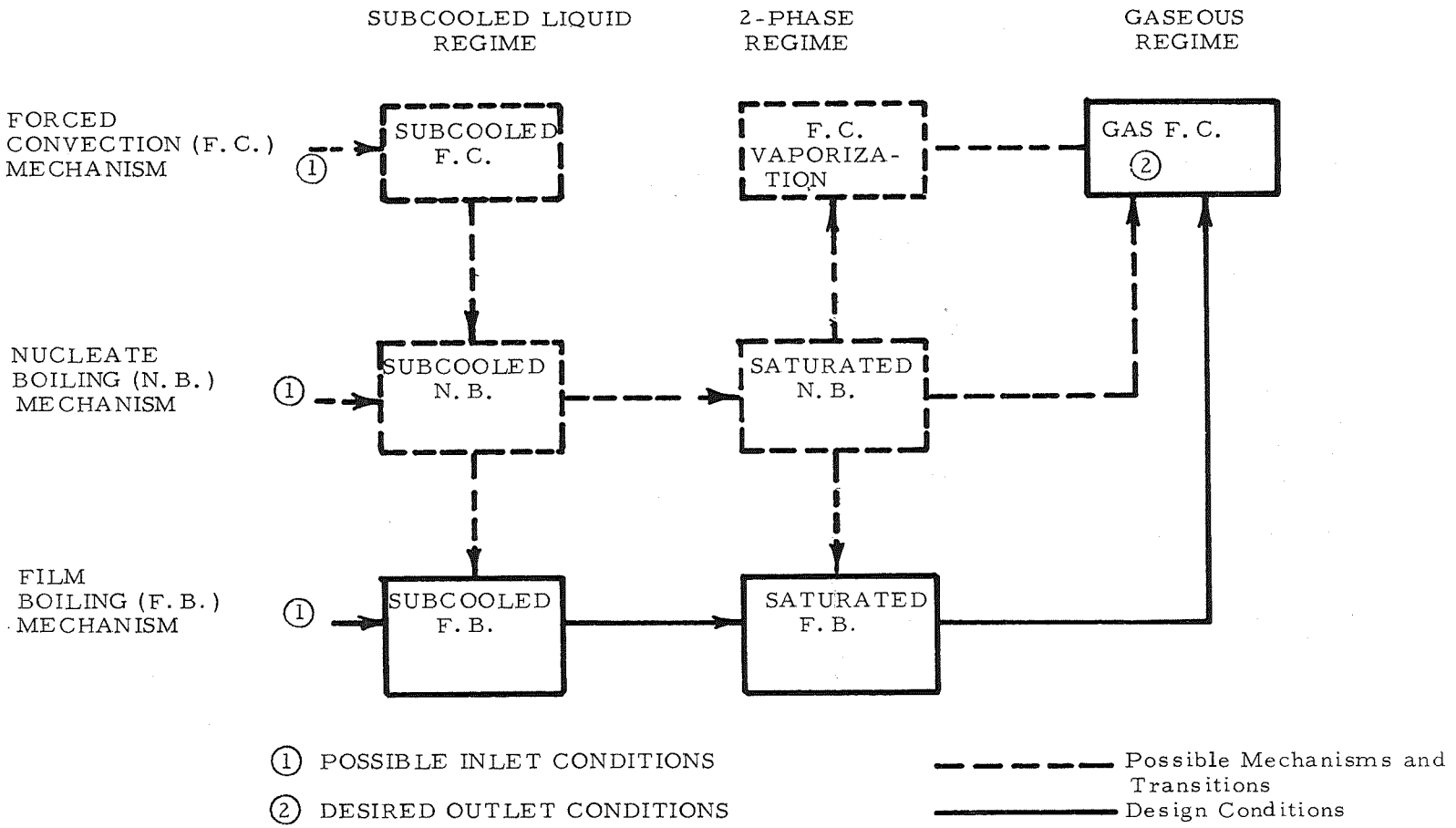

Coolant Side Heat Transfer Mechanisms

Figure 52

Report 697-I

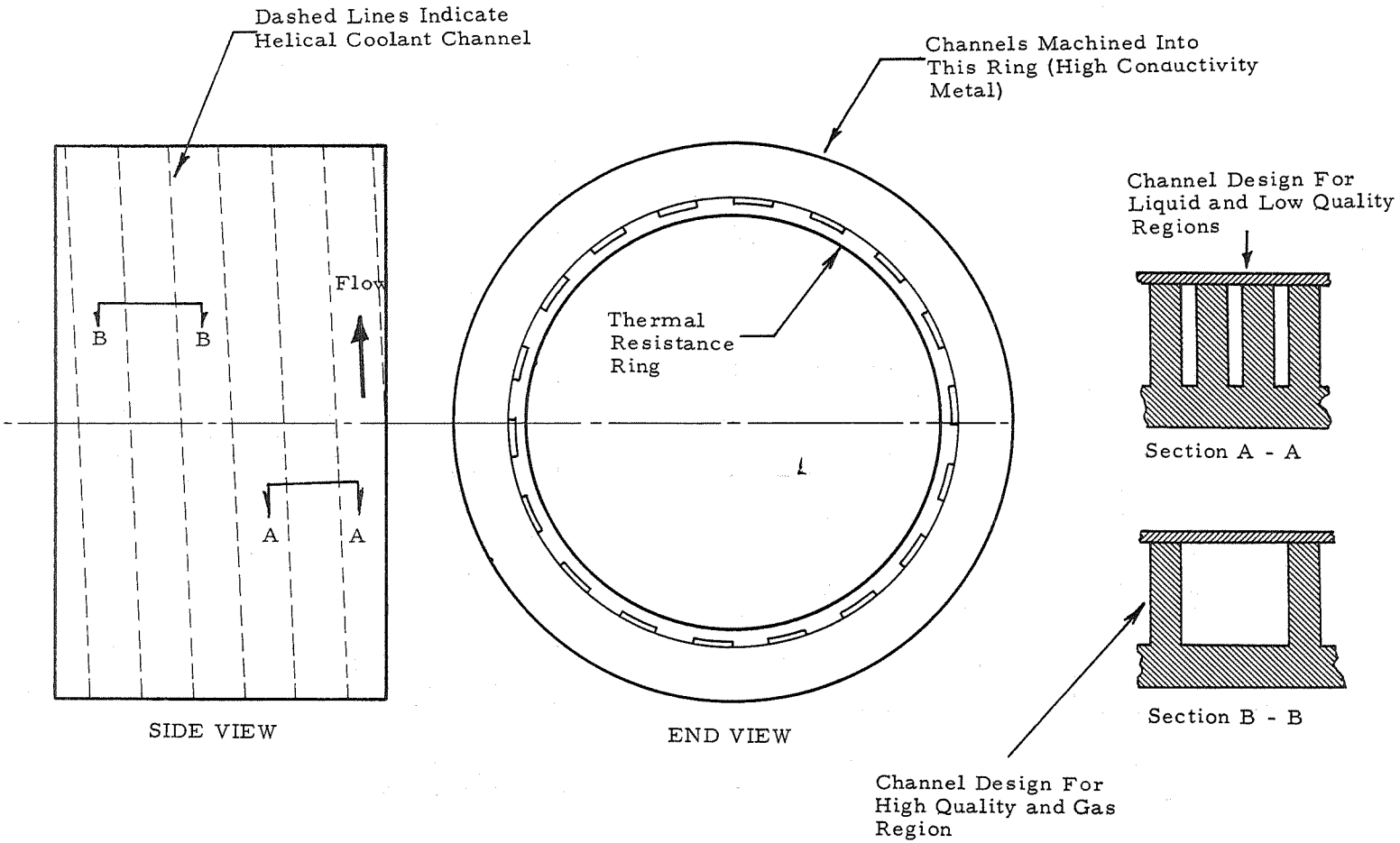

Conceptual Cooling Jacket Design

Figure 53

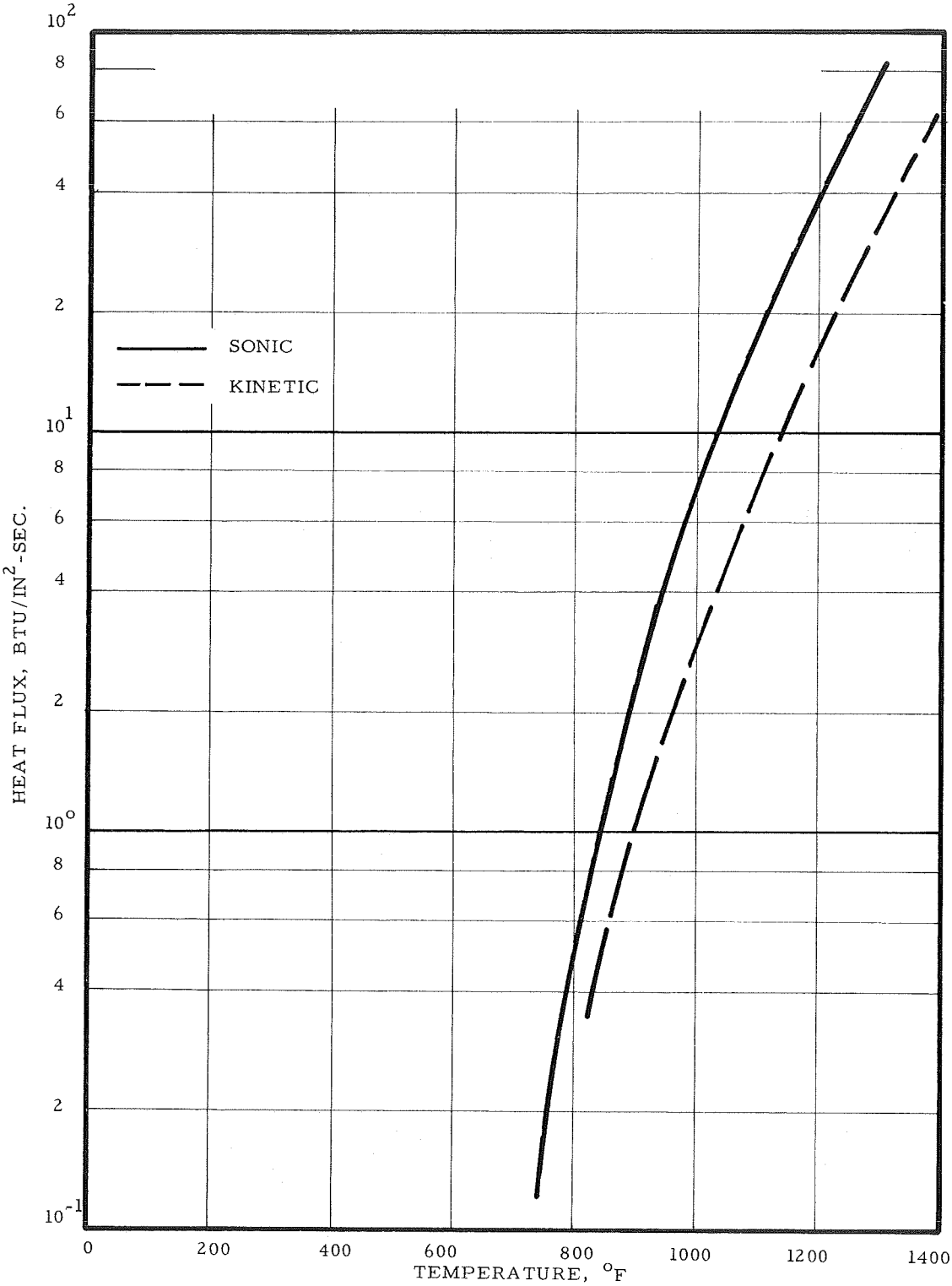

Sodium Heat Pipe Limits at Low Temperature

Figure 54

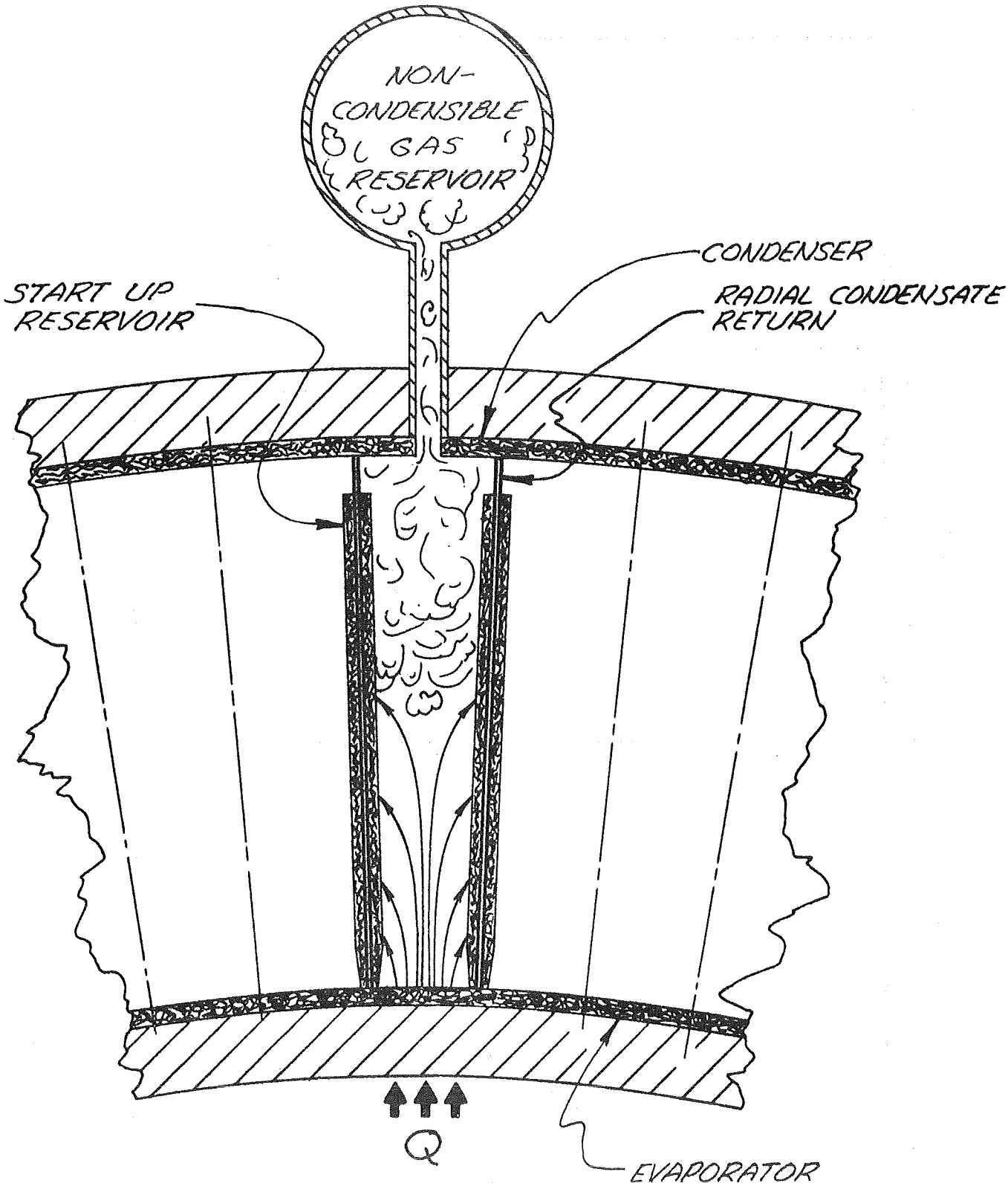

Cold Start Design Concept

Figure 55

Appendix A

HEAT PIPE BIBLIOGRAPHY

This bibliography was prepared as part of Task I and consists of five parts which are described below.

Part 1: Literature published by government agencies, corporations, and universities or colleges in the United States.

Part 2: Articles contained in technical journals, periodicals, and books.

Part 3: Papers presented at technical conferences.

Part 4: Publications in foreign countries.

Part 5: Patents relevant to heat pipes.

Report 697-I, Appendix A

HEAT PIPE BIBLIOGRAPHY

Part 1: AGENCIES/CORPORATIONS/UNIVERSITIES

AEROJET-GENERAL CORPORATION
San Ramon, California

Thermophysical and Heat Transfer Properties of Alkali Metals, P. Y. Achener and Others, Nuclear Division, San Ramon, California, AGN-8195, Volumes I and II. (CA 69:110579c).

AEROSPACE CORPORATION
El Segundo, California

Determining the Wicking Properties of a Compressible Material for Heat Pipe Application, R. A. Farran and K. E. Starner, TR-0158 (3240-10)-11, April 1968.

ARGONNE NATIONAL LABORATORY
Argonne, Illinois

The Prediction of Liquid Superheats Required for Initiation of Nucleate Boiling in Liquid Metals, R. E. Holtz, ASME Paper 64-NA/HT-31, 1964.

Effect of Pressure - Temperature History Upon Incipient Boiling Superheats in Liquid Metals, R. E. Holtz, ANL-7184, June 1966 (CA 67:5958M).

On the Superheating of Sodium at Low Heat Fluxes, R. E. Holtz, R. M. Singer, ANL-7383, November 1967 (CA 69:78726k)

BOEING COMPANY
Huntsville, Alabama

Survey of Heat Pipes, M. E. Schlapbach, Report No. D5-13432, February 1968, AD-838 675L.

GENERAL ELECTRIC COMPANY
Cincinnati, Ohio

Fabrication and Test of an Aluminum Heat Pipe, Memo Report HTC-7, February 1967.

HITTMAN ASSOCIATES, INC
Baltimore, Maryland

The Mattrac Module Feasibility Study, M. B. Eck, Final Tech. Report No. HIT-269, Contract DAAK02-67-C-0065, November 1967 (Conf.) have DDC abstract).

JET PROPULSION LABORATORY
Pasadena, California

The Heat Pipe and Its Operation, J. Schwartz, Report 701-21, January 1969.

JOHN HOPKINS UNIVERSITY
Baltimore, Maryland

Controllable Heat Pipe Experiment, T. Wyatt, Applied Physics Laboratory, Report SDO-1134, March 1965.

The Geos-2 Heat Pipe System and its Performance in Test and in Orbit, Applied Physics Lab Report S20-3-25, 29 April 1968.

Heat Pipe Application for Spacecraft Thermal Control, Applied Physics Lab Technical Memo TG-922, AD 662-241, August 1967.

LAWRENCE RADIATION LABORATORY
Livermore, California

Advanced Space Nuclear Power Program, Quarterly Report for April-June 1966, UCRL 50004-66-2.

Advanced Space Nuclear Power Program, Quarterly Report for October-December 1966, UCRL 50004-66-4.

Advanced Space Nuclear Power Program, Quarterly Report for January through March 1967, UCRL 50004-67-1.

Advanced Space Nuclear Power Program, Quarterly Report for July through September 1967, UCRL 50004-67-3 (Part 1).

Advanced Space Nuclear Power Program, Quarterly Report for January through March 1968, UCRL 50004-68-1 (Part 1).

A Critical Review of Heat Pipe Theory and Applications, H. Cheung, UCRL 50453, July 1968.

Conceptual Design of a 10 MWe Nuclear Rankine System for Space Power, J. H. Pitts and C. E. Walker, UCRL 50382, January 1968.

Concept For a Gas Buffered Annular Heat Pipe Fuel Irradiation Capsule, R. W. Werner and J. D. Lee, UCRL 50510.

Heat Pipe Radiation Design, G. A. Carlson, Contract W-7405-ENG-48, Report AEC UCID-15165, June 1967. (NSA 21:34399)

Heat Pipe Radiator for a 50-MW and Space Power Plant, R. W. Werner and G. A. Carlson, Contract W-7405-ENG-48, Report AEC UCRL 50294, 30 June 1967.

Out of Core Thermionic Space Power, W. E. Loewe, UCRL 70816, March 1968.

Reactivity Self-Control on Power and Temperature in Reactors Cooled by Heat Pipes, V. E. Hampel and R. P. Koopman, UCRL 71198, November 1968.

LOS ALAMOS SCIENTIFIC LABORATORY
Los Alamos, New Mexico

Advances in Heat Pipe Technology, G. M. Grover, et al., LA-DC-9619, June 1968.

The Effect of Vibration on Heat Pipe Performance, J. E. Deverall, Report AEC LA-3798, 4 October 1967. (NSA 22:4399)

Heat Pipe Capability Experiments, J. E. Kemme, Report LA-3585-MS, October 1967.

Heat Pipe Design Considerations, J. E. Kemme, LA-4221-MS, August 1969.

Heat Pipe Performance in a Space Environment, J. E. Deverall and E. W. Salmi, LA-DC-9028, October 1967.

"Heat Pipe Space Radiators", T. P. Cotter, Lectures on Nuclear Thermionic Electrical Propulsion for Space, LA-3412-MS, July 1965 (CRD).

High Performance Heat Pipes, J. E. Kemme, LA-DC-9027, October 1967.

High Thermal Conductance Devices Utilizing the Boiling of Lithium or Silver, J. E. Deverall, J. E. Kemme, Report AEC LA-3211, April, 1965.

Laminar Incompressible Flow in Channels with Porous Walls, B. W. Knight and B. B. McInteer, LADC-5309.

Mercury as a Heat Pipe Fluid, J. E. Deverall, LA-4300-MS, January 5, 1970.

Orbital Heat Pipe Experiment, J. E. Deverall, E. W. Salmi, Contract W-7405-ENG-36, Report AEC LA-3714, June 1967. (NSA 21:30614).

Theory of Heat Pipes, Contract W-7405-ENG-36, T. P. Cotter, Report AEC LA-3246-MS.

Satellite Heat Pipe, J. E. Deverall, J. E. Kemme, Report LA-3278-MS, 20 April 1965. (STAR N65-23238).

Space Electric Power R&D Program, Contract W-7405-ENG-36, Report AEC LA-3881, February 1968. (NSA 22:19033), Report AEC LA-3986-MS, July 1968, Part 1

Status Report on Theory and Experiments on Heat Pipes at Los Alamos, T. P. Cotter, et. al., LA-DC-7206, 1965.

Survey of Los Alamos and Euratom Heat Pipe Investigations, W. A. Ranken and J. E. Kemme, LA-DC-7555, 1965.

Quarterly Status Report on Advanced Reactor Technology (ART), Contract W-7405-ENG-36.

Period Ending 30 April 1965, LA-3316, May 1965.
Period Ending 31 July 1965, LA-3370MS, August 1965.
Period Ending 31 October 1966, LA-3625, November 1966.
Period Ending 31 January 1967, LA-3666-MS, February 1967.
Period Ending 30 April 1967, Part I, LA-3708-MS, May 1967.
Period Ending 31 July 1967, Part I, Report No. LA-3760-MS, August 1967.
Period Ending 1 January 1968, Part I, LA-3881-MS, February 1968.
Period Ending 30 April 1968, Part I, LA-3941-MS, May 1968.
Period Ending 31 July 1968, Part I, LA-3986-MS, August 1968.

Quarterly Status Report on the Space Electric Power R&D Program for the Period Ending:

31 January 1968, LA-3881-MS
30 April 1968, LA-3941
31 July 1968, LA-3986
31 October 1968, LA-4039
31 January 1969, LA-4109
31 January 1970, LA-4374-MS

MARTIN MARIETTA CORPORATION
Baltimore, Maryland

Heat Pipe Design Manual, Nuclear Report AEC MND-3288, February 1967.

McDONNELL DOUGLAS ASTRONAUTICS COMPANY
Richland, Washington

Low Temperature Heat Pipe Research Program, E. C. Phillips, NASA CR-66792, Contract NAS 1-8000.

NASA

A Nuclear Thermionic Space Power Concept Using Rod Control and Heat Pipes, J. L. Anderson and E. Lantz, NASA TN D-5250, May 1969.

Analysis of Low Temperature Direct-Condensing Vapor-Chamber Fin and Conducting Fin Radiators, H. C. Haller and Others, November 1965, NASA Report TN-D-3103.

Analytical Comparison of Rankine Cycle Space Radiators Constructed of Central, Block and Double Vapor Chamber Fin Tube Geometries, H. C. Haller, S. Lieblein, February 1968, NASA-TN-D-4411.

Electron-Bombardment Filament Designs for Heating Cylindrical Thermionic Converters, P. Cipollone, Lewis Research Center, NASA-TMX-1630, August 1968.

Experimental Feasibility Study of Water-Filled Capillary-Pumped Heat Transfer Loops, F. J. Stenger, Lewis Research Center Report NASA TM X-1310, November 1966.

Nuclear Thermionic Space Power Systems Concept Employing Heat Pipes, C. A. Heath, E. Lantz, Lewis Research Center Technical Note TN D-4299, March 1968. (STAR N68-19146).

Reactor Concept for Space Power Employing Thermionic Diodes and Pipes, C. A. Heath and E. Lantz, Lewis Research Center, NASA-TM-X-52370, 1967.

NORTHRUP CORPORATION
Hawthorne, California

Heat Pipe Design and Analysis, Northrup Corporate Laboratories, Report NCL 68-11R, March 1968.

PRATT AND WHITNEY AIRCRAFT
East Hartford, Connecticut

Vapor-Chamber Fin Studies, Transport Properties and Boiling Characteristics of Wicks, H. R. Kunz and Others, Contract NAS 3-7622, Report PWA-2953, June 1967, NASA CR-812.

Vapor Chamber Fin Studies - Operating Characteristics of Fin Models, H. R. Kunz, et. al., August 1968, NASA CR-1139.

RCA CORPORATION
Lancaster, Pennsylvania

The Development of a 600°C Heat Pipe Assembly:

1st Quarterly Report, NYOO-3507-4, 5/65 (CRD)
2nd Quarterly Report, NYOO-3507-9, 8/65
First Year Summary Report, NYOO-3507-13, 12/65 (CRD)
3rd Quarterly Report, AOO-3507-1, 4/66 (C)
4th Quarterly Report, AOO-3507-2, 7/66 (C)
5th Quarterly Report, AOO-3507-3, 10/66 (C)
Interim Summary Technical Report, AOO-3507-4, 1/67 (C)

The Development of a Flame Fired Thermionic Generator, AD 634-538, April 1966 (Final Report), Semiannual Report: AD 629-762.

The Development of a Fossil Fuel Fired Heat Pipe for Use With Thermionic Converters, AD 801-745L, (Final Report).

1st Quarterly Report - AD 476-305
2nd Quarterly Report - AD 482-513
3rd Quarterly Report - AD 486-680L

The Development of a Heat Pipe for Automatic Temperature Control, Summary Technical Report AT(30-1)-3507, Report TL-317-28-994-134, December 1965 (Conf.)

The Development of Heat Pipes for Use With Energy Conversion Devices, F. G. Block, et. al., SC-M-66-624, October 1966. (CRD)

The Development of an Insulated Thermionic Converter-Heat Pipe Assembly, AD 813-424, April 1967, (Final Report).

1st Quarterly Report - AD-468-477
2nd Quarterly Report - AD-471-918
3rd Quarterly Report - AD-476-304
4th Quarterly Report - AD-480-985
First Year Summary Report - AD-482-409
5th Quarterly Report - AD-487-228
6th Quarterly Report - AD-800-993
7th Quarterly Report - AD-804-594

The Development of Thermionic Heat Pipe Space Power Technology

1st Quarterly Report - RCA/JPL-951754-1 (CRD), January 1967
2nd Quarterly Report - RCA/JPL-951754-2 (CRD), April 1967
Final Report, TL 358-53-994-18

Discussion of Heat Pipe Principles, January 1966.

Feasibility Investigation of the Vapor Chamber Fin, R. C. Turner, AD 839-469, August 1968.

The Heat Pipe, A Unique and Versatile Device for Heat Transfer Applications, RCA Ref. 994-619.

Radioisotope Thermionic Generator Research, AD 823-842, Final Report, AFAPL-TR-67-111, October 1967.

Appendix 6 to Final Report - AD-385-995 (CRD)
1st Quarterly Report - AD 802-685
2nd Quarterly Report - AD 804-302
3rd Quarterly Report - AD 810-753

Thermionic Isotope Space Power Technology, NASA-CR-78657, March 1966. (CRD)

SANDIA CORPORATION
Albuquerque, New Mexico

Heat-Pipe Operating Principles and Performance Characteristics, K. T. Feldman and G. H. Whiting, SC-TM-66-2632, March 1967.

The Heat Pipe, Report AEC SC-TM-66-2632, March 1967.

Space Isotope Power Program, Contract AT(29-1)-789, Report AEC SC-PR-66-498, August 1966 (Conf.)

SCOTT-ENGINEERING SCIENCES
Pompano Beach, Florida

Heat Pipe Analysis, Design, and Experiments, K. T. Feldman, Publication No. 9068, December 1968.

THERMO ELECTRON CORPORATION
Waltham, Massachusetts

Heat Pipe Thermionic Converter Development, P. Brosens, NASA-CR-93664, (Final Report), December 1967.

2nd Quarterly Report - NASA-CR-83920, 1/67
3rd Quarterly Report - NASA-CR-88119, 4/67
5th Quarterly Report - NASA-CR-91437, 10/67

TRW SYSTEMS GROUP
Redondo Beach, California

Analytical and Experimental Study of Heat Pipes, L. G. Neal, Report 99900-6114-R000, January 1967. (STAR N68-12857)

Heat Pipe Devices for Space Suit Temperature Control, A. P. Shlosinger, NASA CR-1400, October 1969.

On the Operation of Heat Pipes, B. D. Marcus, 9895-6001-TU-DOD, May 1965.

UNIVERSITIES AND COLLEGES

Condensation of Sodium at High Heat Fluxes, R. E. Barry, Ph.D. Thesis, University of Michigan, 1965.

Design Operation of a Heat Pipe, R. T. Burges, Jr., Naval Post-Graduate School, Monterey, California, AD 836518, June 1968.

The Effect of Nucleate Boiling on Heat Pipe Operation, W. L. Mosteller, U.S.Navy Postgraduate School, April 1969. (STAR N69-39478).

The Effect of Wick Geometry on the Operation of a Longitudinal Heat Pipe, H. E. Kilmartin Jr., M. S. Thesis, Naval Postgraduate School, Monterey, California, June 1969. (STAR N70-11169).

Engineering Design of a Heat Pipe, J. H. Cosgrove, Ph.D. Thesis, North Carolina State University, 1966, (STAR:N68-29703).

An Experimental and Analytical Study of Water Heat Pipes for Moderate Temperature Ranges, B. G. McKinney, University of Alabama, NAS-TMX-53849, June 1969. (STAR N69-38853).

Heat Transfer Coefficients in the Boiling and Condensation of Liquid Metals: Potassium and Rubidium, Columbia University M. SC. Thesis, 1961.

Two-Phase Momentum Flux and Design of a Heat Pipe, Massachusetts Institute of Technology Report TID-2224, 30 June 1965. (STAR N66-23113).

Heat Transfer During Film Condensation of Potassium Vapor on a Horizontal Plate, PM Meyrial and Others, M.I.T. Dept. of Engineering, 17 April 1968.

Heat Transfer During Film Condensation of a Liquid Metal Vapor, S. P. Sukhalme and W. M. Rohsenow, M.I.T., Dept. of Mechanical Engineering, Report No. 9167-27, April 1964.

Investigation of Liquid Metal Boiling Heat Transfer, R. E. Balzhiser and Others, University of Michigan, Contract AF 33(616)-8277, RTD-TDR-63-4130, 9 November 1963.

January	1962, R-04526-3P
April	1962, R-04526-4P
February	1963, AEC NP-12699
August	1963, R-05750-3P
November	1963, RTD TDR-63-4130
February	1964, R-05750-9P
August	1965, R-05750-23P

A Study of the Operating Characteristics of the Heat Pipe. Part 1: An Analytical Model For the Prediction of Operating Limits of Heat Pipes. Part 2: Capillarity in Porous Media, Final Report on Contract AT(40-1)-3411, J. K. Ferrell, J. H. Cosgrove, A. Carnesale, E. M. Schoenborn, North Carolina State University, ORO-3411-12-Pt1-Pt2, April, 1969. (STAR N69-40085).

A Study of the Operating Characteristics of the Heat Pipe, Part 3: Vaporization Heat Transfer from Flooded Wick Covered Surfaces, Final Report on Contract AT(40-1)-3411, J. K. Ferrell and J. Alleavitch, ORO-3411-12-Pt3, April 1969. (STAR N69-40393).

U. S. ARMY

Preliminary Evaluation of Gas Turbine Regenerators Employing Heat Pipes, C. C. Silverstein, Baltimore, Md., AD 671-028, USAAVLABS-TR-68-10, Contract DAAJ02-67-C-0053, April 1968. (STAR N68-31316).

WESTINGHOUSE ELECTRIC CORPORATION (ASTRONUCLEAR LABORATORY)

Compact Thermoelectric Converter, Phase II-B, Contract AT(30-1)-3584.

Quarterly Report, April 1967, Report AEC NYOO-3584-6(C)
Quarterly Report, July 1967, Report AEC NYOO-3584-7(C)
Quarterly Report, Oct. 1967, Report AEC NYOO-3584-8(C)
Quarterly Report, Jan. 1968, Report AEC NYOO-3584-9(C)
Quarterly Report, April 1968, Report AEC NYOO-3584-10(C)
Quarterly Report, July 1968, Report AEC NYOO-2584-11(C)

Compact Thermoelectric Converter, Phase II-C, Contract AT(29-2)-2638, Quarterly Report, October 1968, NYOO-3584-12(C).

WRIGHT-PATTERSON AFB

Cryogenic Heat Pipe, W. L. Haskin, Flight Dynamics Lab, Report AFFDL-TR-66-228, June 1967. AD-657-025.

HEAT PIPE BIBLIOGRAPHY

PART 2: JOURNALS/PERIODICALS/BOOKS

Anand, D. K., et. al., "Effects of Condenser Parameters on Heat Pipe Optimization," J. Spacecraft and Rockets, Vol. 4, No. 5, 695-696, May 1967.

Anand, D. K., "On the Performance of a Heat Pipe," J. Spacecraft and Rockets, Vol. 3, No. 5, 763-765, May 1966. (CA 67:83324r)

Allingham, W. D., and McEntire, J. A., "Determination of Boiling Film Coefficient for a Heated Horizontal Tube in Water-Saturated Wick Material," J. of Heat Transfer, 71-76, February 1961.

Anderson, J. L., and Lantz, E., "A Thermionic Heat Pipe Space Power Concept," Trans. Am. Nuc. Soc. 11:14, 1968.

Arcella, F. G. and G. S. Dzakowic, "Heat Pipes Function Isothermally and Adaptably," Space/Aeronautics, Vol. 52, No. 3, August 1969, 58-60.

Barnett, C. S., "An Out-of-Pile Heat Pipe Thermionic Space Power Concept," Trans. Am. Nuc. Soc. 9:2, November 1966.

Bodhansky, J., and Schins, H. E. J., "A New Method for Vapor Pressure Measurements at High Temperature and High Pressure," J. Appl. Physics 36:11, 3683-3684, November 1965.

Caswell, B. F., and Balzhiser, R. E., "The Critical Heat Flux for Liquid Metal Systems," Heat Transfer - Los Angeles, Chem. Engr. Prog. Symp. Ser., 62(64), 41-46, 1966.

Chen, J. C., "Incipient Boiling Superheats in Liquid Metals," J. Heat Transfer, 90(3), 303-12, 1968. (CA 69:68528z)

Chisholm, D., and Leishman, J. M., "Condensation in Surface Heat Exchangers," Chem. Process Eng., Heat Transfer Surv., 160-164, August 1967. (CA 68:14373q)

Collier, J. G., "Boiling of Liquid Alkali Metals," Chem. Process Eng., Heat Transfer Surv., 65-71, 78, August 1968. (CA 69:97934t)

Cosgrove, J. H., and Others, "Operating Characteristics of Capillary-Limited Heat Pipes," J. of Nuclear Energy, Vol. 21, No. 7, 547-548, July 1967. (NSA 21:39121)

Costello, C. P., and Frea, W. J., "The Role of Capillary Wicking and Surface Deposits in the Attainment of High Pool Boiling Burnout Heat Fluxes," AIChE Journal, Vol. 10, 368-393, May 1964.

Costello, C. P., and Redeker, E. R., "Boiling Heat Transfer and Maximum Heat Flux for a Surface With Coolant Supplied by Capillary Wicking," Chem. Engr. Progress Symp. Series, Heat Transfer - Houston, Vol. 59, No. 41, 104-113, 1963.

Deverall, J. E., and Others, "Heat Pipe Performance in a Zero Gravity Field," J. Spacecraft Rockets, Vol. 4, No. 11, 1556-1557, November 1967.

Eastman, G. Y., "RCA Tests Heat Pipes," Energy Conversion Digest, 6:8, September 1967.

Eastman, G. Y., "The Heat Pipe," Scientific American, 38-46, May 1968.

"Heat Pipe Sweats to Harness Nuclear Reactor Heat," Electromechanical Design, Vol. 11, No. 10, 20, October 1967.

Feldman, Jr., K. T., and Whiting, G. H., "The Heat Pipe," Mechanical Engineering, Vol. 89, No. 2, 30-33, February 1967.

Feldman, Jr., K. T., and Whiting, G. H., "Application of the Heat Pipe," Mechanical Engineering, Vol. 90, No. 11, 48-53, November 1968.

Green, D. W., and Perry, R. H., "Heat Transfer With a Flowing Fluid Through Porous Media," Heat Transfer - Buffalo, Chem. Engr. Progress Symp. Series, Vol. 57, No. 32, 61-68, 1961.

Goring, R. L., and Churchill, S. W., "Thermal Conductivity of Heterogeneous Materials," Chem. Engineering Progress, Vol. 57, No. 7, 53-59, July 1961.

Grover, G. M., and Others, "Structures of Very High Thermal Conductance," J. of Applied Physics, Vol. 35, 1990-1991, June 1964.

Haskins, W. L., "Cryogenic Heat Pipe," Research Tech. Brief, Vol. 5, No. 8, 14-15, August 1967.

Holtz, R. E., and Singer, R. M., "Incipient Pool Boiling of Sodium," AIChE Journal, 14(4), 654-656, 1968. (CA 69:60279g)

Hsu, Y. Y., "On the Size Range of Active Nucleation Cavities on a Heating Surface," Trans. of ASME, August 1962.

Judge, R. F., "RCA Tests Thermal Energy Pipe," Missiles and Rockets, 36, February 1966.

Kroger, D. G. and Rohsenow, W. M., "Film Condensation of Saturated Potassium Vapor," Int. J. Heat Mass Transfer, Vol. 10, 1891-1894, 1967.

Levy, E. K., "Theoretical Investigation of Heat Pipes Operating at Low Vapor Pressures," ASME Trans., Vol. 90B, No. 4, 547-552, November 1968.

Marto, P. J. and Rohsenow, W. M., "Effects of Surface Conditions on Nucleate Pool Boiling of Sodium," Trans. of ASME, Vol. 88C, 196-204, May 1966.

Moss, R. A., "Application of Neutron Radiography to Heat Pipe Diagnosis," Trans. Amer. Nucl. Soc., 10, 445-446, November 1967.

Neu, H., "Heat Pipes and Their Application for Nuclear Power Supplies in Space," (EURATOM, Ispra, Italy), Atompraxis 12:220-4, (German), April-May 1966. (CA 65:8278b).

Nissan, A. H., Hansen, D., and Walker, J. L., "Heat Transfer in Porous Media Containing a Volatile Liquid," Chem. Engr. Progress Symp. Series, Heat Transfer - Houston, Vol. 59, 1963.

Noyes, R. C., "An Experimental Study of Sodium Pool Boiling Heat Transfer," J. of Heat Transfer, Vol. 85, 125-131, May 1963.

Noyes, R. C., and Lurie, H., "Boiling Sodium Heat Transfer," Proc. Int. Heat Transfer Conf., 3rd, Chicago, 5, p. 92, 1966. (CA 68:14427k)

Othmer, D. F., "Condensation Coefficient of Heat Transfer," Chem. Process Eng., 49(6), 109-112, 1968. (CA 69:20687g)

Pedersen, E. S., "Heat Pipe Thermionic Reactor Concept," Nucl. Engineering, Vol. 12, 112-114, 120-129, February 1967.

Petukhov, B. S., and Others, "A Study of Sodium Boiling Heat Transfer," Proc. Int. Heat Transfer Conf., 3rd, Chicago, 5, 80-91, 1966. (CA 68:4423s)

"RCA 'Pipes' Heat Into Electricity," Electron Design, Vol. 14, No. 5, March 1966.

Scheidegger, A. E., The Physics of Flow Through Porous Media, Univ. of Toronto Press, 1957.

Schretzmann, K., (Nucl. Res. Center, Karlsruhe, Ger.), "The Effect of Electromagnetic Fields on the Evaporation of Metals," Phys. Lett., A 24(9), 478-479, 1967. (CA 67:24747h)

Tang, Y. S., "Liquid-Metal Boiling Heat Transfer," Nuclear Applications, Vol. 1, 521, December 1965.

Thurman, J. L., and Ingram, E. H., "Application of Heat Pipes to Reduce Cryogenic Boiloff in Space," J. of Spacecraft and Rockets, Vol. 6, No. 3, 319-21, March 1969.

Wageman, W. E., and Guevara, F. A., "Fluid Flow Through a Porous Channel," The Physics of Fluids, Vol. 3, 878, 1960.

Yaun, S. W., and Finkelstein, A. B., "Laminar Flow With Injection and Suction Through a Porous Wall," ASME Transactions, 78, 719-24, 1956.

HEAT PIPE BIBLIOGRAPHY

PART 3: TECHNICAL CONFERENCES

AIAA 5TH PROPULSION JOINT SPECIALIST CONFERENCE

Colorado Springs, Colorado, June 1969

Stephanou, S. E. and others, "Application of Heat Pipe Technology to Rocket Engine Cooling (Paper No. 69-582).

AIAA THERMOPHYSICS SPECIALIST CONFERENCE

New Orleans, Louisiana, April 1967

Katzoff, S., "Heat Pipes and Vapor Chambers for Thermal Control of Spacecraft," (AIAA Paper No. 67-310).

San Francisco, California, June 1969

Hinderman, J. D., and Others, "An ATS-E Solar Cell Space Radiator Utilizing Heat Pipes."

Shlosinger, A. P., "Advancements of Space Suit Temperature Control Technology by Application of Modified Heat Pipes."

Tien, C. L., "Two-Component Heat Pipes."

Turner, R. C., "The "Constant Temperature" Heat Pipe - A Unique Device for the Thermal Control of Spacecraft Components."

THE ANNUAL AVIATION AND SPACE CONFERENCE
(Beverly Hills, California, June 1968, ASME)

Anand, D. K., "Heat Pipe Application to a Gravity-Gradient Satellite (Explorer XXXVI)," 634-638.

Conway, E. C., and Kelley, M. J., "A Continuous Heat Pipe for Spacecraft Thermal Control," 655-658.

Deverall, J. E., "Total Hemispherical Emissivity Measurement by the Heat Pipe Method," 649-654.

Farran, R. A., and Starner, K. E., "Determining Wicking Properties of Compressible Materials for Heat Pipe Applications," 659-670.

Levy, E. K., "Investigation of Heat Pipe Operating at Low Vapor Pressures," 671-676. (See also Trans. ASME, 90B(4), 547-552)

Schlosinger, A. P., "Heat Pipes for Space Suit Temperature Control," 644-648.

Turner, R. C., and Harbaugh, W. E., "The Design of a 50,000 Watt Heat Pipe Space Radiator," 639-643.

ANNUAL POWER SOURCES CONFERENCE

Ernst, D. M., and Eastman, G. Y., "Thermionic (Thermal Energy Conversion), Vol. II, Two-Piece Heat Pipe Converter," Proc. Annu. Power Sources Conf., 21, 135-138, 1967. (CA 68:41379c)

Hall, W. B., and Kessler, S. W., "Advances in Heat Pipe Design," Annual Power Sources Conference, Fort Monmouth, New Jersey, May 1966.

ASME ANNUAL WINTER MEETING, 1968

Silverstein, C. C., "Heat Pipe Gas Turbine Regenerators," Paper No. 68-WA/GT-7.

CONFERENCE ON APPLICATION OF HIGH TEMPERATURE INSTRUMENTATION TO LIQUID-METAL EXPERIMENTS (AEC, NASA - September 1965)

Edwards, J. A., and Hoffman, H. W., "Superheat With Boiling Alkali Metals."

CONFERENCE ON CHEMICAL VAPOR-DEPOSITION OF REFRACTORY MATERIALS (Gatlinburg, Tennessee, September 1967)

Glaski, F. A., "A Report on the Current Role of Chemical Vapor-Deposition as a Manufacturing Process," 275-289. (NSA 22:6966)

INTERNATIONAL CONFERENCE ON THERMIONIC ELECTRICAL POWER GENERATION, (European Nuclear Energy Agency and IEEE)

London, England, September 1965

Bacal, M., and Teodorescu, M., "Physical Phenomena in Cross-Field Thermionic Converter."

Bohdansky, J., and Schins, H. E., "Heat Transfer in Heat Pipes Operating at Emitter Temperatures."

Busse, C. A., and Others, "Performance Studies on Heat Pipes."

Busse, C. A., and Others, "Prototypes of Heat Pipe Thermionic Converters for Space Reactors."

Cotter, T. P., and Others, "Status Report on Theory and Experiments on Heat Pipes at Los Alamos."

Stresa, Italy, May 1968

Bahr, A., and Others, "Liquid-Vapor Interaction and Evaporation in Heat Pipes."

Busse, C. A., "Heat Pipe Research in Europe."

Busse, C. A., and Others, "High Temperature Lithium Heat Pipes."

Fiebelmann, P., and Others, "A Heat Pipe Thermionic Reactor Concept."

Grover, G. M., and Others, "Advances in Heat Pipe Technology."

Reiss, F., and Schretzmann, K., "Pressure Balance and Maximum Power Density at the Evaporation Gained from Heat Pipe Experiments."

Van Andel, E., "Heat Pipe Design Theory."

INTERNATIONAL HEAT TRANSFER CONFERENCE

Chicago, Illinois, August 1966

Aladyev, I. T. and others, "Film Condensation of Sodium and Potassium Vapor."

INTERSOCIETY ENERGY CONVERSION ENGINEERING CONFERENCE, ADV. IN ENERGY CONVERSION ENGINEERING

1966

Buzzard, R. J., and Others, "The Development of an Advanced Thermionic-Isotope Space Power Generator," TID-23831. (Classified Paper)

Miami Beach, Florida, August 1967

Brosens, P., "Thermionic Converters With Heat Pipe Radiators," 181-187.

Frank, S., "Optimization of a Grooved Heat Pipe," 833-845.

Parker, G. H., and Hanson, J. P., "Heat Pipe Analysis," 847-857.

Boulder, Colorado, August 1968

Altieri, D., and Others, "Conceptual Design of a Radioisotope-Heat-Pipe-Thermionic Space Power System." (Classified Paper)

Bienert, W. E., and Others, "Application of Heat Pipes to SNAP-29."

Harbaugh, W. C., and Eastman, G. Y., "Experimental Evaluation of an Automatic Temperature Controlled Heat Pipe." (Classified Paper)

Werner, R. W., and Carlson, G. A., "Heat Pipe Radiator for Space Power Plant."

Washington, D. C., September 1969

Freggens, R. A.," Experimental Determination of Wick Properties for Heat-Pipe Applications."

JOINT ATOMIC ENERGY COMMISSION/SANDIA LABORATORIES HEAT PIPE CONFERENCE
(North Carolina State College, October 1966, Report No. SC-M-66-623)

Caresdale, A., and Others, "Operating Limits of the Heat Pipe," 27-44. (STAR N67-26794)

Cotter, T. P., "Status of the Engineering Theory of Heat Pipes." (STAR N67-26791)

Haller, H. C., and Lieblein, S., "Feasibility Studies of Space Radiators Using Vapor Chamber Fins."

Katzoff, S., "Notes on Heat Pipes and Vapor Chambers and Their Application to Thermal Control Spacecraft," 69-89. (STAR N67-26796)

Kemme, J. E., "Heat Pipe Capability Experiments," 27-44. (STAR N67-26793)

NATIONAL HEAT TRANSFER CONFERENCE (ASME-AIChE)

Minneapolis, Minnesota, August 1969

Basiulis, A., and J. C. Dixon, "Heat Pipe Design for Electron Tube Cooling," ASME Preprint 69-HR-25.

Calimbas, A. T., and R. H. Hulett, "An Avionic Heat Pipe," ASME Preprint 69-HT-16.

Chato, J. C., and J. H. Streckert, "Performance of a Wick-Limited Heat Pipe," ASME Preprint 69-HT-20.

Dzakowic, G. S., and others, "Experimental Study of Vapor Velocity Limit in a Sodium Heat Pipe," ASME Preprint 69-HT-21.

Ferrell, J. K., and J. Alleavitch, "Vaporization Heat Transfer in Capillary Wick Structures," AIChE Preprint 6.

Galowin, L. S., and V. A. Barker, "Heat Pipe Channel Flow Distributions," ASME Preprint 69-HT-22.

Gray, V. H., "The Rotating Heat Pipe - A Wickless, Hollow Shaft for Transferring High Heat Fluxes," ASME Preprint 69-HT-19.

Langston, L. S., and H. R. Kunz, "Liquid Transport Properties of Some Heat Pipe Wicking Materials," ASME Preprint 69-HT-17.

Lyman, F. A., and Y. S. Huang, "Analysis of Temperature Distributions in Heat Pipe Wicks," ASME Preprint 69-HT-23.

Marto, P. J., and W. L. Mosteller, "Effect of Nucleate Boiling on the Operation of Low Temperature Heat Pipes," ASME Preprint 69-HT-24.

McSweeney, T. I., "The Performance of a Sodium Heat Pipe," AIChE Preprint 7.

Phillips, E. C., and J. D. Hinderman, "Determination of Properties of Capillary Media Useful in Heat Pipe Design," ASME Preprint 69-HT-18.

Sartor, A. J., and others, "Condensing Heat Transfer Considerations Relevant to Rebidium and Other Alkali Metals," AIChE Preprint 5.

Schwartz, J., "Performance Map of the Water Heat Pipe and the Phenomenon of Non-condensible Gas Generation," ASME Preprint 69-HT-15.

THERMIONIC CONVERSION SPECIALIST CONFERENCE (IEEE)

San Diego, California, October 1965

Hall, W. B., "Heat Pipe Experiments," 337-340.

Ranken, W. A., and Kemme, J. E., "Survey of Los Alamos and EURATOM Heat Pipe Investigations," 325-336, LA-DC-7555.

Houston, Texas, November 1966

Bohdansky, J., and Strub, H., and Von Andel, E., "Heat Transfer Measurements Using a Sodium Heat Pipe Working at Low Vapor Pressure," 144-148.

Busse, C. A., and Others, "Heat Pipe Life Tests at 1600°C and 1000°C," 149-158.

Eastman, G. Y., and Ernst, D. M., "Review of Heat Pipe Work at RCA."

Kemme, J. E., "Heat Pipe Capability Experiments," 159-168.

Harbaugh, W. E., and Longsderff, R. W., "The Development of an Insulated Thermionic Converter/Heat Pipe Assembly."

Shefsiek, R. K., "Thermal Measurements of a Thermionic-Converter Heat Pipe System."

Palo Alto, California, October 1967

Bohdansky, J., et al., "Integrate Cs-Graphite Reservoir System in a Heat Pipe Thermionic Converter," 93-96.

Brosens, P. J., "Advanced Converter Development," 68-73.

Busse, C. A., "Pressure Drop in the Vapor Phase of Long Heat Pipes," 391-398.

Cotter, T. P., "Heat Pipe Startup Dynamics," 344-348, LA-DC-9026. (STAR N68-28359)

Deverall, J. E., and Salmi, E. W., "Heat Pipe Performance in a Space Environment," 359-362.

DeMichele, D. W., and Gietzen, A. J., "Heat Pipe Radiator System Analysis for Thermionic Power Plants." (Classified)

Ernest, D. M., "Evaluation of Theoretical Heat Pipe Performance," 349-354.

Kemme, J. E., "High Performance Heat Pipes," 355-358, LA-DC-9027.

Ranken, W. A., and Summers, C. S., "Isothermal Irradiation Assembly for Study of Fast Neutron Damage to Ceramics."

Framingham, Massachusetts, October 1968

Ernst, D. M., and Others, "Heat Pipe Studies at Thermo Electron Corporation."

Johnson, G. D., "Compatibility of Various High-Temperature Heat Pipe Alloys with Working Fluids."

Kemme, J. E., "Ultimate Heat Pipe Performance."

Monterey, California, October 1969

Longsderff, R. W., "Technology for the Development of a High Voltage Thermionic Module."

HEAT PIPE BIBLIOGRAPHY

PART 4: FOREIGN PUBLICATIONS

Experimental Heat Pipes, K. S. Bainton, United Kingdom Atomic Energy Authority Report AERE-M-1610, June 1965.

Experimentelle Untersuchunger an Natrium-gefuellten Heat Pipes, (West Germany) Institute fuer Neutronenphysik and reaktortechnik Report KFK-512, January 1967.

Heat Pipe Thermionic Reactor Concept, E. S. Pederson, Danish Atomic Energy Commission, RISO-M-514, May 1967.

Liquid Metals for Heat Pipes: Properties, Plots and Data Sheets, H. E. J. Schins (Joint Nucl. Res. Center, Eur. At. Energy Community, Ispra, Italy) Communaute Eur. Energ. At. EURATOM 1967 (EUR-3653). (CA 69:3989q)

Optimization of Heat Pipe Thermionic Converters for Space Power Plants, C. A. Busse, European Atomic Energy Community, ERU 2534.e, 1965.

Superthermal Conductivity: The Heat Tube, A Thermal Transformer, Ye Muslin, 31 December 1968 (STAR N69-16066), Transl. into English from Znanie Sila (Moscow), No. 10, October 1968.

The Use of a New Heat Removal System in Space Thermionic Power Supplies, J. Bohdansky, C. A. Busse, and G. M. Grover, European Atomic Energy Community Report (EURATOM R-2229E), January 1965.

Use of Heat Pipes for Thermionic Reactors, NASA Washington D.C. Tech. Translation TT-F-10928, May 1967. (STAR X67-16798)

HEAT PIPE BIBLIOGRAPHY
PART 5: HEAT PIPE PATENTS

Gaugler, R. S., Heat Transfer Device, U. S. Patent 2,350,348, 6 June 1944.

Grover, G. M., Evaporation-Condensation Heat Transfer Device, U. S. Patent 3,229,759, 18 January 1966.

Grover, G. M., and Others, Nuclear Reactor With Thermionic Converter, U. S. Patent 3,302,042, 31 January 1967.

Grover, G. M., and Others, Capillary Insert for Heat Tubes and Process for Manufacturing Such Inserts, U. S. Patent 3,305,005, 1968.

Bohdansky, J., and Others, Heat Pipes, U. S. Patent 3,402,767, 24 September 1968.

Sweet, C. J., Controllable Heat Pipe Apparatus, U. S. Patent 3,402,761, 1968.

Cooling System for Nuclear Reactors, Canadian Patent No. 764,919, 22 August 1967 (NSA 22:14126).

Bromberg, R., and others, Method of and Means for Cooling the Throat Wall of Rocket Engine Nozzle, U.S. Patent 3,493,177; 3 February, 1970.

Appendix B

DETAILS OF GAS-SIDE HEAT TRANSFER ANALYSIS

TABLE OF CONTENTS

LIST OF FIGURES

I. GAS-SIDE HEAT TRANSFER COEFFICIENT

A. GENERAL PROCEDURE

Heat transfer coefficients were estimated using a pipe flow-type correlation, Equation 1B, which was found to yield adequate design predictions in a recent study at Aerojet, (Ref. 1B).

$$St\ Pr^{0.6} = C_g\ Re^{-0.2} \qquad \text{Eq. 1B}$$

The correlation coefficient, C_g, varies with contraction ratio and area ratio as shown in Figure 1B. The gas properties are evaluated at the freestream temperature.

There is general agreement in the literature that enthalpy is a more appropriate driving potential than temperature for systems such as OF_2/B_2H_6 where dissociated species are present because of recombination in the boundary layer. The extent of recombination is not always known, however, and the appropriate wall enthalpy value is difficult to define. Enthalpy based calculations are preferable in the absence of data because conservative design estimates are usually obtained. However, data obtained for the FLOX/B_2H_6 system on Contract NAS 7-659 (Ref. 2B) indicate that the temperature potential approach defined by Equation 1B predicts the data reasonably well. This can be seen on Figure 1B where it is shown that C_g values inferred from test data on a 1.5 contraction ratio chamber agree with the design curve within about 20%. It is believed that these data justify the use of Equation 1B for estimating heat flux distributions in OF_2/B_2H_6 thrust chambers.

B. CONCEPT EVALUATION STUDIES (SECTION IV)

In the concept evaluation studies, heat transfer coefficients were calculated from the rearranged form of Equation 1B shown as Equation 2B.

I, B, Concept Evaluation Studies (cont.)

$$h_g = \frac{C_g}{D_c^{0.2}} \left(\frac{0.2 C_p}{Pr^{0.6}}\right)_{fs} \left(\frac{w_t}{A_F}\right)^{0.8} \qquad \text{Eq. 2B}$$

The values calculated from Equation 2B were then empirically related to local area ratio with Equations 3B, 4B, and 5B as shown in Figure 2B. The factor H accounts for the variation in transport properties with mixture ratio and is tabulated in Figure 2B.

Convergent region: $h_g = 0.00185\ (A/A_t)^{-0.5}(H)$ Eq. 3B

Divergent region, $A/A_t < 15$: $h_g = 0.00185\ (A/A_t)^{-1.17}(H)$ Eq. 4B

Divergent region, $A/A_t > 15$: $h_g = 0.001\ (A/A_t)^{-0.9}(H)$ Eq. 5B

Values of h_g for other thrust and chamber pressure combinations were obtained from Equation 6B, which is derived assuming turbulent boundary layer flow, and constant values of specific impulse and characteristic velocity. Boundary layer relaminarization effects were neglected.

$$h_g = h'_g \left(\frac{P_c}{100}\right)^{0.9} \left(\frac{1000}{F}\right)^{0.1} \qquad \text{Eq. 6B}$$

where: $h'_g = h_g$ values for 100 psia chamber pressure, 1000 lb thrust.

Average gas-side heat transfer coefficients were evaluated from the definition of an average value.

$$\bar{h}_g = \frac{\int h_g \, dA}{\int dA} \qquad \text{Eq. 7B}$$

It was assumed that an expression for local h_g of the following form was known.

I, B, Concept Evaluation Studies (cont.)

$$h_g = K\ (A/A_t)^{-b} \qquad \text{Eq. 8B}$$

For the cylindrical region of the combustion chamber, h_g was assumed constant and the average for this region was therefore equal to the constant. In the convergent and divergent regions the geometry of a truncated cone was assumed and the following expression for average h_g in those regions (derived from the foregoing equations) was utilized.

$$\bar{h}_g = \frac{(r_2/r_1)^{2(1-b)} - 1}{(1-b)\left[\left(\frac{r_2}{r_1}\right)^2 - 1\right]} \quad (h_{g_1}) \qquad \text{Eq. 9B}$$

where: the subscripts 1 and 2 refer to the minimum and maximum cone radii.

C. PRELIMINARY DESIGN ANALYSES (SECTION VII)

In the Section VII analysis, Equation 2B was modified to include the barrier flow mass flux in place of the overall average. Equal velocities were assumed. This yielded Equation 10B.

$$h_g = \frac{C_g}{D_c^{0.2}} \left(\frac{0.2 C_p}{Pr^{0.6}}\right)_{fs} \left(\frac{W_t}{A_F}\right)^{0.8} \left(F' + \frac{B}{C}(1 - F')\right) \qquad \text{Eq. 10B}$$

For a 19% barrier flow rate and 0.5 initial barrier mixture ratio, Equation 10B reduces to Equation 11B. The C_g and H values vary along the nozzle wall as shown in Figures 1B and 2B (C_g = 0.032 at the throat for 1.56 contraction ratio).

$$h_g = 0.00232\ H\ (A/A_t)^{-0.9} \left(\frac{C_g}{0.032}\right) \qquad \text{Eq. 11B}$$

II. FILM COOLANT TEMPERATURES (SECTION IV,C)

For the gas film cooled region downstream of the liquid film cooled length, film coolant temperatures for the P_c = 100 psia chamber pressure and 1000 lb_f thrust case were calculated from one of Aerojet's gaseous film cooling models (Ref. 3B). The model was simplified by assuming that the internal diameter and the gas-side heat transfer coefficient in the combustion chamber represent average values for the entire gas film cooled region, and that the velocities of the main stream and film coolant gases are about the same. With these assumptions, the equation for approximating T_F downstream of the liquid length becomes:

$$\frac{T_{aw} - T_F}{T_{aw} - T_{Fo}} = e^{-\beta X} \qquad \text{Eq. 12B}$$

where: $$\beta = 1.628 \left(\frac{\pi D_c \, h_g}{C_p} \right) \left(\frac{1}{\pi D_c} \, \frac{C_p}{k} \right)^{0.125} w_{fc}^{-0.875}$$

Values of T_f for other operating conditions were obtained from the 1000 lb_f, 100 psia results by characterizing the film coolant distribution along the chamber wall with a reference dimension X_{ref}, defined by Equation 13B.

$$X_{ref} = X \left(\frac{P_c}{100}\right)^{0.46} \left(\frac{F}{1000}\right)^{-0.54} \qquad \text{Eq. 13B}$$

Equation 10B was derived assuming the following proportionalities which follow from the assumption of constant specific impulse and characteristic velocity.

$$h_g \propto P_c^{0.9}/F^{0.1}$$

$$D \propto (F/P_c)^{1/2}$$

$$W_{Fc} \propto F$$

II, Film Coolant Temperatures (cont.)

Heat transfer coefficient values for Equation 9B were calculated from the equations shown in Figure 2B. In order to simplify the analysis, the mixture ratio variation was eliminated by assuming MR = 1.0. The errors introduced by this simplification tend to balance out when heat fluxes are calculated because conservative T_f values (probably high) and optimistic h_g values (probably low) are obtained.

REFERENCES

1B. N. E. Van Huff, Design Criteria Monograph, Fluid-Cooled Combustion Chambers, Contract NAS 3-12018 (to be published).

2B. FLOX/Diborane Technology-Boundary Reactions, Final Report on Contract NAS 7-659, Aerojet-General Corporation, Report 659-F, September 1969.

3B. New Adiabatic Film Cooling Model with Plots, L. M. Nole, 11 May 1965, Aerojet Internal Computing Sciences Division Report.

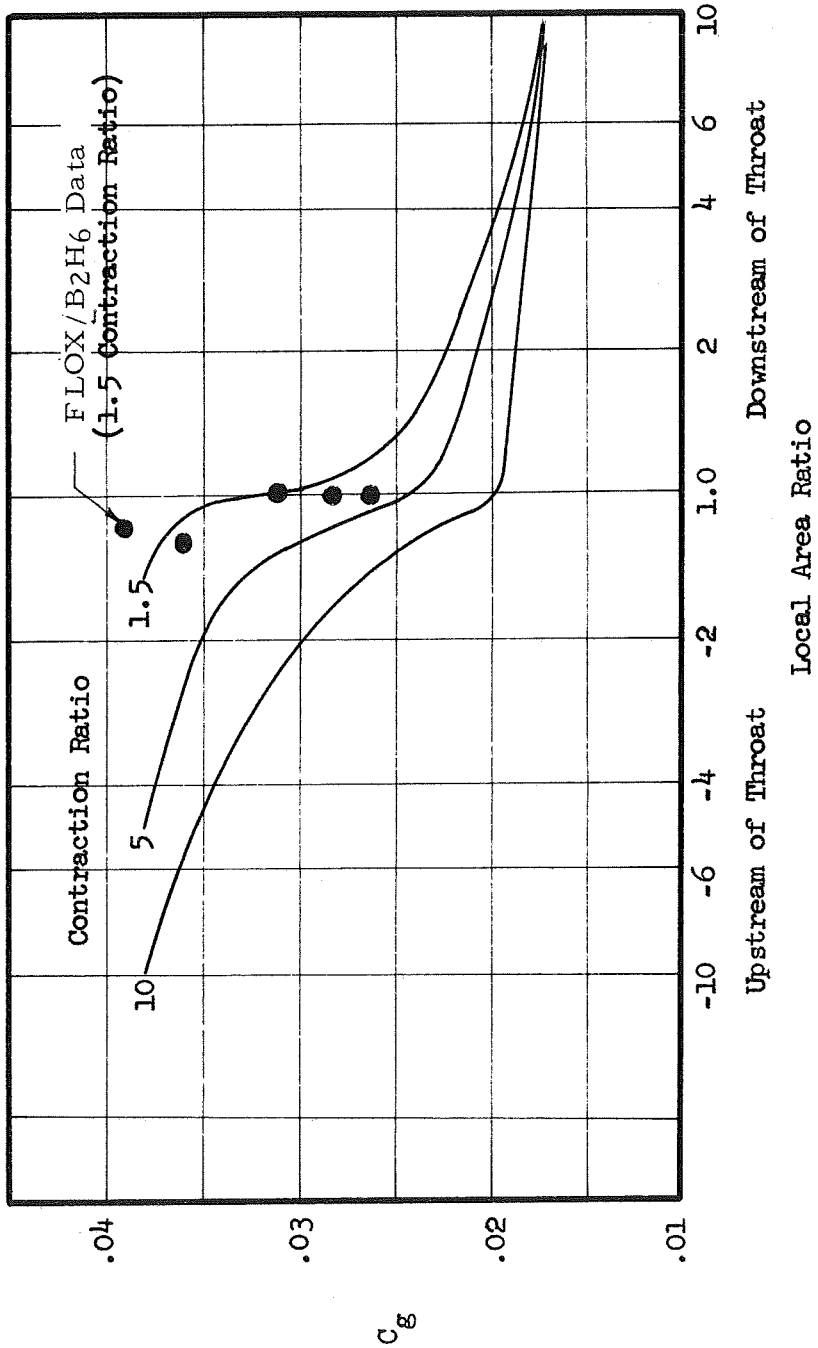

Gas-Side Correlation Coefficient

Figure 1B

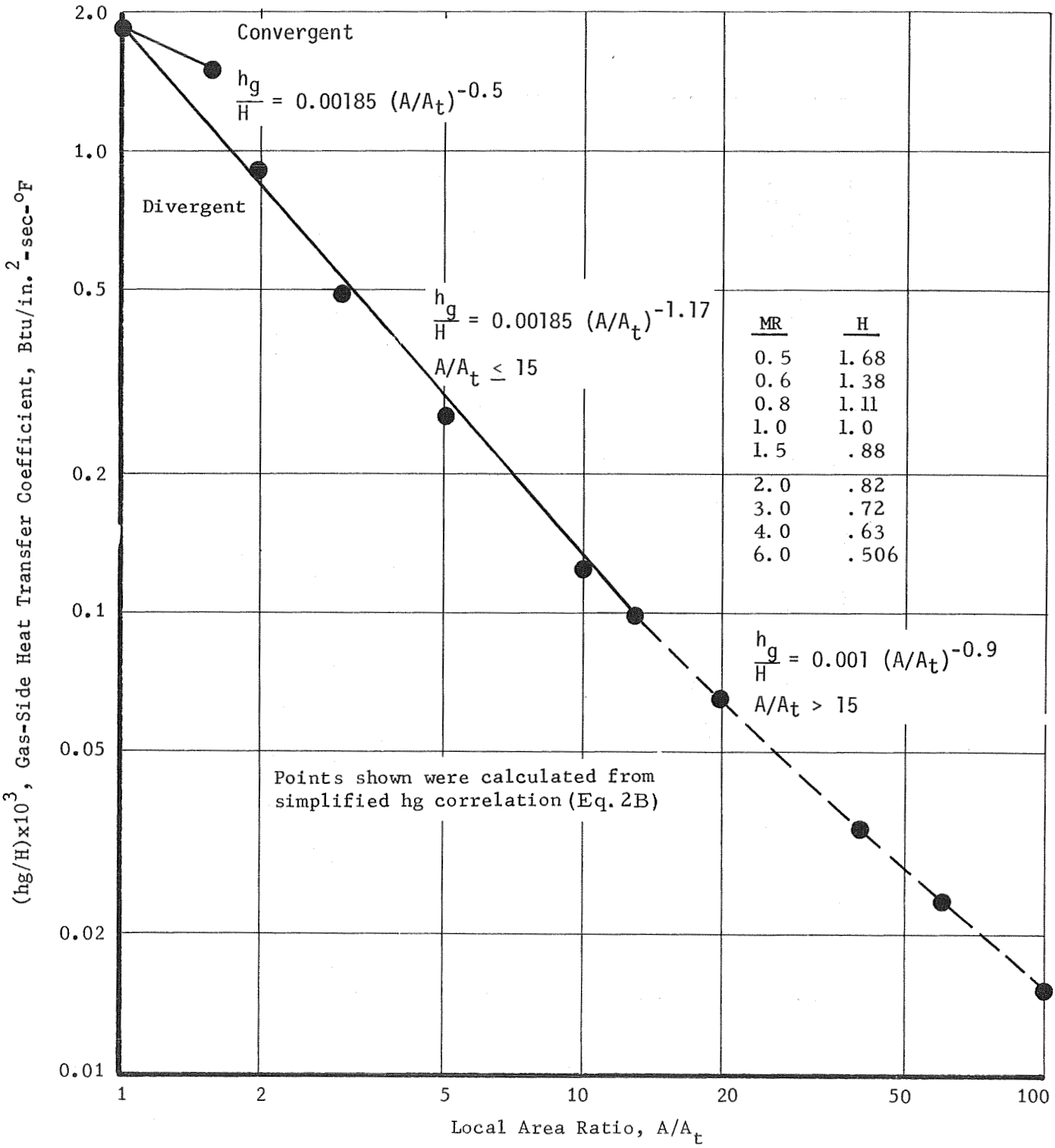

Gas-Side Heat Transfer Coefficient Distribution

Figure 2B

DISTRIBUTION LIST

Distribution List for Interim Report

Contract NAS 7-697

Copies	Recipient	Designee
	NASA Headquarters Washington, D.C. 20546	
1	Contracting Officer	(X)
1	Patent Office	(X)
	NASA Lewis Research Center 21000 Brookpark Rd. Cleveland, Ohio 44135	
1	Office of Technical Information	(X)
1	Contracting Officer	(X)
1	Patent Office	(X)
	NASA Manned Spacecraft Center Houston, Texas 77001	
1	Office of Technical Information	(X)
1	Contracting Officer	(X)
1	Patent Office	(X)
	NASA Marshall Space Flight Center Huntsville, Alabama 35812	
2	Office of Technical Information, MS-IP	(X)
1	Technical Library	(X)
1	Purchasing Office, PR-EC	( )
1	Patent Office, M-PAT	( )
1	Keith Chandler, R-P&VE-PA	(X)
1	Technology Utilization Office, MS-T	(X)
	NASA Pasadena Office 4800 Oak Grove Drive Pasadena, California 91103	
1	Patents and Contracts Management	(X)
	Jet Propulsion Laboratory 4800 Oak Grove Dr. Pasadena, Calif. 91103	
2	Technical Manager Robert W. Riebling 125-224	(X)

DISTRIBUTION LIST (cont.)

Copies	Recipient	Designee
3	Chief, Liquid Propulsion Technology RPL Office of Advanced Research and Technology NASA Headquarters Washington, D. C. 20546	(X)
1	Director, Technology Utilization Division Office of Technology Utilization NASA Headquarters Washington, D. C. 20546	(X)
25	NASA Scientific and Technical Information Facility P.O. Box 33 College Park, Maryland 20740	(X)
1	Director, Launch Vehicles and Propulsion . SV Office of Space Science and Applications NASA Headquarters Washington, D. C. 20546	(X)
1	Director, Advanced Manned Missions, MT Office of Manned Space Flight NASA Headquarters Washington, D. C. 20546	(X)
1	Mission Analysis Division NASA Ames Research Center Moffett Field, California 24035	(X)

NASA Field Centers

2	Ames Research Center Moffett Field, California 94035	Hans M. Mark
1	Goddard Space Flight Center Greenbelt, Maryland 20771	Merland L. Moseson Code 620
2	Jet Propulsion Laboratory California Institute of Technology 4800 Oak Grove Drive Pasadena, California 91103	Henry Burlage, Jr. Propulsion Div. 38

DISTRIBUTION LIST (cont.)

Copies	Recipient	Designee
2	Langley Research Center Langeley Station Hampton, Virginia 23365	Ed Cortwright Director
2	Lewis Research Center 21000 Brookpark Road Cleveland, Ohio 44135	Dr. Abe Silverstein Director
2	Marshall Space Flight Center Huntsville, Alabama 35812	Hans G. Paul Code R-P&VED
2	Manned Spacecraft Center Houston, Texas 77001	J. G. Thibodaux, Jr. Chief, Prop. & Power Div.
2	John F. Kennedy Space Center, NASA Cocoa Beach, Florida 32931	Dr. Kurt H. Debus
	Government Installations	
1	Aeronautical Systems Division Air Force Systems Command Wright-Patterson Air Force Base Dayton, Ohio 45433	D. L. Schmidt Code ASRCNC-2
1	Air Force Missile Development Center Holloman Air Force Base New Mexico 88330	Maj. R. E. Bracken
1	Air Force Missile Test Center Patrick Air Force Base, Florida	L. J. Ullian
1	Space and Missile Systems Organization Air Force Unit Post Office Los Angeles 45, California 90045	Col. Clark Technical Data Center
1	Arnold Engineering Development Center Arnold Air Force Station Tullahoma, Tennessee 37388	Dr. H. K. Doetsch
1	Bureau of Naval Weapons Department of the Navy Washington, D. C. 20546	J. Kay RTMS-41

DISTRIBUTION LIST (cont.)

Copies	Recipient	Designee
1	Defense Documentation Center Headquarters Cameron Station, Building 5 5010 Duke Street Alexandria, Virginia 22314 Attn: TISIA	
1	Headquarters, U.S. Air Force Washington, D. C. 20546	Col. C. K. Stambaugh AFRST
1	Picatinny Arsenal Dover, New Jersey 07801	I. Forsten, Chief Liquid Propulsion Laboratory
2	Air Force Rocket Propulsion Laboratory Research and Technology Division Air Force Systems Command Edwards, California 93523	RPRPD/Mr. H. Main
1	U.S. Army Missile Command Redstone Arsenal Alabama 35809	Dr. Walter Wharton
1	U.S. Naval Ordnance Test Station China Lake, California 93557	Code 4562 Chief, Missile Propulsion Div.
	CPIA	
1	Chemical Propulsion Information Agency Applied Physics Laboratory 8621 Georgia Avenue Silver Spring, Maryland 20910	Tom Reedy
	Industry Contractors	
3	Aerojet-General Corporation P.O. Box 1947 Technical Library Bldg 2015, Dept. 2410 Sacramento, California 95809	R. Stiff

DISTRIBUTION LIST (cont.)

Copies	Recipient	Designee
1	Aerospace Coropration 2400 East El Segundo Boulevard P.O. Box 95085 Los Angeles, California 90045	John G. Wilder MS-2293
1	Atlantic Research Corporation Edsall Road and Shirley Highway Alexandria, Virginia 22314	Dr. Ray Friedman
1	AVCO Systems Division Wilmington, Massachusetts	Howard B. Winkler
1	Beech Aircraft Corporation Boulder Division Box 631 Boulder, Colorado	J. H. Rodgers
1	Bell Aerosystems Company P.O. Box 1 Buffalo, New York 14240	W. M. Smith
1	Bellcomm 955 L'Enfant Plaza, S. W. Washington, D. C.	H. S. London
1	Bendix Systems Division Bendix Corporation 3300 Plymouth Road Ann Arbor, Michigan 48105	John M. Brueger
1	Boeing Company P.O. Box 3707 Seattle, Washington 98124	J. D. Alexander
1	Boeing Company 1625 K Street, N. W. Washington, D. C. 20006	Library
1	Boeing Company P.O. Box 1680 Huntsville, Alabama 35801	Ted Snow

DISTRIBUTION LIST (cont.)

Copies	Recipient	Designee
1	Camin Laboratories, Inc. 104-14 South Fourth St., Brooklyn, N. Y. 11211	Mr. Samuel Fialkoff
1	Missile Division Chrysler Corporation P.O. Box 2628 Detroit, Michigan 48231	Mr. John Gates
1	Wright Aeronautical Division Curtiss-Wright Corporation Wood-Ridge, New Jersey 07075	G. Kelley
1	Research Center Fairchild Hiller Corporation Germantown, Maryland	Ralph Hall
1	Republic Aviation Corporation Fairchild Hiller Corporation Farmingdale, Long Island, New York	Library
1	General Dynamics, Convair Division Library & Information Services (128-00) P.O. Box 1128	Frank Dore
1	Missile and Space Systems Center General Electric Company Valley Forge Space Technology Center P.O. Box 8555 Philadelphia, Pa.	F. Mezger F. E. Schultz
1	Grumman Aircraft Engineering Corp. Bethpage, Long Island New York 11714	Joseph Gavin
1	Honeywell, Inc. Aerospace Div. 2600 Ridgway Rd Minneapolis, Minn.	Mr. Gordon Harms
1	Hughes Aircraft Co. Aerospace Group Centinela and Teale Streets Culver City, Calif. 90230	F. H. Meier V. P. and Div. Mgr., Research & Dev. Div.

DISTRIBUTION LIST (cont.)

Copies	Recipient	Designee
1	Walter Kidde and Company, Inc. Aerospace Operations 567 Main Street Belleville, New Jersey	R. J. Hanville Dir. of Research Engr.
1	Ling-Temco-Vought Corporation P.O. Box 5907 Dallas, Texas 75222	Warren G. Trent
1	Arthur D. Little, Inc. 20 Acorn Park Cambridge, Massachusetts 02140	Library
1	Lockheed Missiles and Space Co. Attn-Technical Information Center P.O. Box 504 Sunnyvale, California 94088	J. Guill
1	Lockheed Propulsion Company P.O. Box 111 Redlands, California 92374	H. L. Thackwell
1	The Marquardt Corporation 16555 Saticoy Street Van Nuys, Calif. 91409	Howard McFarland
1	Denver Division Martin Marietta Corporation P.O. Box 179 Denver, Colorado 80201	Dr. Morganthaler A. J. Kullas
1	Orlando Division Martin Marietta Corp. Box 5837 Orlando, Florida	J. Ferm
1	Astropower Laboratory McDonnell-Douglas Aircraft Company 2121 Paularino Newport Beach, California 92663	Dr. George Moc Director, Research
1	McDonnel-Douglas Aircraft Corp. P. O. Box 516 Municipal Airport St. Louis, Missouri 63166	R. A. Herzmark

DISTRIBUTION LIST (cont.)

Copies	Recipient	Designee
1	Missile and Space Systems Division McDonnell-Douglas Aircraft Company 3000 Ocean Park Boulevard Santa Monica, Calif. 90406	Mr. R. W. Hallet Chief Engineer Adv. Space Tech.
1	Electronics Components Division RCA Corporation Lancaster, Pennsylvania 17604	G. Y. Eastman
1	Space and Information Systems Division North American Rockwell 12214 Lakewood Boulevard Downey, California 90241	Library
1	Rocketdyne (Library 586-306) 6633 Canoga Avenue Canoga Park, Calif. 91304	Dr. R. J. Thompson S. F. Iacobellis
1	Northrop Space Laboratories 3401 West Broadway Hawthorne, California 90250	Dr. William Howard
1	Aeronutronic Division Philco Corporation Ford Road Newport Beach, California 92663	D. A. Garrison
1	Rocket Research Corporation 520 South Portland Street Seattle, Washington 98108	Foy McCullough, Jr.
1	Sunstrand Aviation 2421 11th Street Rockford, Illinois 61101	R. W. Reynolds
1	Stanford Research Institute 333 Ravenswood Avenue Menlo Park, California 94025	Dr. Gerald Marksman
1	TRW Systems Group TRW Incorporated One Space Park Redondo Beach, Calif. 90278	G. W. Elverum

DISTRIBUTION LIST (cont.)

Copies	Recipient	Designee
1	TAPCO Division TRW Incorporated 23555 Euclid Avenue Cleveland, Ohio 44117	P. T. Angell
1	Thiokol Chemical Corporation Huntsville Division Huntsville, Alabama 35807	John Goodloe
1	Research Laboratories United Aircraft Corp. 400 Main St. East Hartford, Conn. 06108	Erle Martin
1	Hamilton Standard Division United Aircraft Corp. Windsor Locks, Conn. 06096	Mr. R. Hatch
1	United Technology Center 587 Methilda Avenue P.O. Box 358 Sunnyvale, California 94088	Dr. David Altman
1	Florida Research and Development Pratt and Whitney Aircraft United Aircraft Corporation P.O. Box 2691 West Palm Beach, Florida 33402	R. J. Coar
1	Vickers, Inc. Box 302 Troy, Michigan	